

Review

Open Access



Recent progress in strategies for preparation of metal-organic frameworks and their hybrids with different dimensions

Yichun Su¹, Guoqiang Yuan¹, Jinliang Hu³, Wenhao Feng¹, Qingyu Zeng¹, Yangyi Liu^{1,2,*}, Huan Pang^{1,*} 

¹School of Chemistry and Chemical Engineering, Yangzhou University, Yangzhou 225000, Jiangsu, China.

²School of Electrical Engineering, Engineering Technology Research Center of Optoelectronic Technology Appliance, Tongling University, Tongling 244061, Anhui, China.

³Jiangsu Yangnong Chemical Group Co. Ltd., Yangzhou 225009, Jiangsu, China.

***Correspondence to:** Dr. Yangyi Liu, School of Chemistry and Chemical Engineering, Yangzhou University, Yangzhou 225000, Jiangsu, China; School of Electrical Engineering, Engineering Technology Research Center of Optoelectronic Technology Appliance, Tongling University, Tongling 244061, Anhui, China. E-mail: liulyy@mail.ustc.edu.cn; Prof. Huan Pang, School of Chemistry and Chemical Engineering, Yangzhou University, Yangzhou 225000, Jiangsu, China. E-mail: huanpangchem@hotmail.com/panghuan@yzu.edu.cn

How to cite this article: Su Y, Yuan G, Hu J, Feng W, Zeng Q, Liu Y, Pang H. Recent progress in strategies for preparation of metal-organic frameworks and their hybrids with different dimensions. *Chem Synth* 2023;3:1. <https://dx.doi.org/10.20517/cs.2022.24>

Received: 4 Sep 2022 **First Decision:** 16 Nov 2022 **Revised:** 29 Nov 2022 **Accepted:** 7 Dec 2022 **Published:** 1 Jan 2023

Academic Editors: Bao-Lian Su, Hai-Bo Yang **Copy Editor:** Peng-Juan Wen **Production Editor:** Peng-Juan Wen

Abstract

As a new kind of organic-inorganic hybrid porous material, metal-organic frameworks (MOFs) exhibit a wide application prospect in gas storage and separation, catalysis and sensing due to their characteristics of large specific surface area, high porosity and coordination unsaturation. As more and more types of MOFs were reported, the synthetic strategies of MOFs-based materials have become a hot research topic. According to the morphological dimension, MOFs can be roughly divided into one-dimensional, two-dimensional and three-dimensional structures. Herein, we summarize the synthetic methods and principles of MOFs from multi-dimensional perspectives, and explore the growth mechanism of MOFs with different morphologies based on dynamic and thermodynamic tuning. Finally, based on the above summaries, the challenges and opportunities of MOFs in the future are discussed.

Keywords: MOFs, MOF-based hybrids, different dimensions, dynamic and thermodynamic tuning



© The Author(s) 2023. **Open Access** This article is licensed under a Creative Commons Attribution 4.0 International License (<https://creativecommons.org/licenses/by/4.0/>), which permits unrestricted use, sharing, adaptation, distribution and reproduction in any medium or format, for any purpose, even commercially, as long as you give appropriate credit to the original author(s) and the source, provide a link to the Creative Commons license, and indicate if changes were made.



INTRODUCTION

Since 1995, when Yaghi *et al.* reported the synthesis of coordination compounds from transition metal cobalt and rigid organic ligand, metal-organic frameworks (MOFs) have attracted much attention as a new type of organic-inorganic hybrid porous material^[1-9]. Subsequently, they synthesized the three-dimensional pore structure MOF-5 with Zn (II) and the rigid organic ligand terephthalic acid^[10]. This material is thermally stable and its backbone structure is maintained after the guest molecule is removed. Therefore, the researchers varied the length of the dicarboxylic acid ligand based on MOF-5 to achieve functionalization and size variation of the MOF with the same topology. As ligands continue to be expanded, so does the understanding of MOF. MOFs are inorganic nodes and organic ligands linked to form infinitely extended network structures with periodicities, also known as porous coordination polymers (PCPs)^[11,12]. Compared with conventional inorganic polymers, MOFs can be rationally designed and tuned by selecting specific metal nodes and organic linkers, and exhibit characteristics of well-aligned structures, high specific surface area, large-sized porosity, unsaturated coordination sites and ligand structural diversity^[13,14]. The unique structures and properties of MOFs make them promising for a wide range of applications in various fields, including gas storage and separation, catalysis, ion exchange, drug delivery, as well as bio-sensors^[15-26].

Generally, up to date, MOFs-based materials have undergone a four-generation journey^[1]. The stability of first-generation MOFs is low and the structures of the MOFs tend to collapse easily due to the inseparable guest anions in the pore of the frameworks. Researchers have since developed second-generation MOFs materials based on the first generation with organic ligands containing mainly carboxyl groups. The second generation of MOFs has stable porosity, which compensates for the low stability of the first generation. The third-generation MOFs show framework flexibility and dynamics when exchanging guest or external stimuli, exhibiting various intelligent properties. For example, Dybtsev *et al.* have synthesized materials with a two-dimensional structure using zinc nitrate and terephthalic acid, and the structure of the MOFs shows a certain dynamic behavior after exchanging the ligand, and the pore channels in the MOFs could keep changing accordingly under the influence of light or different solvent guest molecules^[27]. The fourth generation of MOFs, also called post-processing MOFs, is accompanied by postsynthetic modifications of MOFs and can be applied in various fields^[28]. In principle, the synthetic strategies and applications of third- and fourth-generation MOFs were extensively explored.

In recent years, with the number of reported MOFs increasing rapidly, the synthetic strategies of MOFs have been widely developed. Recently, the design and controllable synthesis of MOF nanocrystals with different phases and morphologies by tailoring thermodynamic and kinetic processes has become a hot topic^[29-33]. For example, typical kinetic parameters are related to the activation energy, which reflects the effect of temperature on the reaction rate. Different reaction temperatures, solvents, time, concentrations, pH values and molar ratios of metal ions to ligands can all have an effect on the growth of MOFs. Growth factors also influence the pore size of the structure, leaving one and mostly two-dimensional structures that are not porous, and only three-dimensional and a small number of two-dimensional have porosity. So far, most of the reported MOFs are microporous (pore size < 2 nm). Micropores are necessary to ensure the interaction between substrate and MOFs, the stability of small-sized actives and size selectivity^[34]. Therefore, in order to construct MOF crystals with desired sizes and thus achieve structures with the target function, understanding and controlling the crystallization process of MOFs is critical^[35].

Essentially, the synthetic strategies of MOFs can be roughly divided into physical (microwave, ultrasound, ball milling, *etc.*) and chemical methods (electrochemistry, mechanochemistry, etching, *etc.*). Based on the morphology, MOFs can be classified according to their morphological structures into one-dimensional (1D)

chains, two-dimensional (2D) layers and three-dimensional (3D) framework structures^[36]. In view of the diversity of synthesis strategies, this article will focus on the macro-morphology of MOF crystals in terms of classification into 1D, 2D and 3D MOFs materials. [Table 1](#) shows the advantages and limitations of each dimensional MOFs. When preparing MOFs with special morphologies or crystal facets, thermodynamical and kinetic adjustments are often adopted in the synthetic processes, which is conducive to enhancing the performances, for example, recrystallization, interface synthesis and self-assembly. The aim of this review is to promote a deeper understanding of metal-organic skeletal materials, to grasp their structural characteristics and to increase research efforts on these materials. In this review, we summarize and provide an overview of the synthesis of metal-organic framework materials from multi-dimensional perspectives by combining physical and chemical methods, introduce various widely used and relatively novel synthetic methods in the past 20 years, and describe the preparation of some typical MOF-based hybrids and their applications, as shown in [Scheme 1](#), in which the relationship between the thermodynamical and kinetic adjustments and the structural control of MOFs will be emphasized.

The hydrothermal/solvothermal method is one of the classical synthetic strategies due to its ease of operation. Metal salts and ligands are added to water or organic solutions and then encapsulated in a reactor and heated to a certain temperature, often resulting in materials with excellent physicochemical properties^[37-46]. The synergy between temperature, pressure and solvent allows the metal salts and ligands to begin to participate in the reaction. The high temperature and pressure environment in the reactor also provides a powerful aid to crystal nucleation growth. Note that various surfactants or covering agents are often introduced into the reaction to control the morphology and size of the MOFs. [Table 2](#) summarizes some recent examples of hydrothermal/solvothermal synthesis of MOFs. In addition to hydrothermal/solvothermal methods, many synthetic strategies have been explored, but rarely generalized. Solid-state mechanochemical methods require no solvents, low temperature and only mechanized stress^[55]. A common solid-state synthesis method refers to mechanical grinding, where MOFs are formed by mixing all components well and reacting directly. Katsenis *et al.* worked on the final synthesis of ZIF-8 from ZnO and 2-methylimidazole in 2017 using mechanochemical methods^[56]. The method is cost-saving and environmentally friendly. Nevertheless, mechanochemical methods often make it difficult to isolate crystals suitable for X-ray single-crystal diffraction. This paper will focus on other typical synthetic methods as well as newer methods that have been developed in recent years. Last but not least, challenges and promising developments in the field of MOF are also discussed.

SYNTHESIS OF MOFS WITH 1D STRUCTURES (1D MOFS)

1D MOFs can be classified into nanowires, nanotubes, nanorods and nanoribbons. In the past 20 years, 1D MOFs have shown promising applications in electronics, photonics, biology and energy storage and conversion due to their unique anisotropy^[57-60]. 1D MOFs create opportunities for new applications of MOFs due to their unique combination of both nanostructured advantages and porous properties. However, research on 1D MOFs is still in its infancy and is still mainly focused on the development of new synthetic methods. As shown in [Figure 1](#), the most common chemical synthesis methods can be classified into template and template-free strategies.

Template strategies

Assembling nanoparticles into one-dimensional nanostructures through nanoparticles is an emerging research area over the years, which not only builds a bridge between the nanoscale and the micron-scale, but also offers endless applications in optoelectronic engineering, biotechnology, magnetic components and more^[61]. In contrast, for 1D MOFs, template methods are one of the effective methods for synthesizing size- and composition-controlled nanomaterials^[62-64]. Template strategies can be further divided into hard template methods and sacrificial template methods.

Table 1. Comparison of MOFs in various morphological dimensions

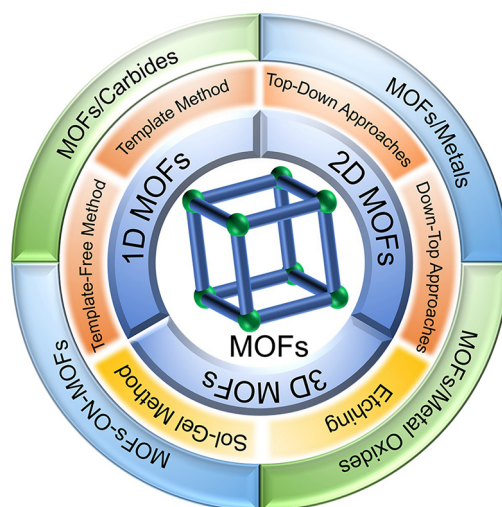
Morphology	1D MOFs	2D MOFs	3D MOFs
Strength	High aspect ratios Excellent flexibility	Large surface areas Stable mechanical properties	High porosity Frame stability
Limitation	Structural instability Poor regulation	Uneven sizes Uncontrollable thickness	Micronization difficulties

MOFs: Metal-organic frameworks; 1D: one-dimensional; 2D: two-dimensional; 3D: three-dimensional.

Table 2. Examples of hydrothermal/solvothermal synthesis of MOFs

MOF	Feature	Synthesis methods	Synthesis conditions	Refs.
MIL-47(V)	1D Micro Rod	Solvothermal	180 °C 20 h	[46]
MIL-53(Fe)	1D Micro Rod	Solvothermal	150 °C 6 h	[47]
MIL-110(Al)	1D Nanotube	Hydrothermal reaction	90 °C 3 h	[48]
Fe-MOF	2D Nanobelt	Solvothermal	110 °C 24 h	[45]
Ni-MOF	2D Nanosheets	Solvothermal	80 °C 18 h	[40]
Zr-MOF	2D Nanosheets	Solvothermal	120 °C 24 h	[49]
Cu-TCPP	2D Nanosheets	Solvothermal	80 °C 3 h	[50]
Cu-MOF	2D Nanosheets	Hydrothermal reaction	140 °C 72 h	[51]
Co-MOF	3D Bulk	Solvothermal	130 °C 3 d	[43]
MFM-303 (Al)	3D Needle Bar	Hydrothermal reaction	210 °C 3 d	[52]
MUT-4(Zn)	3D Columnar	Solvothermal	120 °C 24 h	[44]
UiO-68-TZDC	3D Octahedron	Solvothermal	100 °C 72 h	[41]
MIL-101(Cr)	3D Octahedron	Hydrothermal reaction	180 °C 15 h	[39]
NNU-29	3D Bulk	Hydrothermal reaction	180 °C 72 h	[53]
NiCo-MOFs	3D Bulk	Solvothermal	140 °C 48 h	[54]

MOFs: Metal-organic frameworks; 1D: one-dimensional; 2D: two-dimensional; 3D: three-dimensional.



Scheme 1. The main synthetic strategies for MOFs-based materials. MOFs: Metal-organic frameworks; 1D: one-dimensional; 2D: two-dimensional; 3D: three-dimensional.

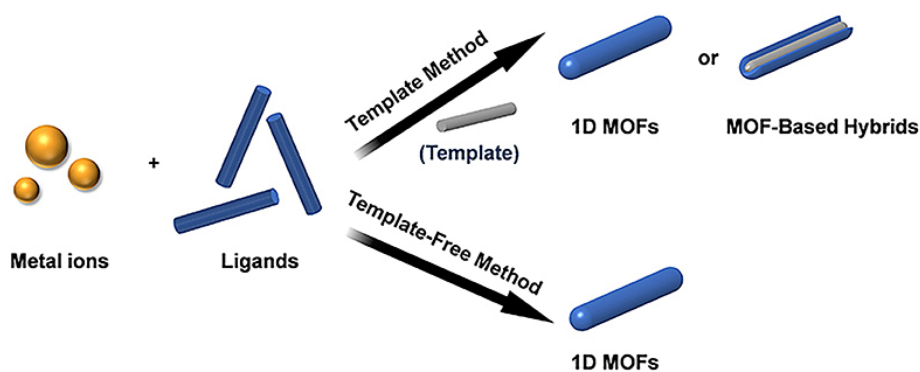


Figure 1. Schematic diagram of two illustrative strategies for the preparation of 1D MOFs. MOFs: Metal-organic frameworks; 1D: one-dimensional.

Hard template method

The hard template method induces the nucleation and growth of MOFs nanostructures on the surface of template materials, such as graphene oxide, Te nanowires and ZnO nanorods, to form MOFs-based one-dimensional hybrid materials^[65–69]. The morphology of the material and the pore size is modulated with templates. Back in 2010, Jahan *et al.* had successfully synthesized unusual MOFs nanowires by using benzoic acid functionalized graphene oxide (BFG) as a structurally oriented hard template to induce nucleation of MOF-5 on its surface and growth along the [220] crystallographic plane direction^[70]. In order to synthesize MOF/BFG complexes, they tried adding different amounts of BFG (1, 4 and 5 wt%) as the precursors and eventually found that the diameter of the nanowires closely correlated with the lateral size of the functionalized graphene. In 2012, Pachfule *et al.* speculated that the nano-hollow structure might have special encapsulation capabilities due to its constraint^[65]. Subsequently, highly crystalline MOFs were grown in the inner cavities of one-dimensional carbon nanofibers (CNF) using pre-synthesized CNF as templates with reasonable experimental parameters. The analysis of the powder X-ray diffraction data indicated that the MOF phase was the thermodynamically unstable MOF-2 [Zn(bdc)], rather than the expected MOF-5 [Zn₄O(bdc)₃], and high-resolution transmission electron microscopy of the MOF-2@CNF composite also clearly showed MOF-2 nanocrystals stacked in the inner cavities of the one-dimensional carbon nanofibers. To further explore the crystal growth, they functionalized the CNF, introduced functional groups and then performed MOF synthesis, and found that the MOF-2 crystals grew on the outer surface of the CNF, indicating the importance of surface functionalization of carbon templates. Commercial trace-etched polycarbonate (PCTE) membranes have also been widely used as hard templates for the synthesis of inorganic nanowires. Caddeo *et al.* then used polycarbonate (PC) templates to deposit Cu nanowires, which were then converted to Cu₃(BTC)₂ MOF nanowires by electrochemical oxidation by injecting an organic linker solution into the template^[71]. Since the MOF is formed inside the template, the shape is consistent with the host nanochannel and MOF nanowires with diameters between 80 and 260 nm can be obtained. In 2018, Arbulu *et al.* used PCTE to synthesize continuous 1D ZIF-8^[72]. ZIF-8 nanomorphology is related to Zn metal salt concentration and PCTE membrane pore size [Figure 2A–C].

In general, the development of applications for MOFs is strongly influenced by the superstructure. With the aid of templates, MOFs can be assembled into superstructures in solvents, but templates for highly homogeneous 1D nanomaterials are not available and the synthesis of superstructures is limited as a result. Recently, Li *et al.* reported the synthesis of MOF materials with 1D nanofiber morphology using

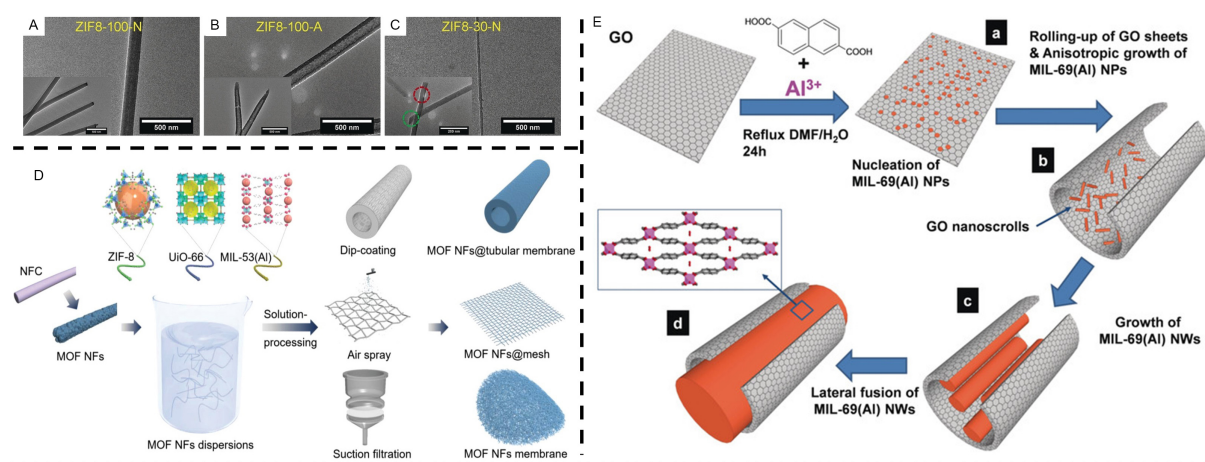


Figure 2. (A-C) TEM images of different 1D ZIF-100 nanostructures. (D) Schematic diagram of the NFC template for the synthesis of MOF nanofibers. (E) Mechanistic scheme summarizing the principal phases of the formation of MIL-69(Al) NWs. (A-C) Adapted with permission^[72]. Copyright 2018, John Wiley and Sons. (D) Adapted with permission^[73]. Copyright 2022, John Wiley and Sons. (E) Adapted with permission^[76]. Copyright 2020, John Wiley and Sons. MOFs: Metal-organic frameworks; 1D: one-dimensional; NFC: nanofibrillated cellulose; NWs: nanowires; NPs: nanoparticles.

nanofibrillated cellulose (NFC) as a template^[73]. The synthesized core-shell nanofibrous materials have the advantages of a high aspect ratio, great flexibility, good dispersion and ease of large-scale assembly. The prepared ZIF-8, UiO-66 and MIL-53 (Al) nanofibers have high aspect ratios of over 100 and can be used to assemble into a variety of macroscopic materials [Figure 2D]. NFC is considered to be a good amphiphilic material due to the presence of both hydrophilic and hydrophobic alkane fractions, and can be dispersed in both polar aprotic organic solvents and non-polar solvents alone. This unique property makes NFC an ideal template for the synthesis of 1D flexible MOF nanofibers. The synthetic strategy that uses solution treatment is expected to ensure the production of MOF nanofibers at scale and promote the industrialization of MOFs.

It is well known that low-symmetry nanocrystals (NCs) are important in areas such as catalysis, sensing and electronics^[74,75]. While the majority of MOF nanoparticles (NPs) are obtained as polycrystalline powders or spherical nanocrystals (NCs), and only a very few one-dimensional anisotropic MOF nanostructures were identified. In 2020, Muschi *et al.* formulated an original approach to synthesize MIL-69 (Al) nanowires (NWs) grown along the [001] crystal plane direction by using graphene oxide as a template modifier^[76]. Graphene oxide nanowires are one-dimensional carbon materials formed by rolling graphene oxide sheets from one side or edge into Archimedean-type helices^[77]. Inspired by this, they exploited the potential rolling of graphene oxide and the following anisotropic growth of MIL-69 (Al) in the inner cavities of graphene oxide nanoscrolls to contain the formation of single-crystal MOFs [Figure 2E]. The anisotropic growth is motivated by the interaction forces between the MIL-69 (Al) NPs and the hydroxyl and carboxyl functional groups of the graphene oxide.

Sacrificial template method

The sacrificial template method is more attractive than the hard template method, which can easily remove the template but hardly triggers the collapse of the 1D MOF structures^[78]. This is a process in which a number of 1D metal oxides or hydroxides are used as templates for their own *in-situ* dissolved metal ions properties, ultimately inducing the formation of 1D MOFs. In recent years, metal nanoparticles (MNPs) doped in MOFs have been widely used in the field of multiphase catalysis^[79-81]. However, the key to the catalytic efficiency of MNPs@MOFs lies in how to shorten the distance between the reactants and the active

sites to achieve this process, which means that the spatial distribution of MNPs in MOFs needs to be precisely tuned. In 2017, Yang *et al.* employed spherical metal oxides both as a support for MNPs and as a sacrificial template for growing MOFs to achieve precise encapsulation of controlled positioning of MNPs in 1D MOFs [Figure 3A]^[82]. Initially, the MNPs were first loaded onto the metal oxides, and the organic ligands in solution were coordinated with the metal ions in oxides, and the MNPs were then encapsulated into the MOF crystals [Figure 3B-E]. The concentration of the organic ligand regulates the spatial position of the MNPs in the MOFs. When the concentration of organic ligands is high, the nucleation of MOFs follows a “dissolution precipitation mechanism”^[83,84]. As increasing the concentration of $\text{Zn}(\text{Hmim})_4^{2+}$, ZIF-8 crystals were slowly deposited on the metal oxide surface to form a polycrystalline layer, while MNPs were encapsulated between the interface of ZnO and ZIF-8 as they remained on the metal oxide surface. When the concentration of organic ligands is low, the conversion follows a “local conversion mechanism” and the MNPs are immobilized on the surface of the MOFs^[85]. It was found that the method was applicable to a wide range of MNPs and MOFs, and that the synthesized MNPs@MOFs had significantly enhanced catalytic activity. In 2018, Li *et al.* also used metal oxides encapsulated into ZIF-8 to achieve good catalytic performance^[86].

Among all nanostructured materials, nanotubes have attracted a particular attraction due to the characteristic application properties shown in adsorption, catalysis and sensing due to the fact that these fascinating tubular nanostructures provide three different contact regions, i.e., the interior, the exterior surface as well as the ends^[87-90]. Nanotube-structured electrode materials are capable of enhancing electrochemical properties not possible for conventional bulk materials, thanks to higher surface areas and shorter diffusion paths that enhance the attraction for free electrons^[91-95]. Among the various structural designs, hierarchical tubular structures (HTSs) have received considerable attention for their advantages such as pore volume for expanding the electrode/electrolyte contact area. In 2016, Chen *et al.* devised a multi-step strategy to use zeolite imidazolate framework (ZIF-67) as a single source of carbon and cobalt in the resultant composites through a controlled chemical transformation, and a two-step annealing process to obtain a layered CNT/ Co_3O_4 hollow tubular structure, which has excellent as an anode material for Li-ion batteries^[96]. They selected electrospun polyacrylonitrile (PAN)-cobalt acetate [$\text{Co}(\text{Ac})_2$] composite nanofibers as a bifunctional template and made use of the strong coordination of 2-methylimidazole and the cobalt source on the template, resulting in the growth of uniform ZIF-67 nanocrystal shells on the nanofibers [Figure 3F-I]. After DMF treatment, the nanofibers were removed to form tubular structures. In the final step, carbon nanotubes are retained after annealing treatment, yielding layered CNT/ Co_3O_4 microtubes. The transformation from cobalt solid nanoparticles to Co_3O_4 hollow particles can be attributed to the Kirkendall effect during the annealing process^[97]. In the same year, Liu *et al.* used Cu_2O as a template and successfully converted pristine nanowires into layered HKUST-1 nanotubes by immersing Cu_2O nanowires in a mixture of acetic acid, ethanol and $\text{H}_3\text{BTC}/\text{DMA}$ using the characteristics of acetic acid to dissolve Cu_2O ^[98]. They have experimentally found that the solvent group is critical to the growth of nanomaterials and that the solvent plays an important role in the balance between the dissolution rate, nucleation rate and crystal growth of copper ions.

Electrospinning

Electrospinning has been widely used as a method for preparing nanowire fibers due to the mature synthetic technology and low cost^[99,100]. A simple electrostatic spinning device consists of three main components [Figure 4A], a high-voltage power supply, a capillary/syringe with a needle and a grounded collector^[101]. The choice of precursor solution is also one of the keys, with the viscosity of the precursor determining the size and morphology of the fiber materials^[102,103]. The mechanism of electrospinning is predicated on the ejection and elongation of a molten viscous polymer under a high-voltage electric field, followed by solidification at

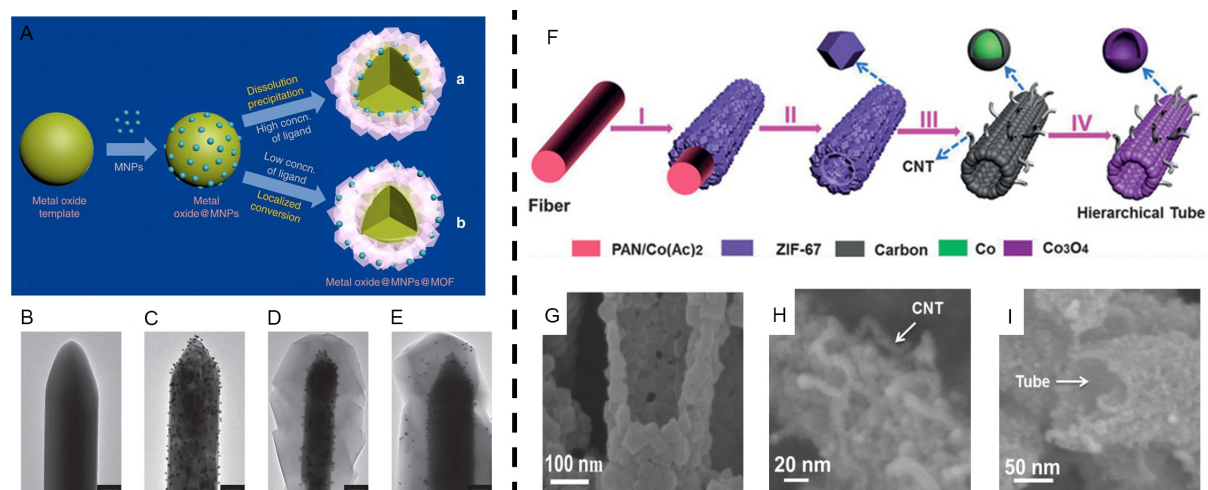


Figure 3. (A) Spatial localization of MNPs in MOF crystals regulated by template-sacrifice method. (B-E) TEM images of ZnO NRs (B), ZnO NRs@Au (C) and (D and E) ZnO NRs@Au@ZIF-8 composites with Au NPs at different locations: (D) inside and (E) near to the surface of ZIF-8. (F) Formation of the hierarchical CNT/Co₃O₄ microtubes. (G-I) FESEM of the synthesized ZIF-67 microtubes. (A-E) Adapted with permission^[82]. Copyright 2017, Springer Nature. (F-I) Adapted with permission^[96]. Copyright 2016, John Wiley and Sons. MOFs: Metal-organic frameworks; MNPs: metal nanoparticles; NPs: nanoparticles; FESEM: field emission scanning electron microscopy.

the collector in the form of a stream of charged liquid. There are two main routes to forming MOF-polymer nanofiber structures via electrostatic spinning, namely “direct electrostatic spinning” and “surface modification”, both of which can be converted into MOF nanofiber derivatives by post-treatment^[104]. In the direct electrostatic spinning method, a slurry containing MOF particles is mixed with polymers and directly electrospun into nanofiber complexes^[105-107]. However, this direct electrostatic spinning method is not suitable for applications pursuing a material pore perspective, due to the fact that the slurry of mixed polymers can clog the pores inside the MOFs. The second method of generating complexes is reached by growing MOF particles *in situ* on the surface of nanofibers^[108,109]. This *in situ* growth mode maintains the advantages of the porosity and high specific surface area of MOFs and can also have good applications in the field of adsorption. The “surface modification” method has become the preferred method for electrostatic spinning in recent years, despite its high experimental requirements. Researchers can design the composition and morphology of the material by doping it with metals or other small molecules after the electrostatic spinning process, thereby expanding the diversity of electrostatically spun nanofibers. In terms of energy materials, the high structural stability of electrostatically spin-synthesized 1D MOFs effectively prevents structural expansion and collapse of the electrode material. The 1D structure also improves the material’s distance for charge transport and ion diffusion during discharge. Electrospinning techniques effectively inhibit the aggregation of MOF particles and improve the utilization of active substances by building a network structure; therefore, they are also considered an effective way to expand the range of practical applications of MOFs^[110-112].

In 2017, Chen *et al.* generated hollow particle-based nitrogen-doped carbon nanofibers (HPCNFs-N) [Figure 4B] by encapsulating ultra-fine ZIF-8 particles into electrospun polyacrylonitrile (PAN) and subsequently carbonizing them, which were found to have strong specific capacitance as supercapacitor materials^[113]. Field emission scanning electron microscopy (FESEM) images revealed that the PAN/ZIF-8 composite nanofibers were directly homogeneous [Figure 4C and D] and after nitrogen heat treatment, the HPCNFs-N samples maintained their previous morphology without significant changes [Figure 4E and F]. In 2020, Huang *et al.* also synthesized polyacrylonitrile-covered ZIF-8@PAN composites directly using

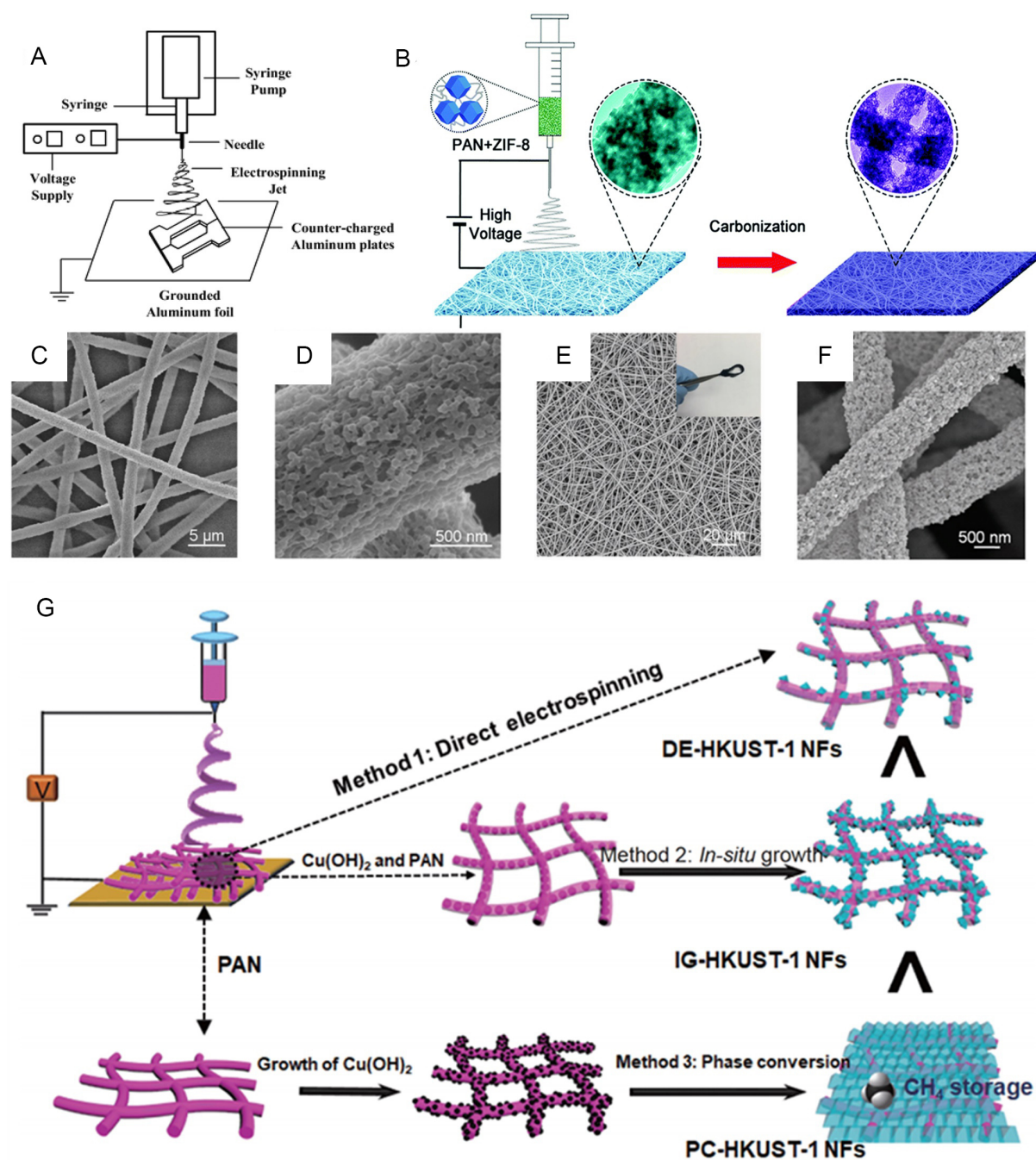


Figure 4. (A) Schematic diagram of the electrostatic spinning unit. (B) The synthesis of hollow particle-based N-doped carbon nanofibers (HPCNFs-N). (C and D) FESEM and TEM images of the PAN/ZIF-8 composite nanofibers. (E and F) FESEM and TEM images of the HPCNFs-N sample. (G) Diagrammatic representation of the different synthetic routes for the structuring of HKUST-1 into MOF NFs. (A) Adapted with permission^[101]. Copyright 2007, American Chemical Society. (B-F) Adapted with permission^[113]. Copyright 2017, The Royal Society of Chemistry. (G) Adapted with permission^[115]. Copyright 2021, Springer Nature. MOFs: Metal-organic frameworks; FESEM: field emission scanning electron microscopy; PAN: polyacrylonitrile; NFs: nanofibers.

electrospinning^[114]. The yolk-shell Sb@C nanoboxes embedded in carbon nanofibers (Sb@CNFs) were prepared after a combination of ion exchange and thermal reduction treatments, and the electrochemical mechanism of the Sb@CNFs electrodes was investigated using *in-situ* TEM characterization techniques. The

direct electrospinning method inevitably blocks the pores of MOFs by polymers, while the phase conversion method bypasses these problems. Dou *et al.* then combined the electrostatic spinning and phase conversion methods to fabricate highly structured MOF nanofibers for methane storage applications^[115]. The surfaces of polyacrylonitrile nanofibers (PAN NFs) were pretreated using $\text{Cu}(\text{OH})_2$, followed by phase conversion to HKUST-1 crystals [Figure 4G]. Compared to direct electrospinning, this conversion method results in a higher loading of MOFs on PAN NFs substrates.

Template-free method

The synthesis of 1D MOF nanomaterials by a template-free method is often expected to produce single-crystalline one-dimensional MOF.

Modifiers-induced growth method

For a long time, scientists have been working on reducing the size of MOFs crystals to the nanoscale without changing the properties of the MOFs crystals themselves and investigating the correlation between the porous properties of the nanocrystals and the interfacial structure. The direct synthesis of 1D MOFs via metal precursors and organic ligands is more difficult and most are usually obtained in alcoholic solvents or ethanol/water mixtures^[116,117]. Over the years, ligand-modulated synthesis of MOFs via monocarboxylic acids, organic bases, dopamine and amphiphilic copolymers as modulators has also been reported^[118-124]. It is important to understand the crystal growth of metal framework materials, and the modulation method involves the use of molecules that are structurally similar to the ligand and a weaker coordination affinity to the metal clusters to compete with the ligand and thus regulate the coordination equilibrium of the crystal morphology growth of MOFs. When the coordination equilibrium between the metal ion and the organic linker is altered, the crystal size, morphology and crystallinity of the MOFs can be controlled^[125-127]. The relatively weak interactions between ligand bonds dominate the assembly process of MOFs and also lead to the formation of crystals. In 2009, Tsuruoka *et al.* used a simple and straightforward method to modulate the coordination equilibrium by adding a modulator with the same chemical function as the linker to the reaction system to enhance the one-dimensional anisotropic fusion of nanocrystals by impeding the coordination interactions between the metal ions and the organic linker^[128]. They synthesized one-dimensional $[\text{Cu}_2(\text{ndc})_2(\text{dabco})]$ nanorods (ndc = 1,4-naphthalene dicarboxylate; dabco = 1,4-diazabicyclo [2.2.2] octane) using acetic acid as a modifier. It was found that the increase in acetic acid concentration significantly inhibited the growth of Cu-NDC in the [100] direction, prompting eventual growth along the [001] direction to form nanorods. In 2016, Pachfule *et al.* successfully synthesized MOF-74-Rod at room temperature using a unique modulator-assisted approach to stabilize the active metal sites on the surface of MOF crystals by introducing salicylic acid modulators into the system to guide the growth of MOF in rod-like morphology [Figure 5A]^[129]. They then used KOH-assisted sonication, where K^+ was inserted into the carbon nanorods in a disordered stack during solution-based sonication, and again during subsequent heat treatment, where the K^+ containing nanorods were unfolded to form a nanoribbon structure. Further acoustic treatment and thermal activation of the rod-like MOF could open up new avenues for the efficient production of one- and two-dimensional carbon materials. Conventional acoustic treatment is ultrasonication, which relies primarily on the transmission of acoustic waves through a medium such as a solution, causing oscillation of the medium particles. In contrast, non-traditional surface acoustic waves (SAWs) are electromechanical waves with nano- or sub-nano-amplitudes that are accompanied by changes in the electric field along the propagation path^[130]. SAWs combine acoustic and electric fields and offer advantages in controlling the thickness of stripped nanosheets. By 2019, they had also synthesized chestnut-shell spherical superstructure metal-organic framework nanorods (SS-MOFNR) by hydrothermal transformation using urea as a modulator^[131]. In control experiments without the addition of urea, the coexistence of unassembled MOF nanorods and partially spherical superstructures was observed using SEM. In contrast, the addition of urea resulted in the formation of morphologically homogeneous and

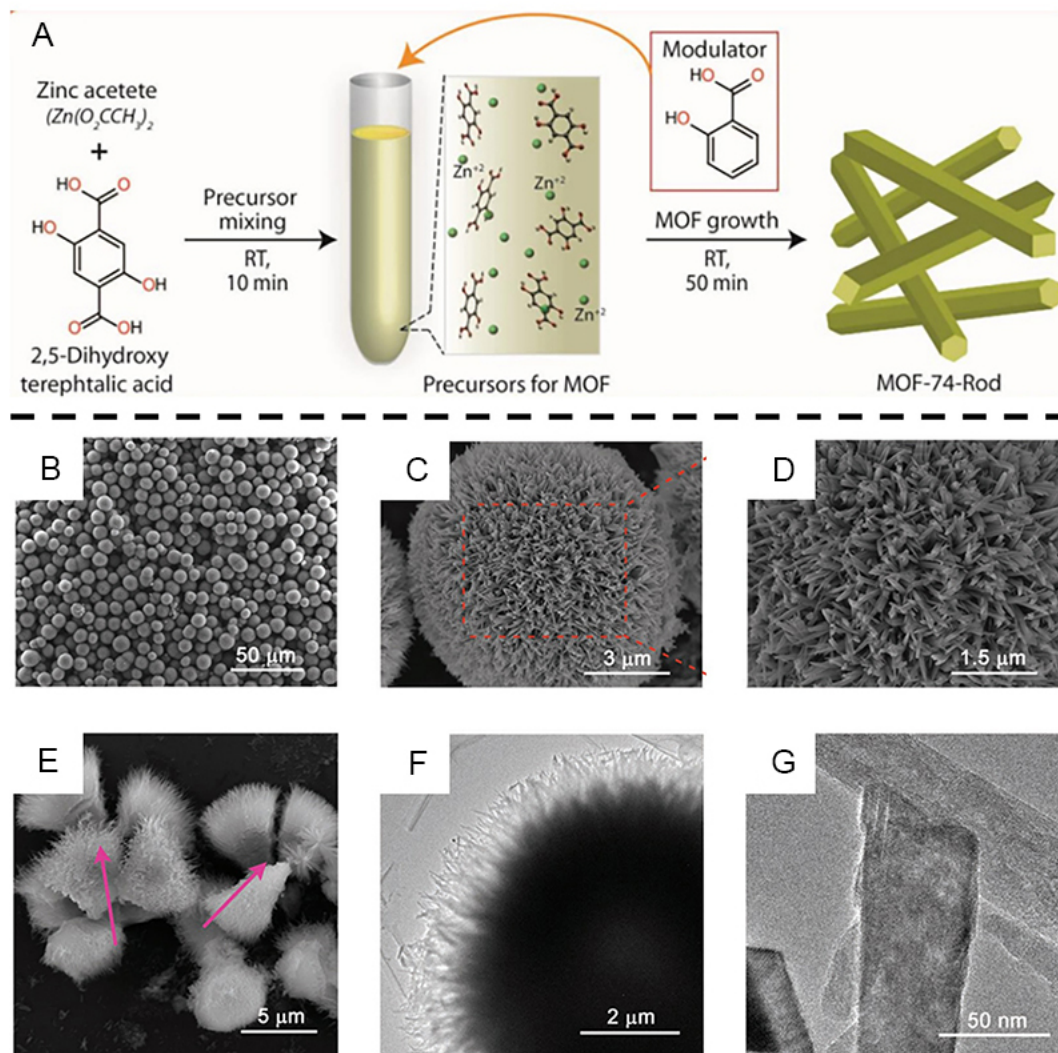


Figure 5. (A) Synthesis scheme for MOF-74-Rod. (B-D) SEM images of SS-MOFNR composed of 1D MOF nanorods. (E) SEM image of a fractured SS-MOFNR showing its internal hollow structure. (F and G) TEM images of SS-MOFNR. (A) Adapted with permission^[129]. Copyright 2016, Springer Nature. (B-G) Adapted with permission^[131]. Copyright 2019, John Wiley and Sons. MOFs: Metal-organic frameworks; SS-MOFNR: spherical superstructure metal-organic framework nanorods; 1D: one-dimensional.

highly crystalline SS-MOFNRs [Figure 5B-G]. By investigating the time-dependent process, it was found that with increasing time, Zn-MOF-74 NPs were first transformed into Zn-MOF-HT nanorods, and finally, micro-sized SS-MOFNRs were slowly assembled, a process that was transformed gradually. The screening of the solvent revealed that water as a solvent was favorable to the formation of 1D MOFs. SS-MOGNR also maintained its original morphology after carbonization with argon, and its performance as a carrier for the Pd immobilization catalyst was improved.

Phase transition method

The single-crystal-to-single-crystal (SCSC) conversion is an intriguing and essential process in chemistry and material science and is an important feature in the preparation of coordination polymers^[132-139]. Over the last few decades, much research demonstrated that SCSC conversions of MOFs could be triggered by external stimuli, including physical and chemical processes, such as temperature, pressure, gas adsorption, etc.^[140-145]. Through these stimuli, the number of ligands and dimensions can be changed, such as 0D to

1D/2D and 1D to 2D/3D, leading to the synthesis of MOFs^[146]. In 2019, Han *et al.* achieved the transition from QUST-81 to QUST-82 through thermodynamically controlled crystal phase transitions in physical stimuli^[147]. Synthesis of QUST-81 crystals at 100 °C, followed by high-temperature heating to 120 °C in the mother liquor again, enables the formation of new stable QUST-82 crystals [Figure 6A and B]. In contrast, there is no dissolution or recrystallization of the single crystal during this process. Single crystal X-ray diffraction (SCXRD) showed that the coordination environment of QUST-82 changed during the crystalline phase transformation, with new coordination bonds forming. The formation of new bonds is also indirectly evidenced by the color of the reactants, with QUST-81 crystals showing a color change from dark green to colorless back to green, indicating the presence of a reduction of Cu²⁺ to Cu⁺ followed by re-oxidation to Cu²⁺ in air. The heterometallic MOF QUST-82 serves as an excellent adsorbent for the elimination of organosulfur. However, there are not many studies on chemical stimuli with the same metal but different coordination environments causing the SCSC transition of MOFs. In particular, there are few discussions on the crystalline transformation of 1D MOFs. Chen *et al.* did advance research^[148]. Starting with 0D Cu nanoparticles [MOP-1, Cu₂₄(m-BDC)₂₄(DMF)₁₄(H₂O)₁₀], they began to explore the effect of SCSC conversions induced by different organic ligands on the structure. They first synthesized 0D rhombic MOP-1 crystals, and SXR data showed them to be connected by a Cu₂(COO)₄ paddlewheel unit and two isophthalic acids (m-BDC). Two terminal ligands are attached to each unit, pointing to the exterior and center of the crystal, respectively. Compared to oxygen atoms, nitrogen atoms are less electronegative and give more electrons, making it easier to give electrons to form coordination bonds with metal salts. They then introduced 1-methylimidazole as a second ligand in an attempt to break the original coordination structure and transform the 0D structure. SXR data confirmed that the introduction of 1-methylimidazole resulted in the coordination of a Cu atom to two oxygen atoms in two m-BDCs and three nitrogen atoms in three 1-methylimidazoles to form a 1D chain structure. In 2017, Yang *et al.* synthesized 1D-NCPs (nanoscale coordination polymers) containing gambogic acid (GA) through a phase transfer strategy^[149]. PEGylated 1D-NCPs were constructed by mixing Mn ions and indocyanine green (ICG, a NIR dye) along with poly-l-histidine-PEG (pHis-PEG). First, metal ions and organic ligands self-assemble through coordination interactions in solution methanol to form a three-dimensional porous structure. It is then transferred into an aqueous solution, where the highly polar water molecules coordinate with the metal ions to form a one-dimensional nanofiber-like structure [Figure 6C]. An interesting phenomenon occurred when the reaction phase was transformed from an organic solvent to an aqueous solution, and the granular structure of the Mn-ICG@pHis-PEG NCPs nanoparticles slowly transformed into a fibrous one-dimensional structure over time. The authors found that the 3D porous structure becomes unstable due to the larger sulfonic acid anions of ICG. In strongly polar aqueous solutions, the Mn²⁺ coordination environment was changed and the hydrogen binding led to the formation of a 1D chain-like structure. For the change of the nanostructure from 3D to 1D, they performed molecular dynamics fitting computational simulations on Mn²⁺ according to the universal force field^[150]. The research found that in methanol, Mn²⁺ is coordinated to six sulfonate anions of organic ligand ICG. Concurrently, Mn²⁺ could also coordinate with the imidazole ring of poly-histidine-PEG. Poly-histidine-PEG relying on imidazole groups can strongly bind metal ions, but poly-histidine-PEG has only one imidazole ring and can only coordinate with one Mn²⁺. Therefore, when Mn²⁺ is coordinated with poly-histidine-PEG and the growth of MOF stops, 3D porous MOFs are formed. After the introduction of highly polar water molecules, the hydroxyl group can connect with the sulfonate anion to form a hydrogen bond to form a 1D structure. This simple crystal phase transfer strategy, which can be extended to various kinds of metal ions, is expected to open up new opportunities for the synthesis of MOFs.

Recrystallization

The anisotropic 1D MOF structures were prepared only by the template method and surfactant-assisted method, but the single-crystal nano MOFs or nano MOFs with high aspect ratios could not be

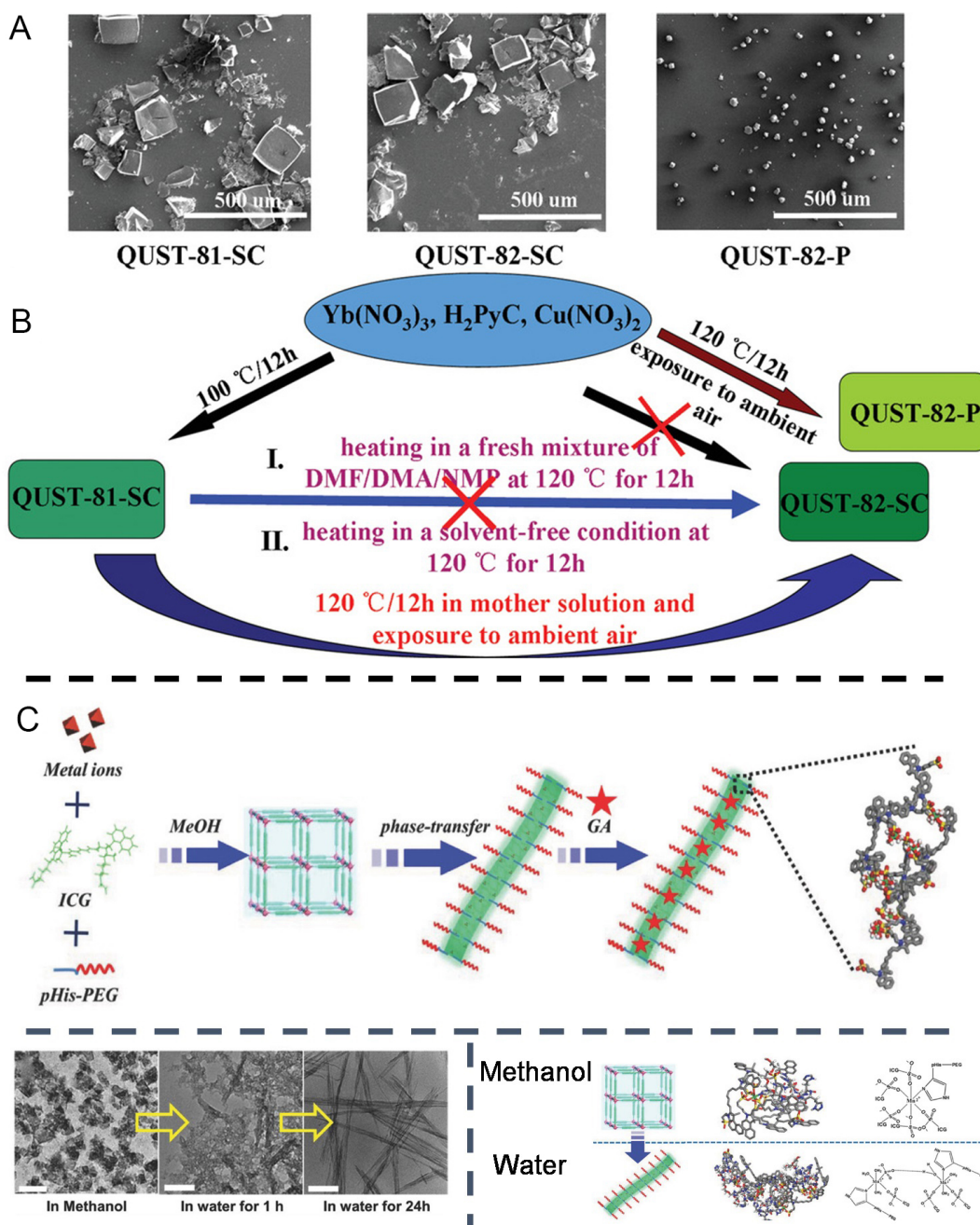


Figure 6. (A) SEM images of QUST-81-SC, QUST-82-SC, and QUST-82-P (SC = single crystal and P = powder). (B) The SC-SC phase transition process between QUST-81 and QUST-82. (C) Scheme to illustrate one-step synthesis of 1D PEGylated NCPs. (A and B) Adapted with permission^[147]. Copyright 2019, John Wiley and Sons. (C) Adapted with permission^[149]. Copyright 2017, John Wiley and Sons. NCPs: Nanoscale coordination polymers; 1D: one-dimensional.

prepared^[70,151]. Taking graphene oxide templates as an example, graphene oxide flakes are thinner and more brittle. The surface is modified with functional groups such as hydroxyl groups, which are easily chelated with metal ions, while the carboxyl groups are mainly distributed on the sides and edges of the flakes. It is therefore difficult to form MOFs with high aspect ratios using it as a structural guide for molecular assembly. Surfactant-assisted methods are often used to modulate the morphology and size of MOFs and are generally used as auxiliary agents. Moreover, surfactants are often classified as anionic, cationic,

amphiphilic and polymeric, and there is some skill in choosing which surfactant to use. Utilizing metal oxides as metal source precursors, the synthesis of MOFs phases by secondary crystallization has been reported previously^[152-154]. However, the synthesis of 1D MOF nanostructures with both single crystal and ultra-long morphologies is still a great challenge. Commonly, the kinetic process of crystallization influences the morphology of the crystals. Different precursors have different solubilities in specific solvents. Lower crystallization rates facilitate the formation of high aspect ratio, anisotropic MOFs. By 2018, Zou *et al.* had successfully fabricated the first high aspect ratio single-crystal Co-MOF nanotubes via an amorphous MOF-mediated recrystallization method (AMMRA)^[155]. To achieve anisotropic, ultra-long single crystals. They first prepared Co-MOF-74 nanoparticles (Co-MOF-74-NP) in the amorphous phase, exploiting the property that the amorphous Co-MOF-74-NP dissolves slightly in water and later recrystallized the Co-MOF-74-NP in aqueous solution (pH = 7.15) to produce ultra-long single crystals of Co-MOF-74 nanotubes (Co-MOF-74-NT) [Figure 7]. Compared to the low aspect ratio Co-MOF-74 micro-rod (Co-MOF-74-MR) (3-30 μm in length, 1-5 μm in diameter), the secondary crystallization method demonstrates the great advantage of nanosize control to achieve a homogeneous morphology of high aspect ratio nanotubes.

SYNTHESIS OF MOFS WITH 2D MORPHOLOGIES (2D MOFS)

Since 2004, when flake graphene was first prepared, various 2D materials have been explored with rapid development^[156]. The synthesis of 2D nanomaterials has gradually become a hot research topic. Studies have shown that almost all inorganic layered materials can be exfoliated into 2D materials^[157]. Moreover, similar to conventional 2D materials, 2D MOFs have a large aspect ratio, fully exposed active sites and fast diffusion channels, making them attractive for applications in electronics, energy conversion and storage and gas separation^[158-160]. Although there are many approaches to the synthesis of 2D MOFs materials to date, they can be broadly classified into two main categories: top-down and bottom-top strategies [Figure 8]. The first one mainly entails the delamination of bulk MOFs, and the latter is based on the direct synthesis of 2D MOFs crystals with high aspect ratios based on metal nodes and organic ligands^[161,162]. Here, we focus on some classical and new synthesis strategies in recent years.

Top-down approaches

As the name implies, the top-down strategy refers to the exfoliation method of the overall MOFs, which can easily overcome the weak interlayer interaction, mainly relying on the weak interaction between the layers of different 2D MOFs, e.g., van der Waals forces, - stacking, *etc.*^[163].

Micromechanical exfoliation

In 2004, Novoselov *et al.* succeeded in obtaining the first graphene with a perfect hexagonal honeycomb lattice by repeatedly peeling off highly oriented pyrolytic graphite using transparent tape, inspired by the use of tape to remove impurities from the surface of graphite while working on metal field effect transistors^[156]. Subsequently, this micromechanical peeling using tape was widely used in preparing 2D materials. Although 2D materials are mostly structures with weak van der Waals force interactions between layers stacked on top of each other, there are strong covalent bonds in each sheet and 2D materials have been gaining popularity in the field of covalent functionalization in recent years. Traditionally, surface modification is carried out after obtaining the ultrathin 2D material. However, due to the poor reactivity of the 2D MOFs, defects and incomplete functionalization were often performed after modification^[164]. In 2018, Lopez-Cabrelles *et al.* designed pre-synthetic ligand functionalization followed by micromechanical exfoliation to successfully prepare defect-free functionalized 2D MOF [Figure 9A and B]^[165]. The crystallinity and integrity of the exfoliated flakes were confirmed by projection electron microscopy and regional electron diffraction patterns [Figure 9C]. Although micromechanical peeling is easy to handle, it is

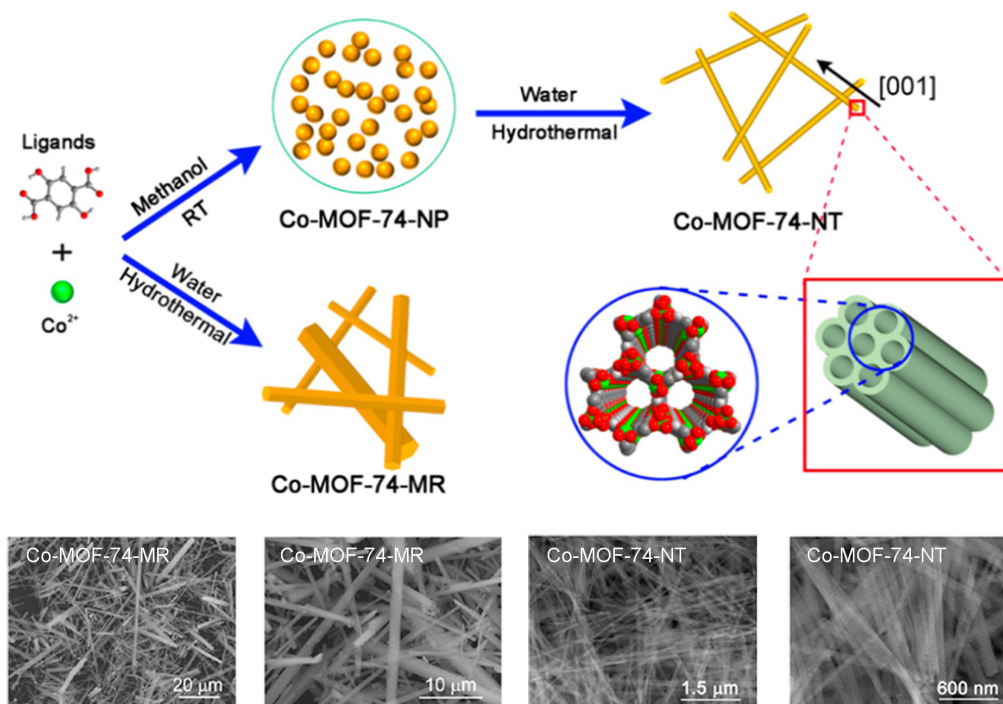


Figure 7. Synthesis protocols for Co-MOF-74-NT and Co-MOF-74-MR. Adapted with permission^[155]. Copyright 2018, American Chemical Society.

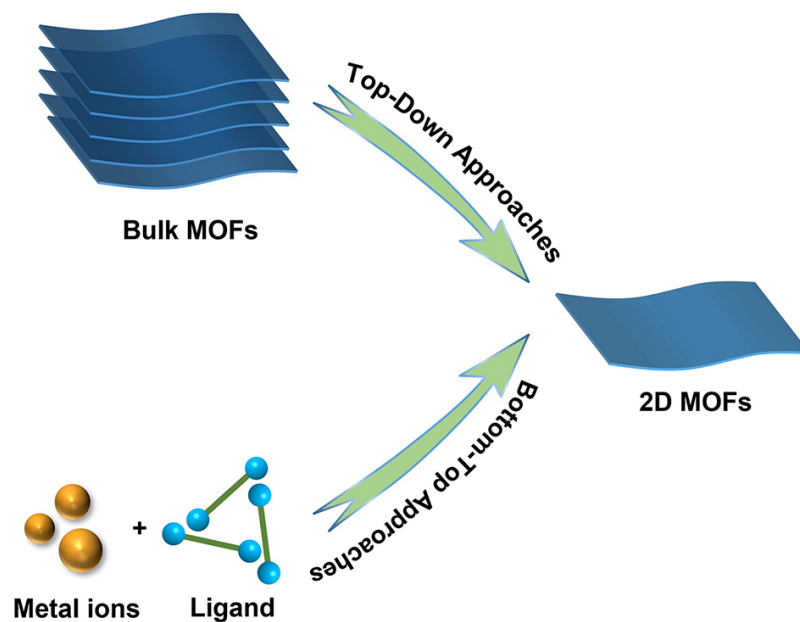


Figure 8. Schematic diagram of the synthesis strategy of 2D MOFs. MOFs: Metal-organic frameworks; 2D: two-dimensional.

less efficient. There is also a risk of disrupting the quantum structure of the material during stripping, resulting in stripping losses and affecting large-scale stripping.

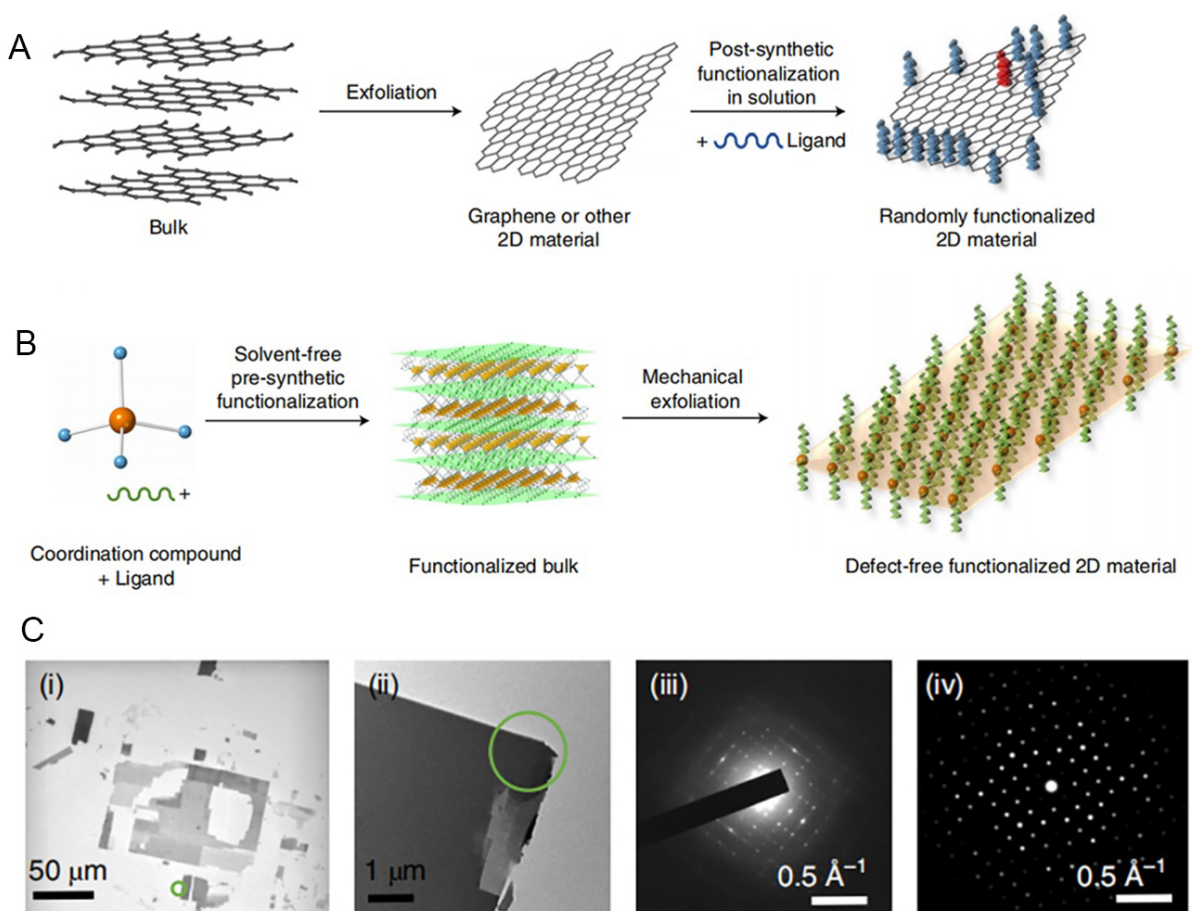


Figure 9. (A) A common strategy for the functionalization of 2D (inorganic) materials, consisting of two steps. (B) Pre-synthetic functionalization, where the functionalized block is first obtained prior to mechanical stripping, resulting in a quasi-perfect array of unaltered functional groups attached to the surface. (C) (i) Low magnification TEM image of a thin section, where the darker grey areas are associated with thicker sections; (ii-iv) The experimental SAED pattern corresponding to the [0 0 1] area axis (iii) was obtained for the selected area [surrounded by the green circle on the TEM image in (ii)] and fitted very well with the simulated SAED pattern (iv). (A-C) Adapted with permission^[165]. Copyright 2018, Springer Nature. 2D: Two-dimensional.

Ultrasonic stripping

As a new member of the 2D material family, 2D MOF materials, although still in the early stages of research, have larger lateral dimensions and ultra-thin thicknesses than other inorganic nanosheet materials, giving them a larger surface area than other inorganic nanosheet materials^[50,166,167]. For 2D MOF crystals, the different layers are attached by weak interactions, including hydrogen bonding and van der Waals forces. If the weak interactions are broken, monolayers of 2D-MOFs can be obtained. This idea has been implemented by a simple ultrasonic peeling method. Ultrasound waves are originated from acoustic cavitation within collapsing bubbles. After the solution has been processed by ultrasound, ultrasound energy accumulates in the oscillating bubbles and can generate high pressures and local temperatures^[168]. Small bubbles in a solution periodically undergo a process of creation, expansion and bursting. As the bubbles burst, energy is applied to the stripped precursor with a shock wave and tensile stresses are generated within the components of the precursor until the nanosheets are stripped. Ultrathin MOF nanosheets (UMOF NSs) can be prepared using the ultrasonic stripping strategy. UMOF NSs are characterized by the following features: nanoscale thickness allowing fast transport, superior electron transfer, ligand-unsaturated metal sites and exposed catalytically active surfaces^[169-171]. In 2016, Zhao *et al.*

then used ultrasonic exfoliation to prepare a series of UMOF NSs with ligand-unsaturated sites and high electrocatalytic activity towards OER at room temperature^[54]. It showed that the coordination-unsaturated metal atoms are the main active centers and this type of UMOF NSs is expected to be a strategy for synthesizing atomically accurate active catalysts.

At present, few systematic studies have been carried out on the exfoliation of bulk materials into ultrathin 2D nanosheets. For this reason, the discovery of new methods to facilitate the exfoliation of freestanding nanosheets is a necessary crystallographic challenge. Previously, the effect of the length of the suspended chains located in the MOF pores on the exfoliation has often been neglected. However, in 2019, Ashworth *et al.* attempted to increase the length of hydrophobic alkyl chains in functionalized ligands to explore their effect on ultrasonically exfoliated MOF materials [Figure 10A]^[172]. To assess the impact of chain length on the particle size of the exfoliated nanosheets, they carried out an analysis using atomic force microscopy (AFM). It was found that as the alkyl chain length increased by two methylene units, the thickness of the nanosheets became thinner but the lateral dimensions increased. The longer alkyl chain length resulted in a lower concentration of suspended material, indicating poorer solvent-nanosheet interaction, directly causing a lower average particle size dispersion for nanosheets that have longer alkyl chains [Figure 10B-G]. Nevertheless, longer alkyl additionally increases interlayer distances and diminishes other interlayer interactions and makes it easier to separate the layers during sonication, while at the same time, the solvent is instrumental in offsetting the energy loss to create new interfaces during the peeling process^[173,174]. In the same year, Tan *et al.* used metal clusters constructed from bulky hydrophobic ligands to prepare extremely thin, anisotropic UMOF NSs under ultrasonic exfoliation^[175]. Ultrasonic exfoliation method can well separate 3D porous layered hydrophobic TBSC-capped Zn_n clusters (H_nTBSC = *p*-*tert*-butylsulfonyl calix[4]arenes, Figure 11A-F). This study provides a new strategy for inducing stereoselectivity in organocatalysis, offering value for the development of UMOF NSs with applications in a variety of enantioselective applications. In 2020, Jian *et al.* reported the preparation of water-resistant monolayer porphyrin framework nanosheets using simple sonication and constructed water-stable Al-MOF films using ultrathin nanosheets^[176]. As shown in Figure 11G, the measured thickness of the Al-MOF nanosheets was approximately 1.9 nm, which is close to the theoretical thickness of 1.35 nm. Strictly speaking, increasing the ultrasonic time can improve the peel yield; regulating the power can affect the peel results. The ultrasonic stripping method ensures both morphology and property integrity, but it is inconvenient to control nanosheet thickness.

Chemical exfoliation

As well as micro-mechanical exfoliation and ultrasonication, chemical exfoliation with the selection of organic small molecules as insertion agents is commonly used for preparing UMOF NSs. In 2017, Ding *et al.* used a novel intercalation and chemical exfoliation method to obtain UMOF NSs (~1 nm) 2D MOF nanosheets from layered MOF crystals^[177]. The obtained UMOF NSs exhibit highly efficient multiphase photocatalytic performance compared to the corresponding layered MOFs bulk. They first designed new MOFs by inserting a chemically unstable bipyridyl ligand, 4,4'-dipyridyl disulfide (DPDS), into the layered MOF crystals and showed that the interlayer distance in the new MOF crystals expanded after inserting DPDS. Then, the nature of the trimethylphosphine (TMP) compound to reduce disulfide bonds was used to sever the DPDS, causing the interlayer forces in the volume-expanded layered MOF crystals to weaken and be exfoliated into ultra-thin nanosheets [Figure 12A]. This method is expected to be of great use in the synthesis of a variety of ultrathin 2D MOF nanosheets with specific structures and properties^[178]. In 2018, Huang *et al.* reported a strategy based on electrochemical/chemical exfoliation of columnar MOFs to selectively break interlayer coordination bonds and to prepare 2D MOFs that could facilitate the oxygen evolution reaction^[179]. Moreover, some functional groups interacting with H⁺ ions, such

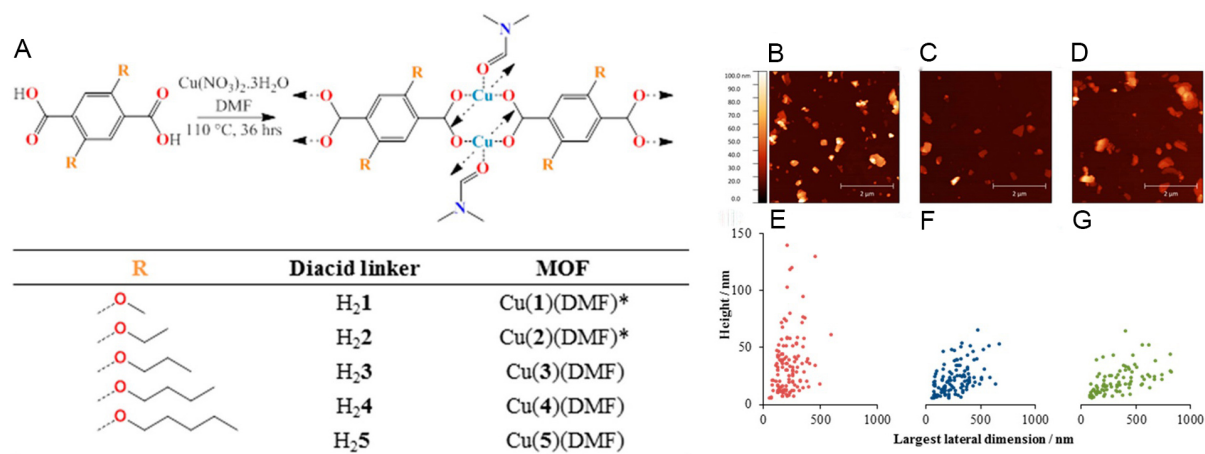


Figure 10. (A) General reaction scheme for the targeted synthesis of MOFs $[\text{Cu}(n)(\text{DMF})]_n$, where $n = 1-5$. Defines the R groups in the dicarboxylic acid ligand precursors H₂1 to H₂5. (B-D) AFM images of Cu(3), Cu(4) and Cu(5) nanosheets following ultrasonic stripping and centrifugation (1500 rpm for 1 h) in MeCN. (E-G) Scatterplot of correlation for MON dimensions. (A-G) Adapted with permission^[172]. Copyright 2019, American Chemical Society. MOFs: Metal-organic frameworks; AFM: atomic force microscopy; MON: MOF nanosheets.

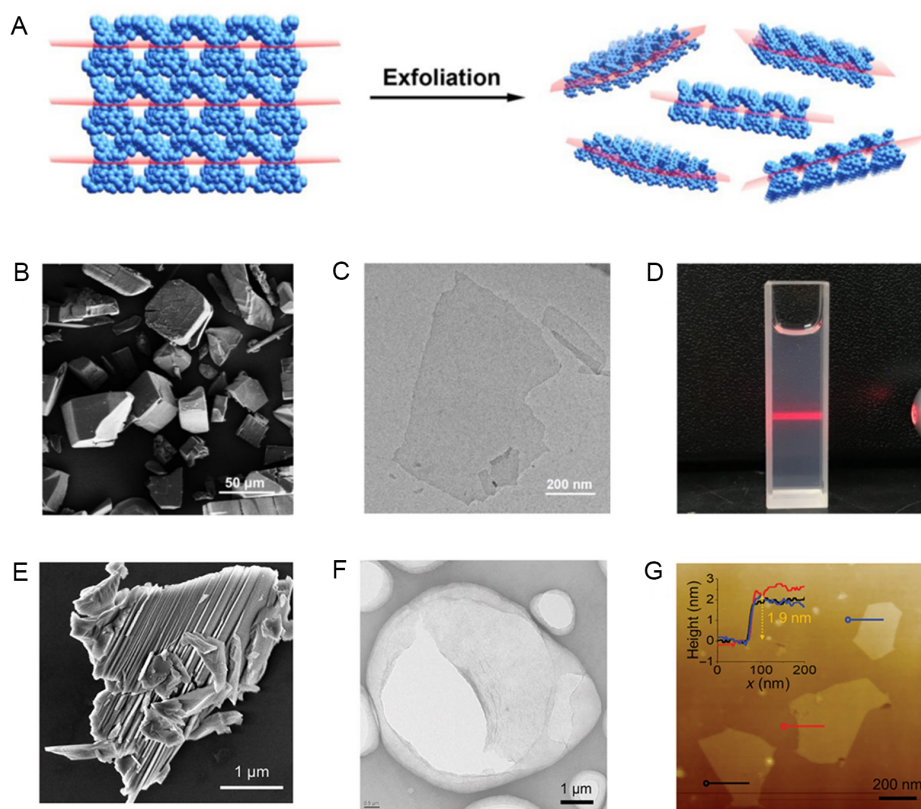


Figure 11. (A) Schematic diagram of exfoliation of MOF 1 blocks into UMOF NSs. (B) SEM image of MOF 1. (C) TEM image of MON 1. (D) MON 1 Tyndall effect of suspensions in *i*-PrOH. (E) SEM image of the Al-MOF bulk crystals. (F) TEM image of exfoliated Al-MOF nanosheets. (G) The AFM image of Al-MOF nanosheets on a silicon wafer, the inset shows the corresponding height profile. (A-D) Adapted with permission^[175]. Copyright 2019, American Chemical Society. (E-G) Adapted with permission^[176]. Copyright 2020, American Association for the Advancement of Science. MOFs: Metal-organic frameworks; UMOF NSs: ultrathin MOF nanosheets; MON: MOF nanosheets; AFM: atomic force microscopy.

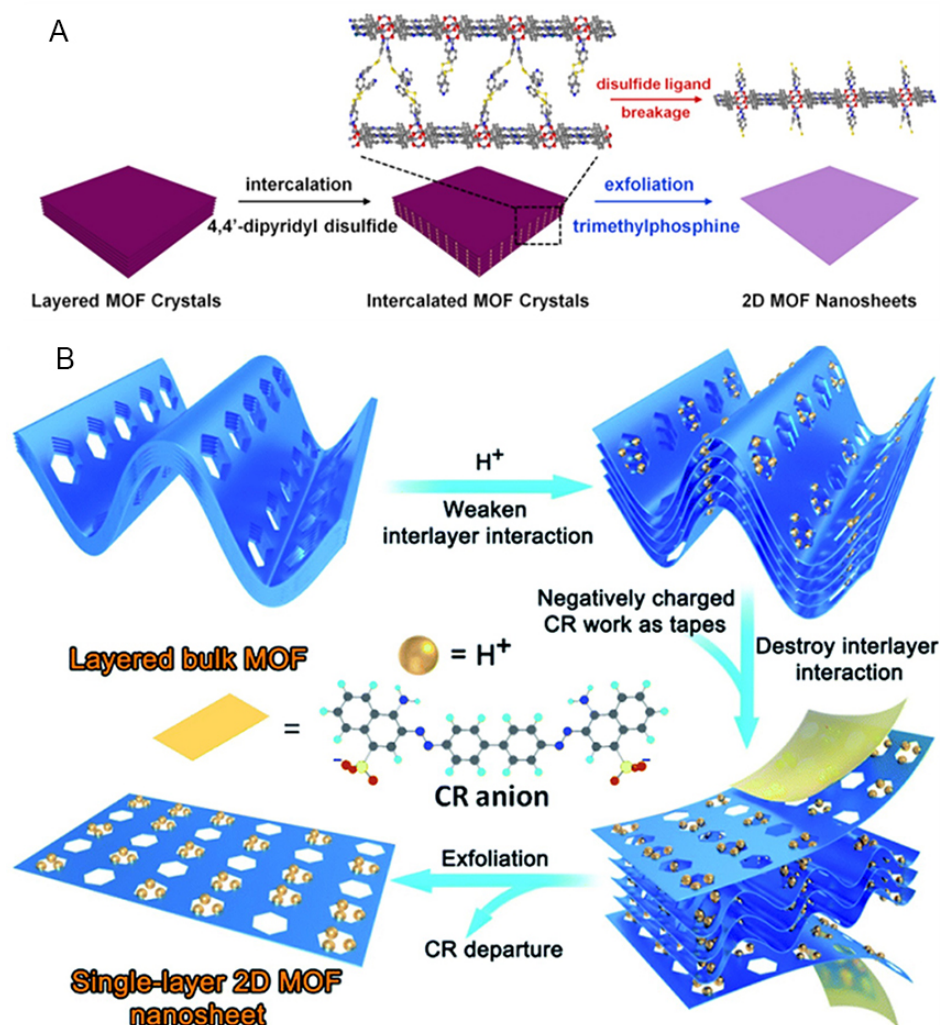


Figure 12. (A) Schematic diagram of the entire formation of 2D MOF nanosheets by chemical exfoliation. Adapted with permission^[177]. Copyright 2017, American Chemical Society. (B) Schematic representation of the synthesizing 2D Zn-MOF nanosheets. Adapted with permission^[180]. Copyright 2021, Royal Society of Chemistry. MOFs: Metal-organic frameworks; 2D: two-dimensional.

as hydroxyl and ester groups, are present in bulk 2D MOFs. In 2021, Liu *et al.* first protonated bulk Zn-MOFs under acidic conditions and then used a negatively charged Congo red (CR) dye as a “tape” to attach to the Zn-MOF surface using electrostatic interactions to further break the weak van der Waals forces [Figure 12B], which further breaks the weak van der Waals forces, resulting in an ultra-thin monolayers (3.4 nm) 2D nanosheet^[180]. While for the *in-situ* exfoliating process, the adsorption of CR molecules prevented the re-accumulation of the exfoliated nanosheets, providing excellent adsorption properties. The chemical exfoliation, though ingratiating, has a certain threshold, usually with a selective link between the insertion agent and the peeled object, and is therefore not widely applicable. Both insertion and stripping processes are involved, and often, the insertion step is the decisive step in the stripping process and the stripping rate is not easily controlled.

Solution stripping

With the further exploration of 2D materials, a number of chemical strategies have been developed and applied to the preparation of UMOF NSs. In 2013, Gallego *et al.* completely exfoliated the laminate by

solvent interaction alone, before which solvent exfoliation (without the application of other external forces) of 3D laminates had almost not been reported^[181]. They achieve complete separation of the crystals by immersing the layered MOF $[\text{Cu}(\mu\text{-pym}_2\text{S}_2)(\mu\text{-Cl})]_n \cdot n\text{Y}$ (where Y can be MeOH, H₂O or 1/2EtOH) in water. The interlayer cavities in the crystal structures can be filled by solvent molecules in a simplistic and repetitive manner. This solvent exchange does not affect the crystallinity of the single crystals. The structural features of the compounds show that the solvent in the interlayer cavities prohibits strong layer-to-layer interactions. This method is very soft in terms of energy due to solvent-assisted procedures, avoiding the potential complications of exfoliation in laminar crystals or solid matrices. In 2017, Wang *et al.* used the freeze-thaw method to exfoliate a kind of bulk MOFs, MAMS-1 $[\text{Ni}_8(5\text{-bbdc})_6(\mu\text{-OH})_4]$, into large, defect-free 2D nanosheets [Figure 13A-D]^[182]. The hexane solution undergoes a transformation between a solid and a liquid state under the influence of temperature, which generates a shear force that leads to the exfoliation of nanosheets. These nanosheets are also used as molecular sieve membrane structures to facilitate gas separation. The Aida team used SMe-H₂ip ligands to synthesize a porous kagome lattice of bulk MOF^[183]. When immersed in a non-plasmonic polar solvent, employing N,N-dimethylformamide (DMF) or tetrahydrofuran (THF), kgm^{SMc} was discovered to swell rapidly like an accordion, gradually exfoliating the monolayer nanosheets. The solvent stripping is similar to the chemical exfoliation where the solvent is used as an insert to strip the material. The disadvantages are slow peel rates, low yields and a narrow range of applications.

Bottom-top approaches

Although top-down methods have wide applicability in the preparation of various UMOF NSs, they often face difficulties in controlling the thickness and size of 2D materials^[184,185]. In contrast, bottom-up approaches offer the advantage of being more efficient, scalable and flexible. This strategy relies heavily on the assembly between metal nodes and organic linkers and is suitable for the preparation of nanosheets that possess isotropic bonds^[186]. Classical bottom-up methods for synthesizing 2D materials generally include interfacial synthesis and layer-by-layer methods, *etc.*

Interface synthesis

Restricting the growth of MOF crystals to the interface of two dissimilar phases is a common method for synthesizing 2D MOF nanosheets (MONs)^[187,188]. Interfacial synthesis confines metal ions and organic ligands at the interface of two phases to form a thin sheet of MOFs. With the aid of non-destructive optical methods, it is possible to monitor the growth of the crystal interface and indicate the presence of a reversible transition layer at the growth interface, which provides guidance for the synthesis of MOFs^[189,190]. Coordination reactions that typically occur at the interface of two phases have the advantage of large area, good size ratio and easy transfer to the device^[191]. By considering the type of interface, interfacial synthesis can be divided into three categories: liquid/air interface, liquid/solid interface and liquid/liquid interface.

Liquid/air interface: accompanied by the evaporation process of the organic solvent at the interface and then the introduction of surface pressure with the Langmuir-Blodgett (LB) technique, the grown monolayer MOFs can be comfortably transferred to the substrate. In 2015, Sakamoto *et al.* used the liquid/air interface reaction to synthesize monolithic nanosheets with a lateral size larger than 10 μm in size^[192]. They added a solution of dichloromethane containing a very small amount of three-way dipyrin ligand molecule (L1) slowly and dropwise to an aqueous phase containing zinc (II) acetate. Along with the rapid volatilization of dichloromethane, an immediate coordination between L1 and zinc (II) ions is achieved, generating a monolayer of MOF (N1) at the interface. Ying *et al.* fabricated flexible $\text{Cu}(\text{dhbc})_2(\text{bpy}) \cdot \text{H}_2\text{O}$ MONs at the air/water interface and dispersed them in an isopropanol solution with a significant Tyndall effect [Figure 14A-D]^[193]. The thickness of the nanosheets shown in Figure 14C can be clearly observed as about 4.4 nm. Subsequently, they combined MONs with graphene oxide nanosheets (GONs) to prepare ultra-thin

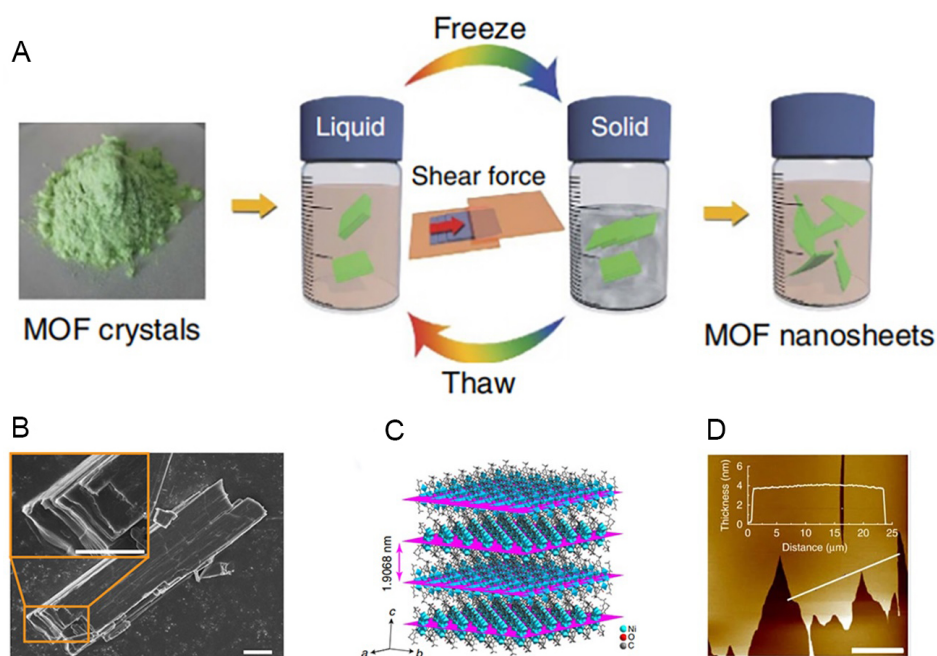


Figure 13. (A) MAMS-1 crystals freeze-thawed and exfoliated into dispersed nanosheets. (B) FE-SEM image of a laminated MAMS-1 crystal. (C) Crystal structure of MAMS-1. (D) AFM image of purified MAMS-1 nanosheets. (A-D) Adapted with permission^[182]. Copyright 2017, Springer Nature. MOFs: Metal-organic frameworks; FE-SEM: field-emission scanning electron microscopy; AFM: atomic force microscopy.

hybrid films (~ 100 nm) that can be used for CO_2 separation. Zhang *et al.* synthesized the conductive MOF film $[\text{Co}_3(\text{HOB})_2]_n$ (HOB = 1,2,3,4,5,6-benzenehexaol) using (Langmuir-Blodgett) LB technology^[194]. Interestingly, this 2D film has good electrical conductivity and detects hydrogen peroxide well with an ultra-low detection rate of 1.05×10^{-8} wt%.

Liquid/solid interface: the reactants frequently constructed MONs by self-assembly at the two-phase interface between a metal or carbon substrate and a solution. Commonly utilized substrates are nickel foam (NF), graphite-carbon ensemble graphene, *etc.*^[195]. In recent years, inorganic salts with cheap prices, large crystallite planes, and high stability have gradually become common substrates for the synthesis of large-area 2D materials^[196,197]. Huang *et al.* then utilized sodium chloride templates to *in-situ* prepare high-quality ultrathin ZIF-67 nanosheets^[198]. The limited solvent and the appropriate amount of sodium chloride were key factors in the synthetic process. The growth of ZIF-67 was confined to the narrow space of sodium chloride microcrystals, ensuring that the ZIF-67 nanoparticles extended along the microcrystalline planes. In 2020, this team proposed a self-dissociative assembly (SDA) strategy to synthesize ultrathin nanosheets that served as highly active oxidative evolution reaction (OER) catalysts^[199]. Firstly, they picked a cobalt-nickel alloy as the template and mixed the template with a solvent that could dissolve the metal source and ligand. In a hydrothermal process, benzenedicarboxylic acid (BDC) oxidized the CoNi alloy template and dissociated Co^{2+} and Ni^{2+} on the template surface. Co^{2+} and Ni^{2+} were, in turn, coordinated with BDC and assembled into ultra-thin CONi-MOF nanosheet arrays (CoNi-MOFNA) on the alloy substrate surface [Figure 14E-H]. During this dissociation-assembly process, the nucleation of MOFs occurs at the surface of alloy, which results in restricted growth sites for locating the metal source and guaranteeing the homogeneity of the nanoarrays.

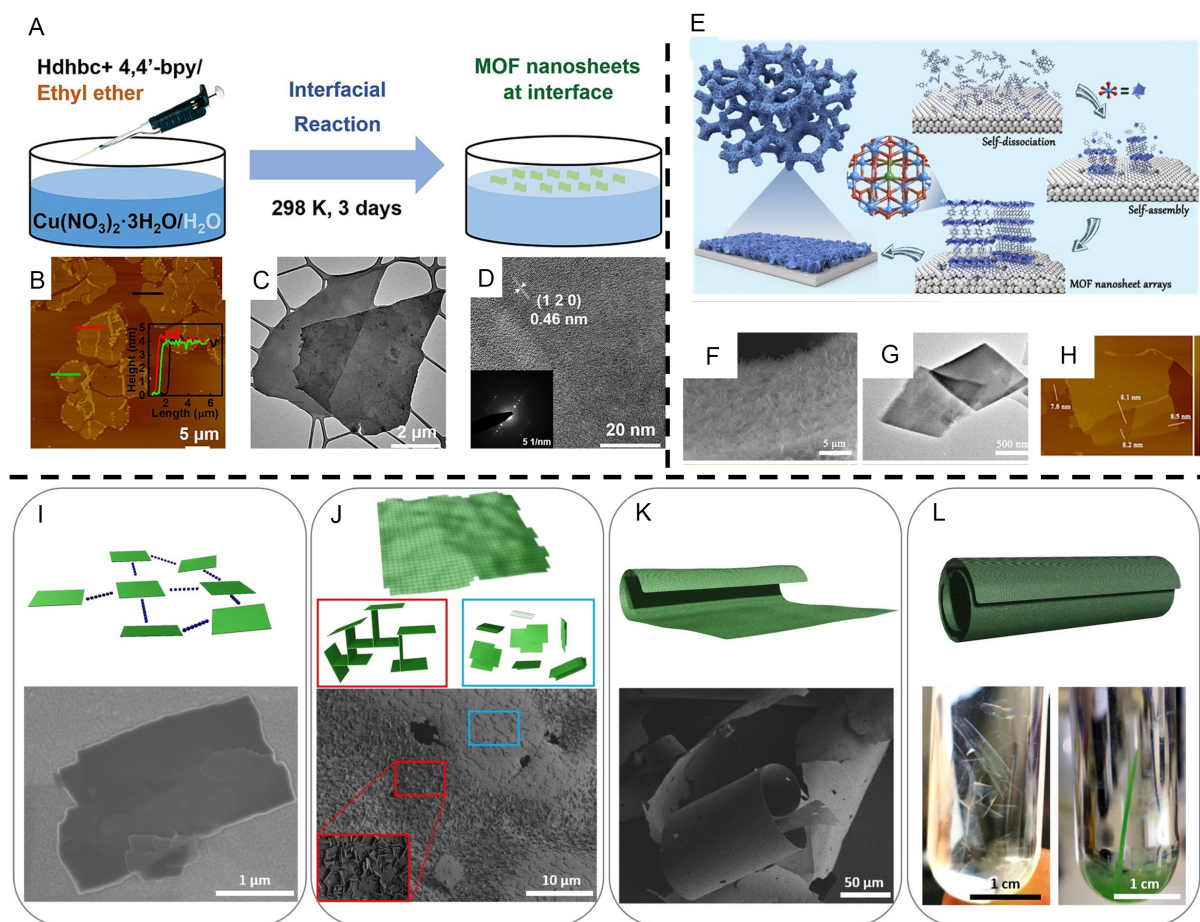


Figure 14. (A) Scheme for the preparation of layered less $\text{Cu}(\text{dhbc})_2(\text{bpy}) \cdot \text{H}_2\text{O}$ MONs at the air/water interface. (B) AFM image of $\text{Cu}(\text{dhbc})_2(\text{bpy}) \cdot \text{H}_2\text{O}$ MONs. Inset: height profiles of MONs corresponding to the three labeled lines. (C and D) TEM and HRTEM image of $\text{Cu}(\text{dhbc})_2(\text{bpy}) \cdot \text{H}_2\text{O}$ MONs. (E) Schematic illustration of SDA strategy for the synthesis of CoNi-MOFNA, (F) SEM image. (G) TEM image. (H) AFM image. (I) Formation of isolated, anisotropically shaped $\text{DUT-134}(\text{Cu}) \cdot \text{DMF}$ microcrystals. (J) Spontaneous self-assembly of the microcrystals into face-to-face or edge-to-face arrangements in fresh DMF solution. (K and L) Freestanding carpets and spontaneous roll-ups resulting in lengths up to ca. 100 μm in diameter and up to 20 mm or longer. Bottom: (I) SEM image of a $\text{DUT-134}(\text{Cu})$ flake. (J) surface of the carpet. (K) macrostructure of the dried carpet. Photos: (L) Translucent DUT-134 carpet in DMF (left) and large “multi-walled” macro-tubes in DMF (right). (A–D) Adapted with permission^[199]. Copyright 2021, John Wiley and Sons. (E–H) Adapted with permission^[207]. Copyright 2019, Elsevier. (I–L) Adapted with permission^[207]. Copyright 2022, John Wiley and Sons. MOFs: Metal-organic frameworks; MONs: MOF nanosheets; AFM: atomic force microscopy; SDA: self-dissociative assembly; DMF: dimethylformamide.

Liquid/liquid interface synthesis: two kinds of solutions with different densities are frequently utilized to dissolve metal salts and ligands, respectively, and the nanosheets are formed in the limited space at the interface of the two phases. Most MOFs are considered to be electrical insulators due to their poor electrical conductivity, but the emergence of new synthetic methods over the last decade or so has revealed some examples of conductive MOFs that allow them to be used as optical electronic components^[200–205]. Arora *et al.* have bridged the gap between materials synthesis and technological applications by synthesizing the first two-dimensional MOFs for photoelectric detection through a liquid/liquid interface strategy^[206]. They took advantage of the difference in density between 2,3,6,7,10,11-triphenylenehexathiol (THT) and water to synthesize $\text{Fe}_3(\text{THT})_2(\text{NH}_4)_3$ films at the THT/water interface. They were also able to achieve controlled growth of the film thickness depending on the reaction time. Structurally, the monolayer $\text{Fe}_3(\text{THT})_2(\text{NH}_4)_3$ film exhibits 2D mesh structures with many planar hexagonal connections, and Fe atoms

were coordinated with THT organic ligands to form honeycomb structures with a pore size of about 1.9 nm. This is the first comprehensive study of the performance of MOF material components in terms of optical response, temperature and wavelength, and these materials will be promising candidates for optoelectronic applications. In 2021, Schwotzer *et al.* focused on the assembly of 2D-MOF nanosheets into complex superstructure crystals, successfully assembling small DUT-134 platelets into giant “carpet” structures by using a liquid-liquid interface approach [Figure 14I-L]^[207]. In a quasi-interfacial synthesis strategy, DMF plays a special role in the process, acting as a binder between the nanoparticles and the “carpet” structure, with the support of DMF leading to the synthesis of thin films. The translucent “carpet” enhances the accessibility of the Cu²⁺ sites after the removal of the solvent, improving the adsorption of H₂S and providing a reference for air filtration. The Cánovas team succeeded in synthesizing large multilayer Fe₃(THT)₂(NH₄)₃ films with a CHCl₃/water interface, and adjusting the reaction time allowed the film thickness to be controlled^[208]. Li *et al.* developed the synthesis of bimetallic Ni-M-MOF (M = Al, Mn, Zn, Co and Cd) nanosheets using the mixed solvent N,N-dimethylacetamide (DMAC) and water^[209]. This ultrathin heterometal can be used as an efficient electrocatalyst for oxygen evolution reactions.

Layer-by-layer assembly

The layer-by-layer (LBL) synthesis method is a sub-method of the liquid phase epitaxy (LPE) procedure. The LBL process is defined as the cyclic immersion of functionalized substrates such as gold and silicon in a solution containing metal ions and a solution containing organic linkers, resulting in highly crystalline surface-anchored MOFs (SURMOFs)^[210-213]. Between each immersion, the samples need to be washed with a pure solvent to remove excess scaffolds^[214]. The thickness of the film can be regulated by the number of repeated immersions. A few years earlier, Sakaida *et al.* reported the first 2D tetracyanonickelate-based MOF by drawing on their previous method of synthesizing 3D MOF^[215]. Since the orientation of the crystals heavily influenced the deposition process, they tried to form self-assembled monolayer (SAM) by first immersing the gold substrates in an ethanolic solution of 4-mercaptopyridine overnight. The substrates were then alternately immersed in the two ethanol solutions for 20 cycles, resulting in the synthesis of highly crystalline films [Figure 15A]. Xiao *et al.* constructed ultrathin TA-Zn²⁺ layers based on tannic acid (TA) and Zn²⁺ on polyethersulfone substrates using the LBL method, and subsequently converted the TA-Zn²⁺ layers into ZIF-8 films by immersing them in the 2-methylimidazole (Hmim) solution as a zinc source^[216]. The LBL method has also been applied to heteroepitaxy and Liu *et al.* have reported the use of the LBL method to fabricate a photoactive MOF-on-MOF heterostructure^[217]. Conductive MOF films have great applications in various fields, such as energy storage and optical field, due to their thin thickness, conductivity and large area size. In 2021, the preparation of 2D Cu₃(HHTP)₂ (HHTP = 2,3,6,7,10,11-hexahydroxytriphenylene) films were achieved by Zhao *et al.* through the layer-by-layer assembly method^[218]. Controlled thickness growth was easily achieved by controlling the growth period [Figure 15B-D]. The synthesized Cu₃(HHTP)₂ pores have a hexagonal structure with a pore diameter of only 1.8 nm, which can improve the transport efficiency of electrolyte ions and greatly encourage the development of energy memory devices.

Surfactant-assisted strategy

The synthesis of 2D MOF nanosheets or nanofilms using interfacial synthesis and LBL methods usually requires specific substrates and relatively complex preparation steps, but the direct synthesis of 2D MOF nanosheets has not been reported. Common surfactants, such as polyvinylpyrrolidone (PVP) and cetyltrimethylammonium bromide (CTAB), not only limit the growth of MOFs along the stacking direction but also assist in stabilizing the MOFs precursors. In 2015, Cao *et al.* firstly reported a surfactant-mediated strategy for the direct production of ultrathin, homogeneous, high-quality 2D MOF nanosheets^[50]. They selected PVP as a surfactant to control the various anisotropic growth of Zn-TCPP crystals to form ultrathin

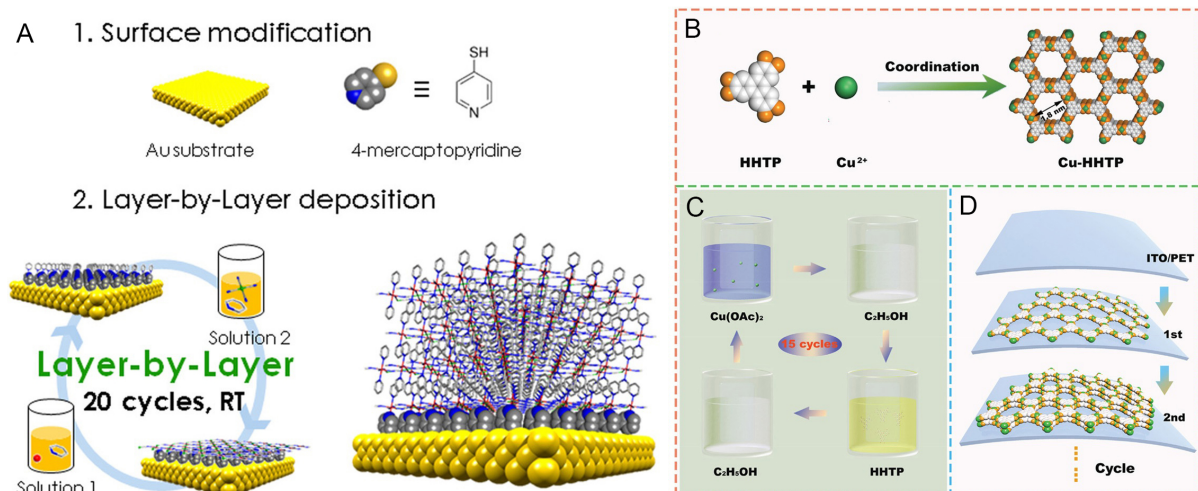


Figure 15. (A) Diagram of LbL film fabrication. (B) Schematic synthesis of Cu₃(HHTP)₂. (C) Diagram of layer-by-layer growth of Cu₃(HHTP)₂ films on ITO/PET substrates by repeated cyclic growth. (D) Top view of Cu₃(HHTP)₂ growth on the surface of an ITO/PET substrate. (A) Adapted with permission^[215]. Copyright 2017, American Chemical Society. (B-D) Adapted with permission^[218]. Copyright 2021, John Wiley and Sons.

MOF nanosheets with a thickness of less than 10 nm [Figure 16A-D]. Later, they investigated the generality of different metals for forming 2D nanosheets and found that 2D nanosheets could be constructed when using Zn, Cu, Cd or Co salts as metal precursors. Subsequently, in 2016, they prepared 2D porphyrin paddlewheel framework-3 (PPF-3) MOF nanosheets using a surfactant-mediated method and obtained 2D composites for super electrode materials by sulfidation and carbonization^[219]. It has been shown that PVP molecules can selectively attach to the surface of MOFs, reducing interlayer contact and stacking, resulting in the growth of MOFs in a two-dimensional direction and eventually forming MONS^[220]. Hang *et al.* used PVP to prepare 2D Zn-TCPP MOF for controlled photodynamic therapy (PDT) materials for the treatment of specific cancers^[221].

In 2020, Wang *et al.* employed the anionic surfactant sodium dodecyl sulfate (SDS) to prepare homogeneous 2D conjugated MOFs (2D c-MOFs)^[222]. In this process, SDS molecules acted as structural modifiers, and the negatively charged hydrophilic groups in the molecule preferentially anchored on the surface of MOFs under electrostatic interactions, alleviating the buildup between layers and facilitating the formation of ultrathin nanosheets [Figure 16E]. HHB-Cu was first constructed and subsequently stripped of HHB-Cu NSs under sonication. The prepared single crystal HHB-Cu NSs are characterized by a thickness of 4-5 nm (~8-10 atomic layers) [Figure 16F-H].

Zirconium-based MOFs have received much attention compared to other metal-based MOFs due to their higher thermal stability and rich structural types^[223,224]. Reports on Zr-MOF nanosheets are limited when compared to many other MOF nanosheets, due to the strong metal coordination bonds^[49]. In contrast, in 2019, Zhang *et al.* demonstrated a simple strategy for the direct synthesis of 2D Zr-BDC MOF nanosheets^[225]. Considering the defective linker in UIO-66, they chose a bio-based surfactant (SAAS-Cm) as a ligand competitor to attach to the defect in Zr-BDC MOFs, leading to anisotropic growth of MOFs. Pseudo-assembly into bulk MOFs occurs during the growth of the crystals, and the interaction forces between the layers of the bulk MOFs are weakened by the interaction of the surfactant hydrophobic chains, which in turn disintegrate into ultrathin nanosheets (3-4 nm). Furthermore, they found that changing the number of alkyl groups on the hydrophobic chains can simply modulate the thickness of 2D nanosheets (3-60 nm).

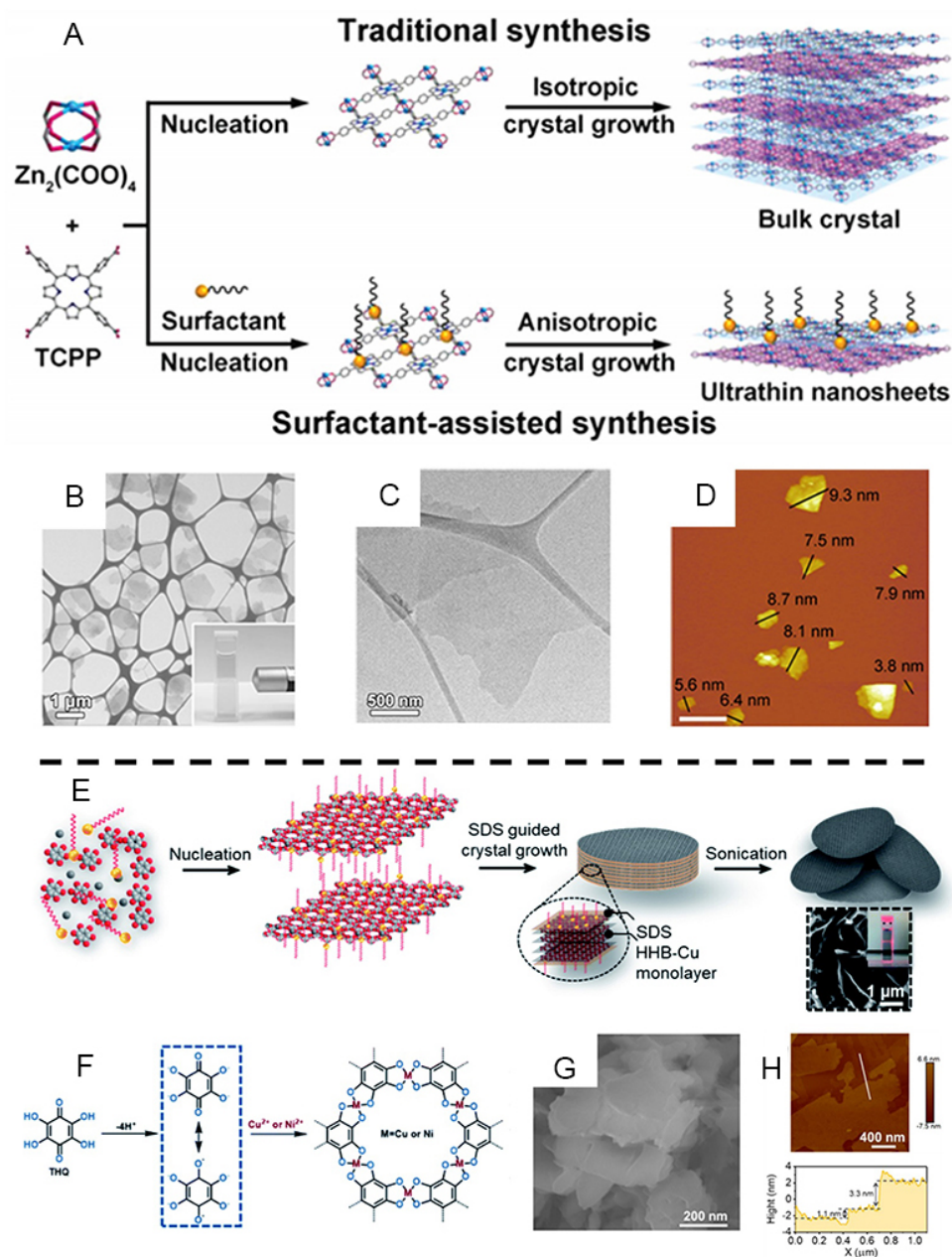


Figure 16. (A) Routine and surfactant-assisted synthesis of MOF. (B) STEM image of Zn-TCPP nanosheets. (C) TEM image of single Zn-TCPP nanosheets. (D) AFM images of Zn-TCPP nanosheets, Scale bar: 2 μm . (E) Scheme for the synthesis of ultrathin HHB-Cu nanosheets using a surfactant-assisted method. (F) Scheme for the synthesis of HHB-Cu. (G) SEM images of HHB-Cu NSs with lamellar morphology and layered structures. (H) AFM image and height profile along the white line marked on the HHB-Cu NSs. (A-D) Adapted with permission^[50]. Copyright 2015, John Wiley and Sons. (E-H) Adapted with permission^[222]. Copyright 2020, Royal Society of Chemistry. MOFs: Metal-organic frameworks; AFM: atomic force microscopy; NSs: nanosheets.

SYNTHESIS OF MOFS WITH 3D MORPHOLOGIES (3D MOFS)

3D MOFs are commonly porous MOFs structures with unique 3D morphology, assembled and stacked from simple individual MOFs building blocks^[18,226-232]. Compared to low-dimensional MOFs materials, 3D

MOFs materials exhibit fantastic morphologies, large specific surface areas and high porosity, making them widely used in many fields, especially in catalysis, gas storage and separation, and energy storage. In catalysis, the high porosity of MOFs facilitates the transfer of substances and provides space for the encapsulation of guest molecules. However, most 3D MOFs materials only exhibit microporous structures (< 2 nm). The problem of small pore size would limit molecular transport and diffusion, reduce efficiency, and increase the catalytic time, which is not in line with the concept of sustainability. In terms of gas storage and separation, the structural hierarchy provided by the variation of MOFs building blocks becomes a favorable option for storing/separating gases. In general, MOFs are used for selective adsorption and separation of specific gases in a gas mixture. The appropriate introduction of mesoporous or defective spaces in microporous MOFs can provide additional adsorption sites, allowing further access to molecules. MOF-based materials also play an integral role in energy storage devices such as supercapacitors and batteries. The synergy between the layered pores in the structure allows MOFs to exhibit excellent electrochemical properties. However, it is still difficult to design and fabricate well-defined 3D MOFs on the nano/micro scale, especially for architectures consisting of morphologically ordered simple building blocks; scientists continue to explore new synthetic methods for 3D MOFs materials with nano/micro-pore structures^[233]. Due to their structural diversity of pores and the presence of unsaturated coordination sites, various synthetic strategies have also received extensive attention.

Etching

Compared with 1D and 2D MOFs, 3D MOFs with more complex structures generally have higher surface-to-volume ratios. Nevertheless, to date, there are poor references for the rational preparation of single-crystal MOFs with complicated open nanostructures^[234,235]. However, some uncommon nanostructures, such as nanocages, nano-hollow spheres, *etc.*, can be prepared by the etching method. For example, partial etching of prefabricated MOF crystals results in partially defective single crystalline hollow MOFs with stable and tunable active centers, facilitating the development of more efficient reaction routes^[236-238]. In 2016, Han *et al.* reported on the use of ammonia to etch Ni-Co Prussian Blue (PBA) cubes to grow anisotropically into cubic nanocages^[239]. Etching occurs preferentially at the apex of the cube and slowly along the diagonal direction, increasing the etching time. Through controlled experiments, it was found that the etching rate was dependent on the defect density in the corner regions of the cube. In the case of Ni-Co PBA crystals, the growth process is from the outside-in, with the inner core being more “loose” and defect-rich than the exterior shell, resulting in a faster etching rate, finally, a pyramid-like nanocage [Figure 17].

MOFs are promising porous crystalline materials as catalyst carrier materials^[80,240-244]. Etching methods tend to etch metal ions so as to achieve a defective morphology. For MOFs, numerous studies have been done on etching from the perspective of ligands. Two years ago, Luo *et al.* tried to etch MOFs by using strong oxidants to oxidize organic ligands, sever the C-C bond and selectively degrade the organic linker into organic small molecules, developing an oxidative linker cutting process^[245]. They used 2,5-dihydroxyterephthalic acid (DOBDC) as a sacrificial connector and selected oxidants of different strengths [nitric acid and reactive oxygen species (ROS)] for comparison, UiO-66-(OH)₂ could be horizontally carved from the inside out or from the outside in, resulting in single crystal hollow and yolk-shell structures [Figure 18A-F]. Analysis of the products after nitric acid and ROS etching of MOFs using ¹H-NMR and LC-MS revealed that in both cases, the C-C bond on the benzene ring in the linker DOBDC was the shear site of the UiO-66-(OH)₂ core. Comparatively, ROS is more reactive, shorter-lived and more rapidly reacts with DOBDC and is removed before diffusion into the core, generating yolk-shell structures. Nitric acid, on the other hand, has a lower oxidation potential and is slower to etch, oxidizing DOBDC to 2,5-dihydroxy-3-nitroterephthalic acid (DONTA) before degrading it to smaller molecules such as formic acid and oxalic acid [Figure 18G and H]. These two cavity structures ensure that the natural active sites on the catalyst surface are fully preserved, providing new inspiration for the design of complex composite catalysts. The

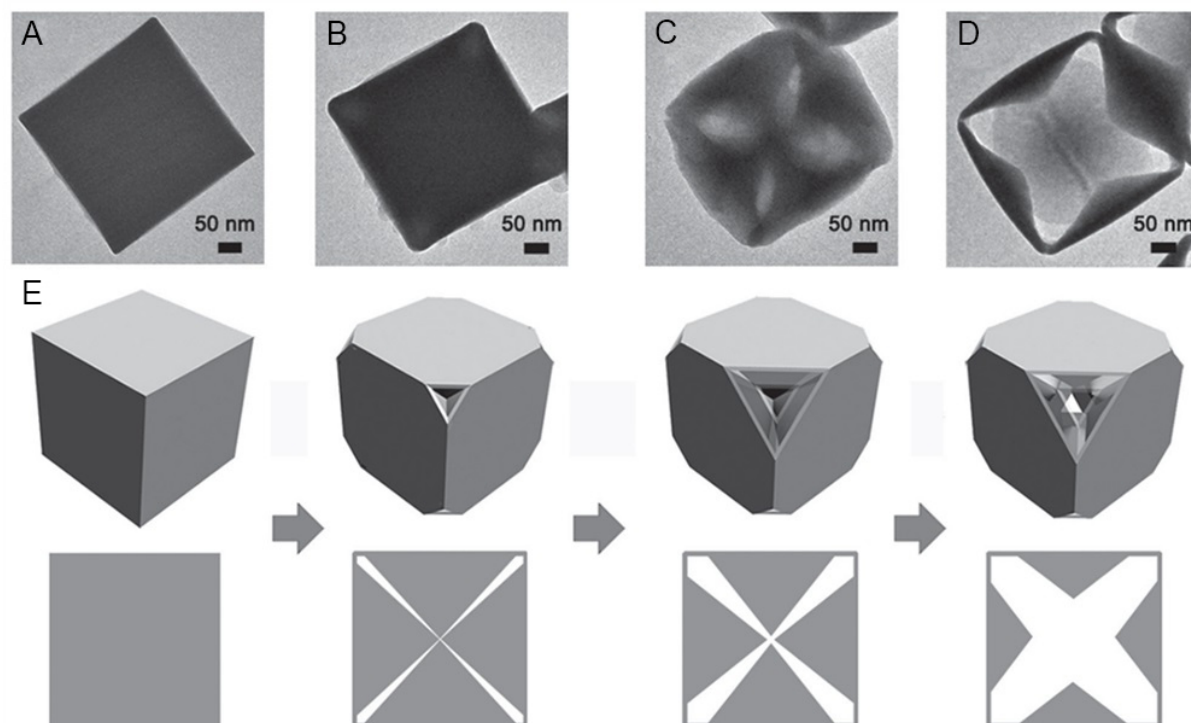


Figure 17. (A-D) TEM image of etched product obtained after reaction of 20 mg Ni-Co PBA cubes with 2.5 mL of ammonia at room temperature for (A) 0 h, (B) 0.5 h, (C) 2 h, and (D) 6 h. (E) The corresponding schematic illustrates the formation of a Ni-Co PBA cage. (A-E) Adapted with permission^[239]. Copyright 2016, John Wiley and Sons. PBA: Prussian blue analogues.

etching process is highly sophisticated, and wet etching is often used in the synthesis of MOFs. Wet etching rates are high, but tend to etch all homogeneous and the etching direction is not well chosen. Acidic or alkaline etchants are commonly used and the drop acceleration rate of the etchant has an important influence on the etching results. The etching process requires good personal protection, gloves and masks, as well as specific wastewater treatment procedures.

Microwave-assisted

Microwave (MW) irradiation was previously a widely used method in organic chemical synthesis, and over the years, it has been used to synthesize inorganic nanomaterials such as zeolites and MOFs^[246-248]. Traditional hydrothermal synthesis involves heating the medium from the outside to the inside; however, the microwave-assisted strategy is different, using microwaves to directly heat the reactants, with heat being generated in the reaction medium from the inside to the outside^[249,250]. Compared to conventional synthesis techniques, microwave-assisted methods offer advantages in terms of crystal nucleation, morphological size of the MOF, reaction yields, and reproducibility^[251-253]. In many research findings, MW radiation has been found to produce smaller-sized MOFs due to enhanced heat and mass transfer capabilities, which usually accelerate the crystal nucleation^[254,255]. In 2016, Babu *et al.* successfully synthesized highly porous 3D MOFs (MOF-205) by MW irradiation^[256]. They controlled the reaction time to probe the crystal formation process and applied them for the immobilization of atmospheric CO₂ due to their unique physical and structural properties. Chen *et al.* synthesized MOF-74 (Ni) using MW-assisted, hydrothermal and condensation reflux methods, respectively^[257]. By comparison, it was found that MW could shorten the synthesis time from 32 h and 24 h to 1 h, which greatly improved the reaction efficiency. In addition, the MW route produced smaller and more stable products. Relying on the abundant metal sites, it is more conducive to the adsorption of CO₂. Wang *et al.* synthesized robust Cu-MOF using a MW reactor under mild conditions at

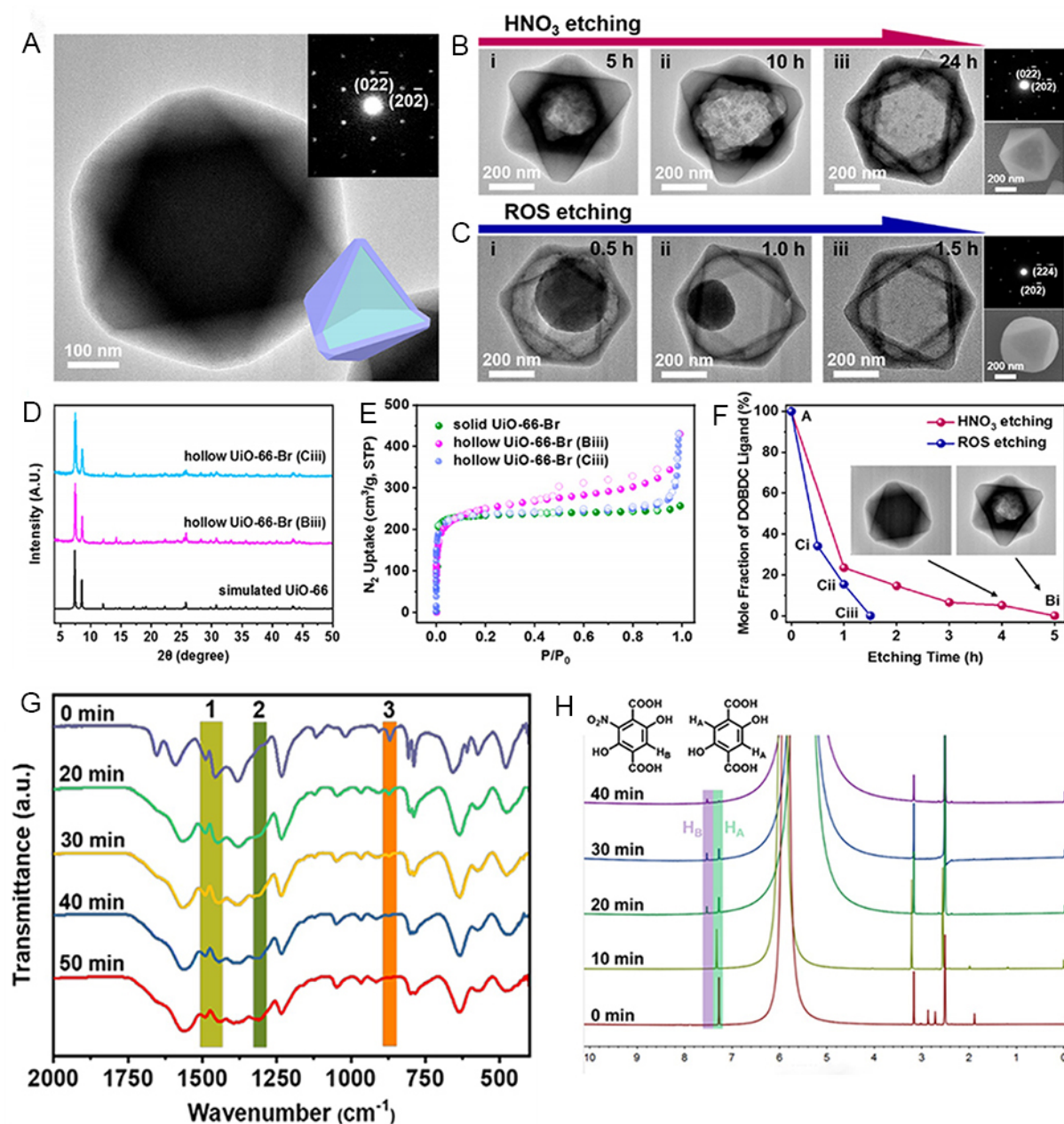


Figure 18. (A) TEM images of UiO-66-(OH)₂@UiO-66-Br particles and their SAED patterns. (B) TEM images of UiO-66-(OH)₂@UiO-66-Br treated with HNO₃ at different times, SAED pattern and SEM image are provided on the right. (C) TEM images of UiO-66-(OH)₂@UiO-66-Br after different times of ROS treatment, SAED pattern and SEM images are provided on the right. (D) Powder X-ray diffraction patterns of hollow UiO-66-Br. (E) N₂ adsorption isotherms of solid UiO-66-Br and hollow UiO-66-Br obtained. (F) Normalized molar fraction of DOBDC in UiO-66-(OH)₂@UiO-66-Br after treatment with HNO₃ and ROS for different times. (G) FT-IR spectra of UiO-66-(OH)₂ etched by 2.5 M HNO₃ for various time. Area 1 is the benzene skeleton vibration. Area 2 is the symmetric stretching of -NO₂. Area 3 is the out-of-plane bending of C=C-H of benzene ring. (H) ¹H NMR spectra of UiO-66-(OH)₂ digested after HNO₃ etching (2.5 M) for different times. (A-H) Adapted with permission^[245]. Copyright 2019, American Chemical Society. ROS: Reactive oxygen species; DOBDC: 2,5-dihydroxyterephthalic acid.

60 °C [Figure 19A]^[258]. The Cu-MOF showed good catalytic activity as a catalyst for the direct catalysis of carboxylation of 1-ethylbenzene and carbon dioxide. Kong *et al.* produced MOF-303 nanocrystals with a controllable size of 50-500 nm by a MW-assisted method^[259]. After doping with methanesulfonic acid

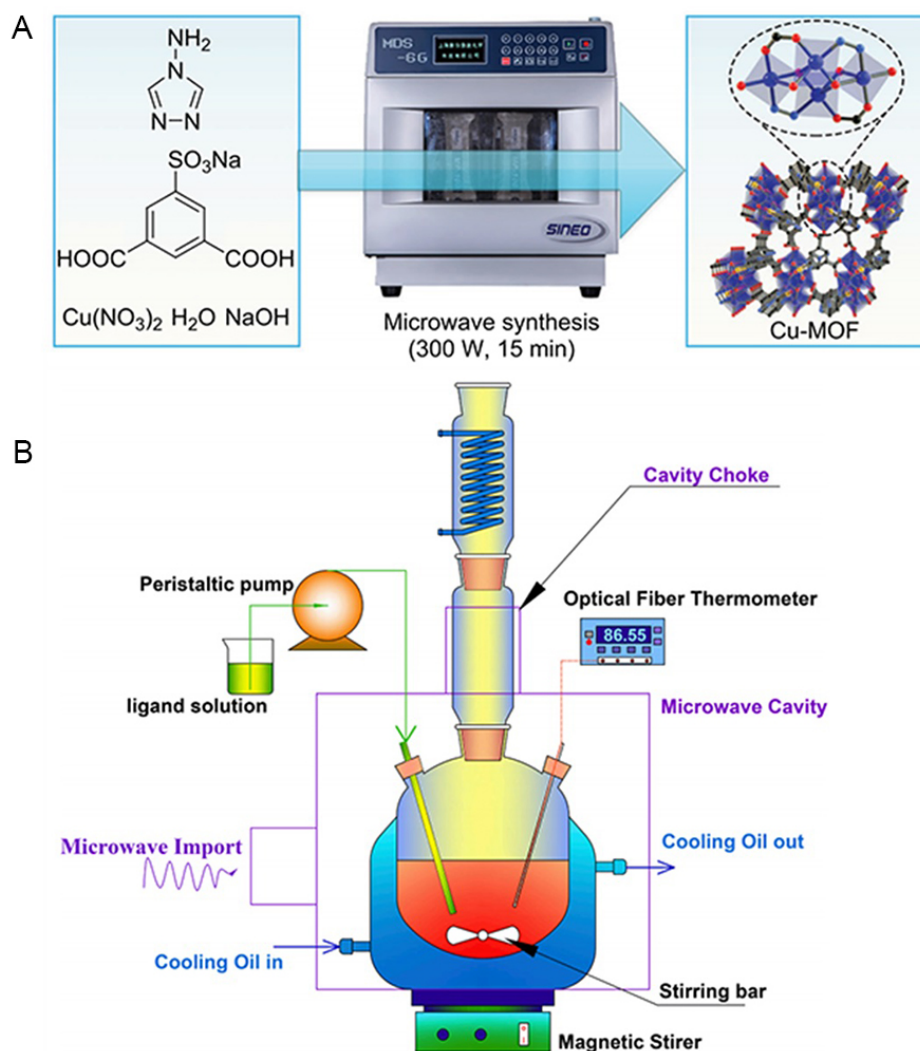


Figure 19. (A) MW-Assisted Synthesis of Cu-MOF. (B) Synthetic procedure and experimental setup for MIL-88B (Fe) synthesis in the MW field. (A) Adapted with permission^[258]. Copyright 2021, John Wiley and Sons. (B) Adapted with permission^[263]. Copyright 2021, Elsevier. MOFs: Metal-organic frameworks; MW: microwave.

(MeSA), MeSA@MOF-303 exhibited high plasmonic conductivity. Although MW-assisted synthesis of MOFs is nowadays a safe and convenient strategy, the lack of reactor engineering in the MW field still hinders the further application of MW technology in synthesizing 3D MOFs^[260,261]. Under MW irradiation, the resonant power distribution is uneven and the heating in the MW field is not uniform, which can easily lead to local overheating and hot spots^[262]. In 2021, Zhao *et al.* studied the use of numerical simulations to find out the hot spot variation pattern by exploring the MW input power, cavity size and stirring rate parameters to find out the variation pattern of hot spots [Figure 19B]^[263]. It was confirmed that adjusting the MW power and cavity structure could help eliminate hot spots and produce MOFs with uniform and regular dimensions. However, the reaction parameters also need to be optimized quite precisely in order to achieve the desired morphology and yields. Compared to conventional heating, microwave heating is rapid, highly concentrated in terms of instantaneous energy and requires no heat transfer. Polar solvents absorb microwave energy and heat up quickly, yet non-polar solvents hardly absorb microwave energy and warm up very slowly. Rapid heating is also a “double-edged sword” and might make it difficult to measure the actual temperature of the sample and maintain a particular temperature.

Self-assembly

The self-assembly method is inspired by nature^[264,265]. It is a process of spontaneous aggregation between atoms of a material and/or their orderly arrangements into novel structures. The assembled structures often have properties beyond imagination. Normally, the poor stability is considered to be a negative disadvantage. However, in some cases, instability may also be a positive and beneficial factor^[266]. Thus in 2015, Huang *et al.* were inspired by the template method and prepared H-MOFs by self-assembly using unstable metal-organic assemblies (MOAs) as templates and stable MOFs as bodies^[267]. The formation and disappearance of MOAs can be controlled during the self-assembly process due to the sensitivity of the template to moisture and acid [Figure 20A]. Considering that the mesopore size of the generated H-MOFs (~11 nm) is much smaller than that of the added MOAs (370~520 nm), they suggested that there was a process of decomposition or rearrangement of MOAs in the reaction and confirmed the speculation by elemental analysis (EA) and inductively coupled plasma (ICP) emission spectroscopy. The *in-situ* regenerated MOAs were used as templates to guide the synthesis of H-MOFs, and it was found that MOAs with different structures and complexities could be used as template precursors for the preparation of H-MOFs. Attempts to assemble from 1D MOFs to sustainable 3D superstructures with the template method are still challenging because (1) the size and geometric symmetry of 1D MOFs are not easy to control, which can lead to disordered assembly; and (2) superstructures are often unstable owing to weak inter-particle forces, which can easily generate further bulky crystals^[268]. Wang *et al.* devised a self-assembly-based dissolution-crystallization-attachment (DCA) strategy, where nanometallic oxides (MOs) were used as metal sources to control the size of MOFs by optimizing the proportion between MOs and acidic ligands, and successfully assembled sea urchin superstructure MOFs (US-MOFs)^[269]. Under the acidic ligand, the MOs will dissolve accordingly, and the rate of MOs dissolution is related to the ligand concentration. The dissolution rate of MOs decreases when the ligand concentration decreases, but MOs promote ligand deprotonation and therefore accelerate the nucleation of MOFs to form nanorod shapes with large length-to-width (L/W) ratios. When the L/W ratio is large enough, the nanorods undergo directional attachment and eventually form US-MOFs. Over the years, there has been a boom in the application of self-assembly as a means of synthesizing new materials, and Zhao *et al.* have synthesized MOF-5 by self-assembly^[270]. In 2022, Hu *et al.* proposed a strategy for guest molecule-driven self-assembly and chiral induction to construct light-functional lanthanide-organic cages^[271]. The guest molecules encapsulated in the bulk cavity are parallel to the tetrahedral cage walls and have a similar π -stacking effect, resulting in a double-walled tetrahedron. This structure is expected to provide new avenues for chiral asymmetric catalysis. Alivand *et al.* used acidic Fe₃O₄ nanoclusters as a multifunctional template to modulate the self-assembly of structurally diverse MOFs to further capture CO₂ by tailoring the hierarchical structure to modulate the acidic sites^[272]. Traditionally spherical colloidal structures have been used to build self-assembled superstructures, but in recent years self-assembly of non-spherical polyhedral particles has also been considered as a viable method to form superstructures, as reported by Avci *et al.* for truncated rhombic dodecahedral (TRD) ZIF-8 particles with good monodispersity and colloidal stability, which can self-assemble into millimeter-sized 3D superstructures by evaporation under heated conditions^[273]. During the self-assembly process, an aqueous solution of the particle colloids was added dropwise to the surface of the glass, which was placed in a 65 °C oven until the droplets dried. Self-assembly of ZIF-8 particles into superstructures was observed by field-emission scanning electron microscopy (FE-SEM) in an ordered arrangement along a 3D orientation [Figure 20B]. The photonic bandgap of the superstructures can be tuned by controlling the ZIF-8 particle size, ultimately facilitating the design of 3D photonic sensing materials. The self-assembly method is highly ordered and directional as it is carried out spontaneously and the assembled structure tends to be in thermodynamic equilibrium. The assembly process is more complex, influenced by the characteristics of the structural units (mass, shape, charge, *etc.*) and the stability is inferior.

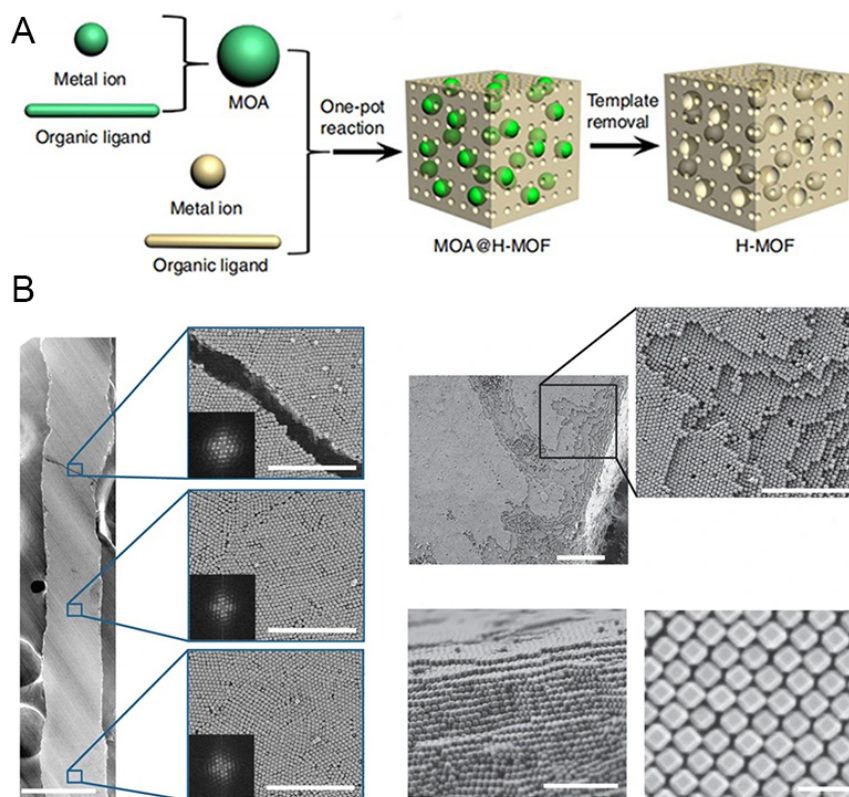


Figure 20. (A) Schematic representation for the fabrication of H-MOF. (B) Representative FE-SEM image of a self-assembled superstructure made from TRD ZIF-8 crystals (size 210 ± 10 nm). (A) Adapted with permission^[267]. Copyright 2015, Springer Nature. (B) Adapted with permission^[273]. Copyright 2017, Springer Nature. MOFs: Metal-organic frameworks; TRD: truncated rhombic dodecahedral; MOA: smetal-organic assemblies.

Sol-gel method

In general, the crystallization of MOFs produces polydisperse microcrystalline powders. There are a large number of voids between the discrete crystals, which can reduce the packing density and thus affect the overall bulk adsorption capacity^[274,275]. While these microcrystalline powders are suitable for scientific research, their chemical nature limits the large-scale applicability of MOFs, with a number of inherent technical problems to be solved, such as poor handling, mechanical instability and mass transfer limitations^[16,276]. The advent of the sol-gel method, however, provides a new way to avoid the microcrystalline powder state and synthesize MOF monoliths^[277,278]. In the case of MOFs, sol-gel methods offer potentially powerful strategies for improving the properties of the material, such as chemical functionalization of pore surfaces or crystal interfaces, hybridization of MOFs with other material types and precise spatial localization and orientation of MOF crystals^[279,280]. The term “sol-gel” relates to the chemical process that generates a sol, a colloidal suspension of submicron-sized particles^[281]. Although some studies have shown that the MOF gel state is formed by the aggregation of dispersed crystalline nanoparticles in the system through weak non-covalent interactions, the formation mechanism of these materials has generally been poorly investigated. Normally, the primary particles that form the gel need to be small enough to ensure that they can grow at the gel interface during drying^[282]. In their study of high density HKUST-1 monomer and UiO-66 in gas absorption, Tian *et al.* found that the drying temperature was critical to determine whether the MOF gels eventually formed robust and dense monoliths, and that the rate for the drying step must be slow^[283,284]. In 2017, Bueken *et al.* studied a series of Zr-based MOFs (UiO-based series, MOF-808 and NU-1000) and found that three parameters, i.e., metal source, water and concentration of

reactants, play a critical role in the formation of gelation^[285]. It is easier to produce gels when using $\text{ZrOCl}_2 \cdot 8\text{H}_2\text{O}$ than ZrCl_4 to produce microcrystalline precipitates.

After several years of exploration, the formation mechanism of MOF gel was subsequently generalized and studied in detail by Hou *et al.* in 2020^[286]. The precursor of MOF monoliths is the MOF gel state. The forming process of the gel state is important in relation to the aggregation of MOF nanoparticles, while the monodispersity of MOF nanoparticles is facilitated by controlling the crystallization process. It is known that the crystallization process occurs in supersaturated solutions, and once the solution is supersaturated, nucleation takes place and crystal seeds start to grow. A sufficient decrease in the concentration of reactants signals the cessation of nucleation and crystal growth. The nucleation and crystal growth rates can be determined using the Avrami and Gualtieri models^[287,288]. MOF gelation starts with crystal competition between MOF nanoparticles as a result of the rapid formation of a high concentration of nanocrystals in solution [Figure 21]. In the sol-gel method, the MOFs are chemically homogeneous, with small particles and high crystallinity, as the precursors are initially dispersed in the solution to form a low-viscosity solution. The good dispersion of the precursors facilitates the smooth progress of the reaction.

Innovation from traditional methods

Since the discovery of MOFs materials in the 1990s, the variety and quantity of MOFs have increased and the methods for synthesizing MOFs have been innovative. With continued exploration, the synthesis of 3D MOFs is no longer limited to a single traditional method, e.g., hydrothermal/solvothermal methods, microwave processing, ultrasonic synthesis, moderator methods, *etc.* The convergence between different strategies may shed new light on the structure and properties of MOFs. Colloids are microcapsules or microspheres that are consisted of closely packed particles with outer shells^[289]. In 2013, Pang *et al.* inspired by colloids, intentionally pursued MOF colloids, reporting the use of emulsions as soft stencils, allowing the assembly of MOFs polyhedral building blocks (BBs) into hollow 3D structures on their surfaces^[290]. Considering that monodisperse BBs are an innate element in the construction of superstructures, in their previous study, they selected tert-butylamines as organic structure directing agents (SDAs) and polyvinylpyrrolidone (PVP) as surfactants to obtain monodisperse BBs under solvothermal conditions^[291]. When PVP was replaced by polyoxyethylene (20) sorbitan trioleate (tween-85), some interesting phenomena happened and the cubic BBs spontaneously assembled into spheres. Moreover, the size of the hollow colloid could be controlled by adjusting the amount of tween-85 [Figure 22A-D]. Under the action of the stirring drive, tween-85 can form emulsified droplets, and the prior formation of monodisperse Fe-soc-MOF cubes in the presence of SDAs then spontaneously self-assembles to form a shell structure on the surface of the emulsified droplets. As the droplet evaporates, the template disappears and eventually forms a hollow colloid [Figure 22E].

Zheng *et al.* found that 4,4'-bipyridyl can be used as a coordination modulator to modulate the morphological transformation of $[\text{Ni}(\text{Tdc})(\text{Bpy})]_n$ MOF from 1D nanofibers to 2D nanosheets and finally to 3D columnar nanocrystals, proposing a dual-ligand-based hard-soft acid-base strategy^[292]. The MOFs prepared by this strategy are efficient electrode materials with good stability, providing a general approach for the realization of morphologically/functionally tunable MOFs in the future. In 2021, the Milko group synthesized single crystals of hollow MOFs with a unique appearance by means of acoustic-chemical-solvent thermal conditions^[293]. The sonication of the solvent was the key step, and a dimethylformamide (DMF)/chloroform mixture was sonicated for 1.5 h. The resulting free radicals were able to interact with the metal salts to reduce their stability. This process exacerbates the formation of multi-domain crystals with internal structural defects by using single crystals as sacrificial templates, which suggests that sonication can alter the ratio of metal ions to ligands, leading to morphological changes in the resulting MOFs. It is often important to design the nanostructure and porosity of crystalline materials, and the synthesis of MOFs

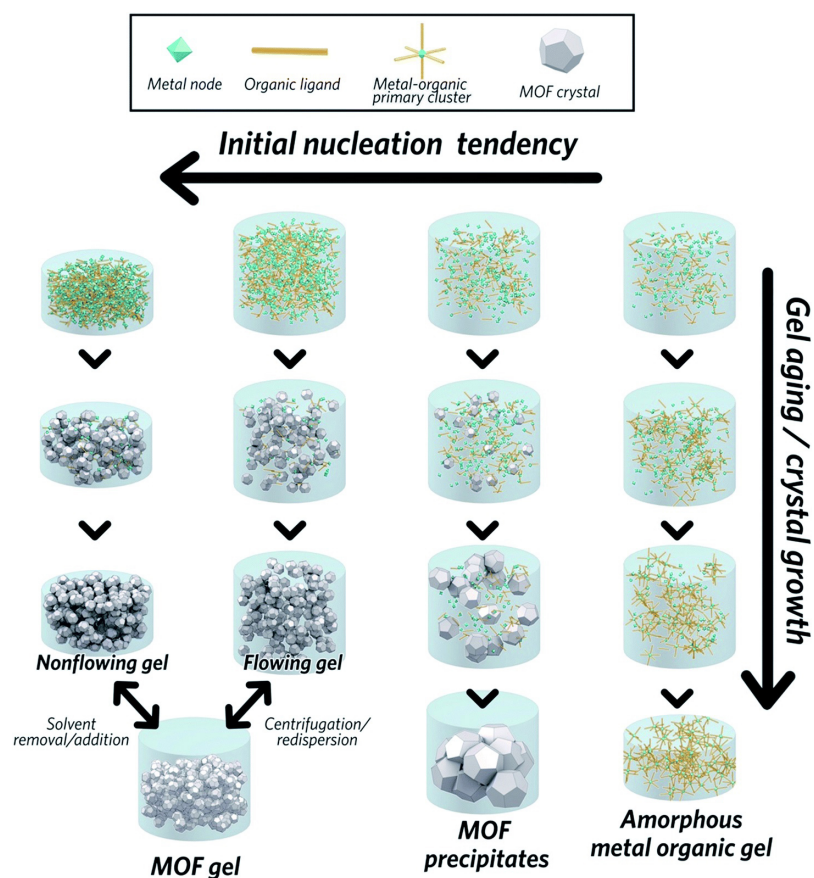


Figure 21. Mechanism of the formation of MOF gels, precipitates and metal-organic gels. Adapted with permission^[286]. Copyright 2020, Royal Society of Chemistry. MOFs: Metal-organic frameworks.

crystals in pre-designed templates often enables more precise control of structural features such as morphology, particle size, porosity and surface regularity.

Spatially confined synthesis has also been shown to prepare MOFs materials of various structures, but the growth mechanism of MOFs single crystals in confined space is yet to be explored. In 2021, Li *et al.* reported the confined growth of ZIF-8 single crystals in three-dimensionally ordered (3DO) macroporous polystyrene materials^[294]. They used a bottom-up strategy to prepare 3DO sphere-assembled ZIF-8 single crystals (3DOSA-ZIF-8) and 3DO single-crystalline ZIF-8 sphere arrays (3DOSC-ZIF-8), respectively, by controlling the concentration of ZIF-8 in 3DOM-PS [Figure 22F]. 3DOSA-ZIF-8 crystals have an octahedral shape and are assembled from spherical crystals with a diameter of about 200 nm, while 3DOSC-ZIF-8 is formed from spherical crystals of highly ordered arrays [Figure 22G and H]. Composition of other MOFs can also be applied to the template method, such as the preparation of 3DO-MOFs, including ZIF-67 and HKUST-1. They explored and revealed that the concentration of precursors has a critical effect on the structure and morphology of 3DO-ZIF-8. Mechanistic studies indicated that the formation of different structures of 3DO-ZIF-8 from low- and high-concentration precursor solutions is due to the discontinuous and continuous distribution of their dried dry gels within the template and their subsequent ability to undergo in situ crystallization, respectively. This study presents a general and effective method to control the growth pattern and engineered nanostructures of layered MOFs single crystals, providing new insights into the growth process and mechanism of MOFs single crystals within the restricted domain template.

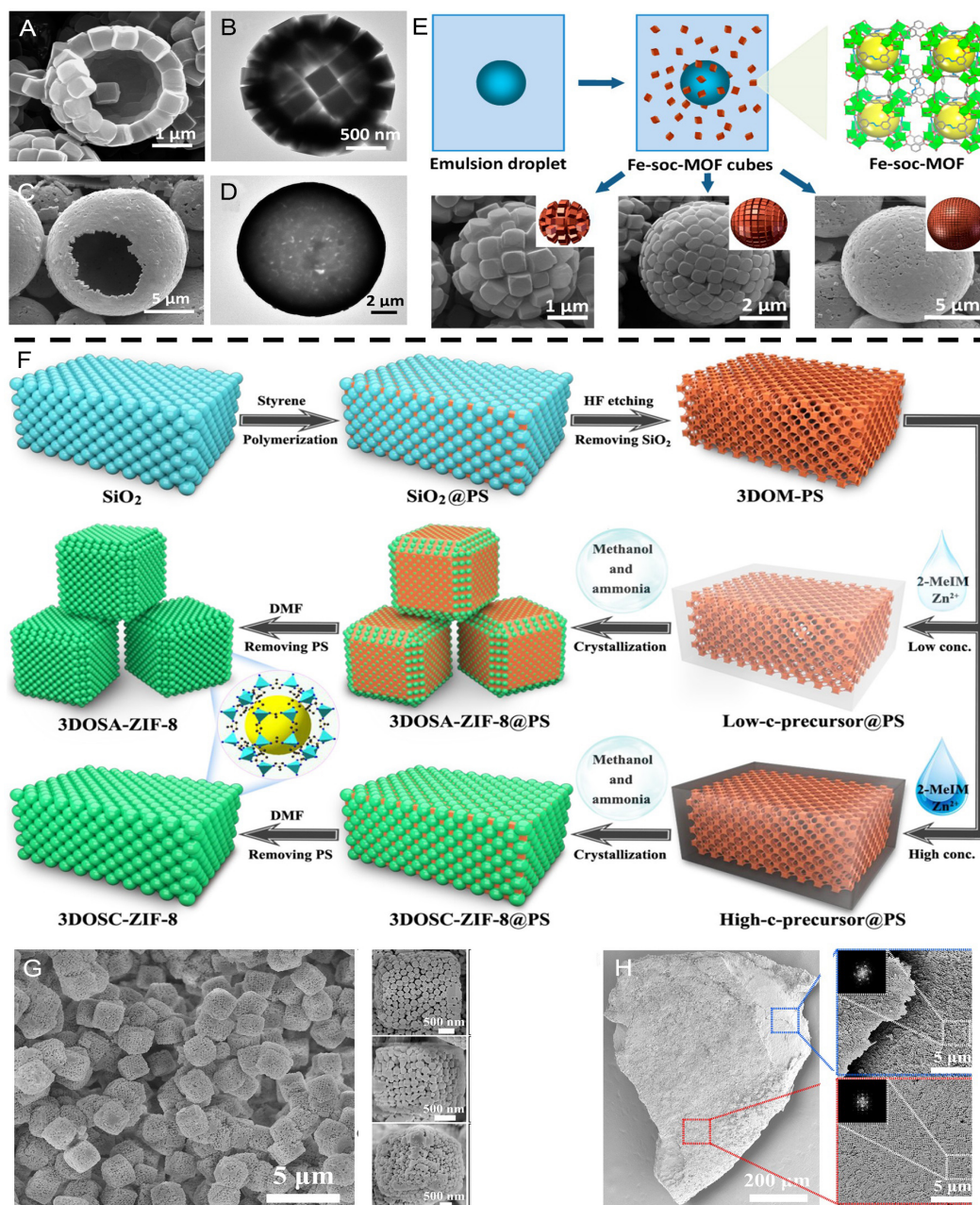


Figure 22. (A and B) SEM and TEM images of small Fe-soc-MOF hollow colloids prepared by addition of 0.05 mL tween-85. (C and D) SEM and TEM images by adding 0.03 mL of tween-85. (E) Schematic representation of the synthesis and integration of Fe-soc-MOF cubes into hollow colloids. (F) Schematic representation of the synthesis of 3DOSA-ZIF-8 and 3DOSC-ZIF-8. (G) SEM image of 3DOSA-ZIF-8, (H) SEM images of 3DOSC-ZIF-8 at different resolutions. (A-E) Adapted with permission^[290]. Copyright 2013, American Chemical Society. (F-H) Adapted with permission^[294]. Copyright 2022, American Chemical Society. MOFs: Metal-organic frameworks.

SYNTHESIS OF MOF-BASED HYBRIDS

Brief introduction

To date, there are more than 10,000 different kinds of MOFs, many low-cost and simple synthetic methods have been developed, and MOFs have become one of the chemical materials with wide application prospects. However, the poor structural stability, water stability and poor electrical conductivity of MOFs compared to conventional porous materials have not yet been addressed. In order to obtain more complex

structures and functions, the synthetic strategy for MOFs-based hybrids by combining the selected MOFs with one or more different units has attracted a great deal of interest from materials scientists^[295,296]. MOF in MOF-based hybrids still retains the advantages of large surface area, high porosity and tuneability of the frameworks^[297]. At the same time, the different units can provide a support platform for the MOFs growth and allow for a homogeneous distribution of the MOF to improve structural stability. The combination of components with well-defined functions and excellent activity may also lead to a coordinated “1 + 1 > 2” effect^[298]. Briefly, the MOF-based hybrids have the advantages of high conductivity, structural stability and more active centers when compared to MOFs. From an application-oriented point of view, the performance of a material is determined by different parameters and a single material is often not sufficient to meet all requirements. MOF-based hybrids can both inherit the advantages of MOF and often show better performance because of the synergistic effect between the component units. With different compositions and exposed active sites, MOFs-based hybrids are widely used in catalysis, gas adsorption and separation. In catalysis, Xu *et al.* then successfully prepared a hybrid of graphene oxide (RGO) and MIL-100 (Fe) for application in the degradation of pollutants^[299]. The pore structures in MOFs can enhance the diffusion of various ions and small molecules that can be absorbed by the other component in the hybrid. The rich active sites and excellent electrical conductivity of the hybrid allow it to be used in the decomposition of organic compounds. In the field of gas separation, the separation of CH₄ has been a hot topic of great interest to industry. Theoretical researches have shown that the region near the imidazole ligand in ZIF-8 exhibits preferential adsorption of CH₄. Inspired by this, Wu *et al.* designed complexes of ZIF-8 with conventional molecular sieves to enhance the selectivity for CH₄/N₂^[300]. Typical MOFs-based hybrids are MOFs/metal oxides, MOF/carbides, MOF/metal nanoparticles and MOF-on-MOF, as shown in [Figure 23](#).

Types of MOF-based hybrids

MOFs/Metal oxides

The doping of metal oxides is a way to stably modify MOFs and improve their performance. One of the keys to research on the sensing aspects of trace gases is the detection of acetone gas^[301]. Long-term exposure to acetone can cause irreversible damage to human health, and MOFs have attracted a lot of attention as new functional nanomaterials for gas sensing. Zhou *et al.* designed and synthesized a ZnO@ZIF-71(Co) composite sensor in order to achieve the detection of acetone^[302]. As is known, the element Co activates oxygen in air to generate reactive oxygen, and Co in the form of oxide or metal has been widely used to study the detection of acetone^[303,304]. While introducing Co into porous MOFs and constructing co-doped such probes is relatively rare. The response amplitude of the complex they prepared was approximately 100 times higher than that of the undoped sensor, and the Co site in ZIF-71 (Co) catalyzes the activation of oxygen and promotes the decomposition of acetone, ultimately improving the sensitivity to trace amounts of acetone (50 ppb). Water pollution has been a hot topic of concern for environmentalists and scientists over the years, and the adsorption of heavy metal ions such as Hg (II), Pb (II) and Cr (V) is a particularly high priority. Porous and tunable MOFs are highly studied in metal adsorption, but their poor water stability limits their application development. Zhang *et al.* used a two-step process to prepare 3D MoO₃@ZIF-8 core-shell nanorod structures for the reduction of highly toxic Cr (V) to non-toxic Cr (III)^[305]. Characterization revealed that new bonds were formed between MoO₃ and ZIF-8 in the complexes. Subsequent analysis of their photoluminescence spectra and transient photocurrent density maps confirmed the generation and transfer of holes. The hybrid heterojunction formed improves the charge separation efficiency. The 3D core-shell structure not only has a large specific surface area but is also much more stable for aqueous environments. The high surface area of ZIF-8 also provides more active sites for electrons and protons. The formation of new bonds enhances the “synergistic effect” of both, as well as the electron capture capacity and photocatalytic activity of the hybrid material. Abdollahi *et al.* developed Fe₃O₄@TMU-32 complexes through a surface charge modulation strategy^[306]. This composite exhibited high adsorption capacity for Hg (II) and Pb (II) metal ions.

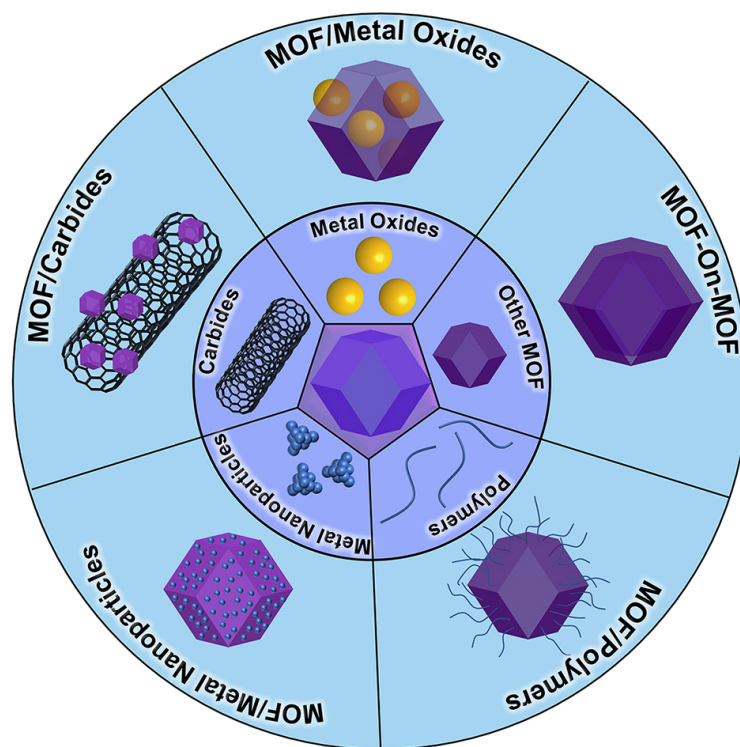


Figure 23. Schematic diagram of the synthetic MOFs-based hybrids. MOFs: Metal-organic frameworks.

In recent years, our group has done a lot of research on MOFs/metal oxides. In 2020, we used a simple hydrothermal method to prepare highly alkaline stable Co_3O_4 @Co-MOF complexes^[307]. Co_3O_4 on the surface of Co-MOF effectively improves the alkaline stability, allowing this composite to remain structurally stable in 3.0 M KOH solution for as long as 15 days [Figure 24A and B]. The material has a high specific capacity of 1020 F g^{-1} at a current density of 0.5 A g^{-1} and the maximum energy density of the constructed flexible device is 21.6 mWh cm^{-3} , offering significant advantages in terms of improved durability and capacitance. When targeting the disadvantage that polyoxometalate (POM) lacks sufficient active sites as a water oxidation catalyst, we propose to compound it with ZIF-67 with sufficient surface area to prepare a yolk/shell ZIF-67@POM hybrid, which can be used as a sustainable heterogeneous water oxidation catalyst [Figure 24C]^[308]. This unique yolk/shell structure has a potential synergy between ZIF-67 and POM, with an overpotential of only 287 mV at a current density of 10 mA cm^{-2} , resulting in excellent electrocatalytic activity toward OER. We also prepared a series of MOF@PBA with multi-level structures by compounding ultrathin MOF nanobelts with PBA through an *in-situ* cation exchange strategy [Figure 24D]^[309]. The multi-level nanostructures exposed more active sites, which promoted charge transfer, and the resulting complexes exhibited efficient catalytic oxygen precipitation under strongly basic conditions.

MOF hybrids have applications not only in catalysis but also in energy storage. The poor electrical conductivity of pure MOFs has been affecting their promotion in the field of energy storage. In 2021, we tried a seed-mediated growth method to prepare Co_3O_4 /ZIF-67 composites [Figure 24E]^[310]. The Co_3O_4 /ZIF-67 composites retain the morphology of ZIF-67 with the edges of Co_3O_4 partially exposed, as shown in Figure 24F-I. The prepared hybrids obtained the semiconductor properties of transition metal oxide (TMOs) and the high specific surface area of ZIF-67, which enhanced the lithium storage performance when the Co_3O_4 /ZIF-67 blend was used as an anode for lithium-ion batteries.

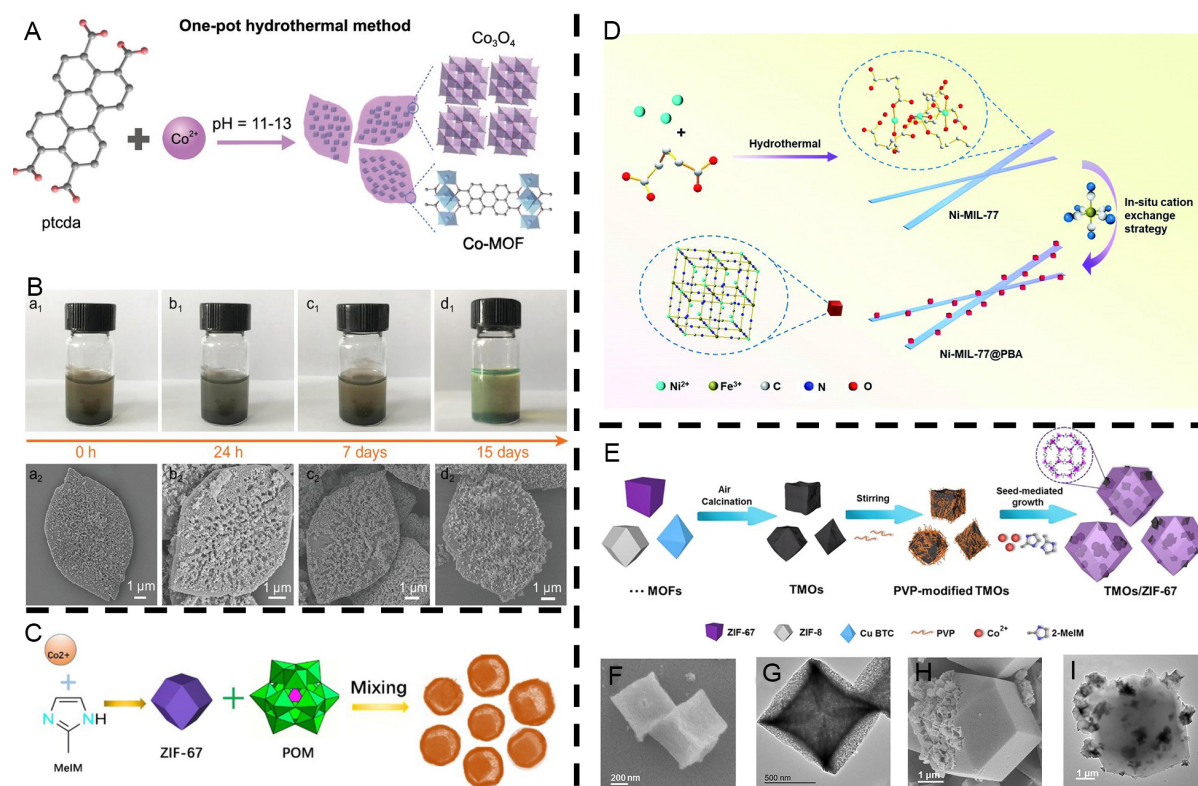


Figure 24. (A) Synthesis of Co_3O_4@Co-MOF hybrids. (B) Optical and SEM images of Co_3O_4@Co-MOF hybrids after different reaction times. (C) Schematic diagram of the synthesis of yolk/shell ZIF-67@POM hybrid material. (D) Formation process of Ni-MIL-77@PBA hybrid structure. (E) Schematic of the fabrication of TMO/ZIF-67 hybrids. ("..." stands for different MOFs). (F and G) SEM (F) and TEM (G) images of ZIF-67 sample after annealing. (H) SEM image of Co_3O_4/ZIF-67. (I) TEM image of Co_3O_4/ZIF-67. (A and B) Adapted with permission^[307]. Copyright 2019, Oxford University Press. (C) Adapted with permission^[308]. Copyright 2019, American Chemical Society. (D) Adapted with permission^[309]. Copyright 2019, Royal Society of Chemistry. (E-I) Adapted with permission^[310]. Copyright 2021, Elsevier. MOFs: Metal-organic frameworks; PBA: Prussian blue analogues.

The hybridization of MOFs and metal oxides is not complicated, but it is difficult to combine them to achieve better properties and applications considering their respective characteristics. For now, the semiconductor properties of most metal oxides, combined with the large specific surface area and porosity of MOFs, hybridization is mainly used in the field of catalysis, and future expansion for other applications is necessary. For example, the relatively good electrical conductivity of metal oxides, the large theoretical specific capacitance and the framework properties of MOFs. Given their characteristics, the prospects of the complexes in energy storage can be envisaged, but the drawbacks of volumetric expansion of the metal oxides and the structural instability of the MOFs are frequently inevitable during charging and discharging. Therefore, adequately combining the advantages and improving the disadvantages is a great challenge for the hybridization.

MOFs/Carbides

Carbon-based materials mainly include graphene, carbon nanotubes and activated carbon, which have been widely used in the field of materials due to their low price. The combination of MOFs and carbon-based materials produce mixtures that make up for the shortcomings of pure MOFs, enhancing the strength, electrical conductivity and stability of the MOFs, which are of great application value.

It is well known that graphene, as a star representative of 2D materials, is widely sought after because of its large specific surface area and high electrical conductivity^[311]. In 2020, Venkadesh *et al.* prepared Cu-MOF/graphene hybrids using solvothermal and electrochemical methods^[312]. The fabricated Cu-MOF/graphene composites showed a porous flower shape with good electrical conductivity, high surface area to enhance the electron transfer with caffeine, and good electrochemical properties for the electrochemical oxidation of caffeine. The developed sensor can accurately determine the concentration of caffeine in coffee and tea with good recovery. 3D graphene (3DG) networks also provide high surface area and high electrical conductivity for charge transport due to their porous nature. 3DG was synthesized by chemical vapor deposition (CVD) growth by Khirak *et al.* and then needle-like CoNi MOFs were grown on the surface of the 3DG network by *in-situ* solvothermal process^[313]. 3DG structures provide highly active sites and accelerate the diffusion of ions from the electrolyte to the active sites. Using the synergistic effect of the metal components, the directional growth of bimetallic MOFs on 3DG facilitates charge transfer^[314]. This material provides a good activity for catalytic cracking of water.

Carbon nanotubes (CNTs) have been investigated for their extremely high aspect ratio and functionalization. Huang *et al.* used a mixed H₂O₂/NaOH solution to post-treat the Ce-MOF/CNTs mixture to induce the oxidation of Ce atoms from Ce³⁺ to Ce⁴⁺^[315]. Electrochemical sensors for the identification of hydroquinone (HQ) and catechol (CC) were prepared. The modified electrodes exhibited two distinct oxidation peaks and higher oxidation currents compared to the untreated composites. Quan *et al.* synthesized CNT by pyrolysis of ZIF-67 and compounded it with aminated MIL-53(Al) to obtain a heterogeneous structure called N-MIL@CNT [Figure 25A]^[316]. It was found that the π - π attraction forces, hydrogen bonding and interfacial synergistic effects induced by this heterostructure contributed to the adsorption of organic compounds. Zeolite imidazolium frameworks (ZIFs), a subset of MOFs, exhibit some chemical and thermal stability in aqueous solutions, making them promising candidates for the adsorption of pollutants^[317]. ZIF-67@C-MOF-74 hybrid was prepared by Rio *et al.* by carbonizing MOF-74 as a precursor^[318]. ZIF-67@C-MOF-74 is easily regenerated and has good extraction capacity for phenolic compounds and can be used as an adsorbent for toxic pollutants.

MOFs/Metal single-atom or nanoparticles

Metal nanoparticles (MNPs), especially noble metals such as Pt, Pd, Ag and Au, are excellent co-catalysts as electron acceptors with low Fermi energy levels^[319,320]. In contrast, porous MOFs with high periodicity and tunable porosity are ideal platforms for loading nanoscale metal particles. Utilizing the closed nature and regular cavities of MOFs can effectively limit the aggregation and fusion of MNPs, resulting in a stable and homogeneous structure that facilitates diffusion and transport^[321].

Single-atom catalysts (SACs), which have caught fire in recent years, have become the new frontier in multiphase catalysis due to their maximum atom utilization efficiency and excellent catalytic performance^[322-324]. Although many innovative synthetic strategies have been explored just to obtain stable SACs, the problems of low metal loading and atom aggregation have not yet been solved. The research team found that MOFs can serve as excellent supports for single metal atoms catalysis^[325-327]. Then Zuo *et al.* prepared ultrathin 2D MOFs (PtSA-MNSs) coordinated with high concentrations of Pt single atoms with the assistance of PVP^[328]. The Pt atoms coordinated within the porphyrin ring are well dispersed after the formation of the MOF. The thickness of the resulting nanosheets is approximately 2.4 ± 0.9 nm [Figure 25B]. The ultrathin structure suggests that more active sites are exposed and also minimizes the transport distance of photon-generated carriers from the interior of the material to the surface, thereby suppressing undesired electron-hole complexation and allowing efficient visible-light-driven H₂ evolution. Generally, MOFs functionalized with noble metal nanoparticles are very effective materials for

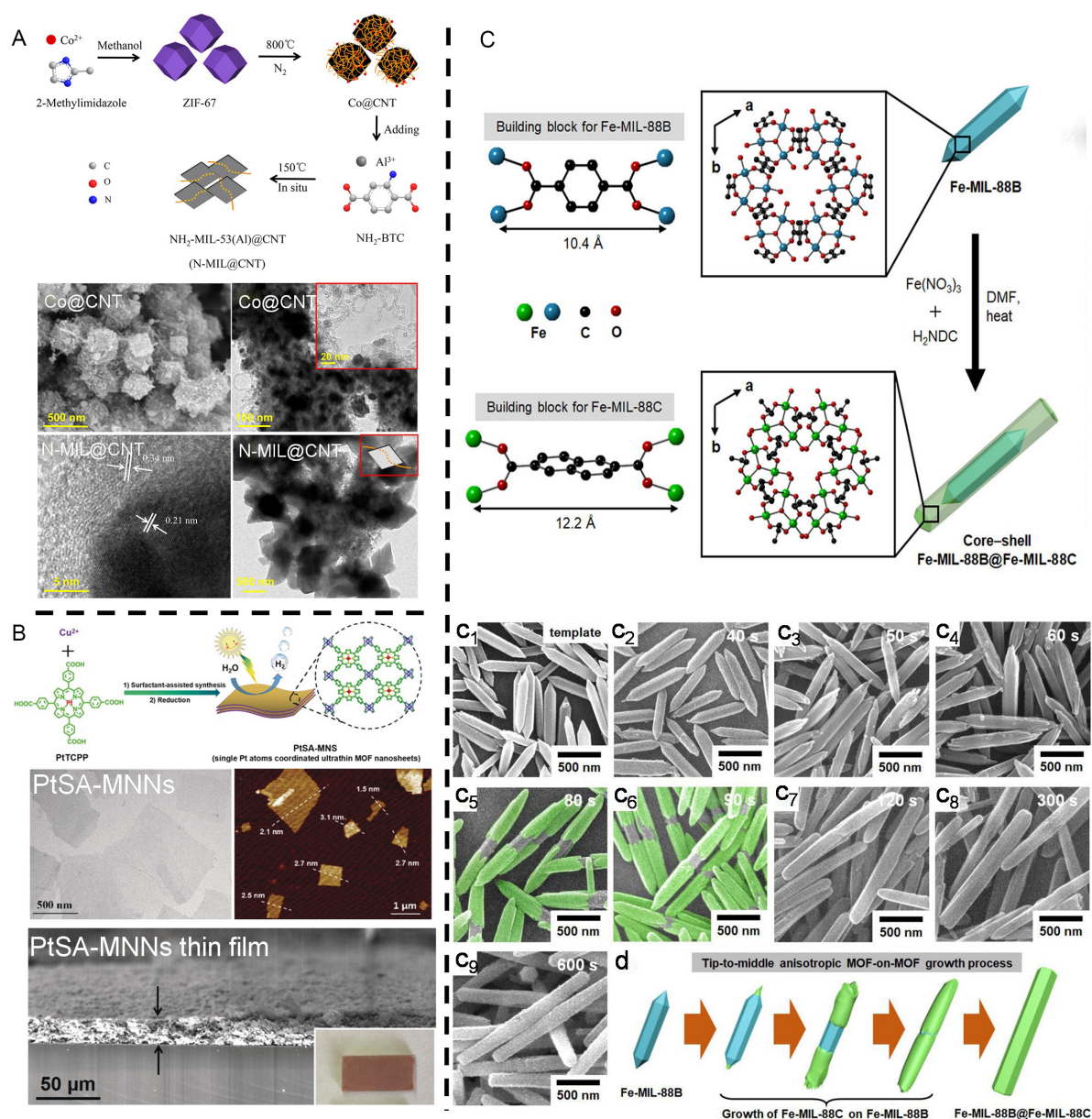


Figure 25. (A) Schematic representation of the synthesis of N-MIL@CNT and corresponding morphological characterizations. (B) Illustration of the synthetic route for the preparation of Pt single-atom coordinated ultra-thin MOF nanosheets (PtSA-MNNS) and corresponding morphological characterizations. (C) Schematic representation of the production of a core-shell type hybrid MOF (Fe-MIL-88B@Fe-MIL-88C) by anisotropic MOF-on-MOF growth, (C₁-C₉) SEM images of Fe-MIL-88B@Fe-MIL-88C during the formation process to monitor MOF-on-MOF growth. (D) Schematic representation of the proposed anisotropic MOF-on-MOF growth process from the tip to the middle. (A) Adapted with permission^[316]. Copyright 2020, American Chemical Society. (B) Adapted with permission^[328]. Copyright 2019, John Wiley and Sons. (C and D) Adapted with permission^[354]. Copyright 2020, American Chemical Society. MOFs: Metal-organic frameworks.

photocatalytic reactions, especially when the metal particles have matching crystal faces with the MOFs. Qiu *et al.* prepared noble metal-doped Zr-MOF catalysts using a facile post-synthesis method and investigated the photocatalytic oxidation process of aromatic alcohols^[329]. They found that Au NPs promoted the oxidation of aromatic alcohols while Pt NPs inhibited the oxidation, and that the low conversion of aromatic alcohols over Pt/Zr-MOFs was due to the exposure of the Pt (200) crystal plane, which resulted in low yields during the production of O_2 . By studying the mechanism, this work will

improve the reference for the development of new photocatalytic materials. The bimetallic-doped MOFs also tend to exhibit notable performance. Among them are Pt-Ni nanoparticles with hollow open frameworks that exhibit superior catalytic behavior. Previous studies have focused on metal nanoparticles, rarely combining them with a second material, let alone encapsulating them as a core structure in a second material. In 2020, Chen *et al.* reported the encapsulation of Pt-Ni nanocentric structures in ZIF-8 alone to achieve core-shell and yolk-shell structures^[330]. They used the surfactant hexadecyltrimethylammonium bromide (CTAB) to encapsulate and control the Pt-Ni nanoframe. The surface-functionalized Pt-Ni nanoframe could be well dispersed in aqueous solution and subsequently added to ZIF-8 solution to prepare single core-shell complexes. 3D tomography confirmed the hollow nanoframe ground embedding.

While a wide variety of complexes of MOFs and metal nanoparticles are available, current methods are far from adequate for practical applications. The influence of both MOFs and MNPs on the catalytic properties of the complexes limits the complete understanding of the catalytic mechanism process. In the future, the development of *in-situ* characterization techniques will help us to understand the formation process and catalytic mechanism of the composites, and the completeness of the characterization tools can reasonably guide us to design specific composite catalysts for specific catalytic reactions.

MOFs/Polymers

With the development of polymer materials, the flexible nature of polymers, which have a softer structure than MOFs, can accommodate MOFs and regulate the growth of MOFs^[331,332]. Given these advantages, the hybridization of MOFs and polymers also creates great synergies, allowing the hybrids to have more complex structures and exhibit specific properties that are functionally superior to the individual components.

Previously, it has been found that MOF/polymers can strengthen the properties of MOFs by maintaining framework stability or enhancing the absorption of analytes^[333]. Cohen utilized a post-synthesis modified polymerization method to composite nylon and MOF via an interfacial polymerization technique^[334]. Compared to non-covalent hybrids, the covalent hybrids significantly increased the rate of decomposition of the simulant by nearly an order of magnitude. This material is expected to be designed as a potential textile. Previously, Hwang *et al.* developed a new nanoscale mesocrystal using a double-hydrophilic block polymer (DHBC) as a crystal modifier, as opposed to an amphiphilic block polymer^[118]. DHBC grows selectively and anisotropically attached to specific surfaces of MOFs, generating vertically aligned hexagonal rod mesocrystals. This work demonstrates the ability of polymers to modulate the growth of MOFs, providing a new means of building a complex and robust morphological platform.

The hybridization of MOFs as carriers with various polymers provides new insights into the future exploration of complex nanostructures. Multifunctional MOF-polymer hybrids are of great potential value in areas such as biomedicine and gas separation^[335]. Nevertheless, the hybrids still have limitations in some aspects (e.g., selectivity and long-term stability) which remain to be improved in the future.

MOF-on-MOF

MOF-on-MOF hybrid frameworks are generally constructed using epitaxial growth. Epitaxial growth is the process of depositing crystalline material on specific crystalline planes of the same orientation and similar lattice spacing of the crystal substrate, which often generates core-shell shaped or layered structures^[336,337]. The key to growth is the selection of suitable host and guest candidate MOFs for the epitaxy of MOF-on-MOF materials. Normally, secondary MOFs with well-matched lattice constants will grow homogeneously in all directions of the original MOF substrate, generating a core-shell structure. In contrast, when the lattice

constants of the host and guest are significantly different, the original MOF substrate will change, which may cause the secondary MOF layer to stop growing and the inherent elasticity of the MOF may offset the interfacial energy, thus continuing to produce epitaxial growth^[338]. Therefore, epitaxial growth methods can generally be divided into isotropic growth MOF-on-MOF and anisotropic growth MOF-on-MOF.

Isotropic growth on MOF substrates is achieved by matching lattice parameters in the a, b and c directions, leading to more flexible core-shell nanostructures^[339-341]. Metal sources and organic ligands are key to triggering isotropic growth. In 2016, Choi *et al.* then successfully synthesized the isotropically growing core-shell MIL-68@MIL-68-Br using MIL-68 as a template and MIL-68-Br as a secondary MOF^[342]. The same metal source, with little difference in ligands, led to almost identical structures for MIL-68 (Orthorhombic, $a = 21.77 \text{ \AA}$, $b = 37.68 \text{ \AA}$, $c = 7.23 \text{ \AA}$) and MIL-68-Br (Orthorhombic, $a = 21.73 \text{ \AA}$, $b = 37.61 \text{ \AA}$, $c = 7.22 \text{ \AA}$), resulting in isotropic growth. The length and thickness of the hexagonal rod structure increased with time. EDX spectral scans confirmed that the Br atoms were distributed as components of the shell structure at the edges of the hexagonal rod structure. Small differences in the ligands can lead to isotropic growth. Similarly, metal ion size can cause changes in cell parameters, but two similarly sized metal sources may be able to ignore differences in cell parameters. In 2018, Pan *et al.* used epitaxial growth to prepare core-shell ZIF-8 ($a = b = c = 16.9910 \text{ \AA}$) and ZIF-67 ($a = b = c = 16.9589 \text{ \AA}$) with similar topology and unitary cellular parameters ZIF-8@ZIF-67^[343]. Due to the relatively similar ion sizes of Zn^{2+} (74.0 pm) and Co^{2+} (74.5 pm), it is easy to form isotropically grown lattice-matched core-shell MOFs. The use of ZIF-67 or ZIF-8 as precursors for the fabrication of isotropic structures has been previously reported by Zhan *et al.*^[344].

Lattice mismatch secondary MOF growth tends to result in abnormally shaped particles that tend to grow anisotropically only on the specific surface of the MOF substrate; hence, the construction of MOF heterostructures has attracted much attention^[345-347]. Recently, anisotropic MOF-on-MOF growth has been shown to be an effective means of achieving MOF heterostructures, controlling the growth rate and orientation of secondary MOFs, *etc.*^[348-353]. The structure of anisotropically grown MOF-on-MOFs is usually sandwich or tubular in shape, but Lee *et al.* found that even if the lattice of secondary MOFs and MOF basal cells do not match, core-shell hybrid MOFs can be generated under anisotropic growth^[354]. The cell parameters show that MIL-88B and MIL-88C have a large mismatched cell lattice in the c-direction, with Fe-MIL-88C ($a = 10.22 \text{ \AA}$, $c = 23.60 \text{ \AA}$, $V = 2020 \text{ \AA}^3$) able to grow anisotropically on the MIL-88B ($a = 11.05 \text{ \AA}$, $c = 18.99 \text{ \AA}$, $V = 1980 \text{ \AA}^3$) template, resulting in a Fe-MIL-88B @Fe-MIL-88C shell-type hybrid MOF [Figure 25C and D]. By monitoring the reaction time, the growth of Fe-MIL-88C first starts at the ends of the template and then propagates towards the center of the template in the c direction, resulting in an increase in the overall size of the template and the formation of a well-defined core-shell hybrid. Gu *et al.* used an anisotropic MOF-on-MOF strategy to prepare two molecules with crystal surface differences into multilayer MOF heterostructures^[355]. A series of intercalated ZIF-L heterostructures were constructed by stacking ZIF-L-Zn and ZIF-L-Co in alternating three-, five-, seven- and multilayer structures, which are expected to be precursors for derivatives with tunable magnetic and catalytic properties.

CONCLUSION AND OUTLOOK

Over the past two to three decades, researchers have explored and developed a variety of synthetic strategies to prepare MOF materials with unique properties and structures, and consequently, tens of thousands of new MOF structures have been explored and discovered. This article summarizes the synthesis principles of MOFs over the years and explores the growth mechanisms of MOFs with different morphologies and dimensions. As an emerging nanocrystalline porous material, the synthetic strategy of MOFs is no longer limited to a single, traditional pathway (such as hydrothermal/solvothermal and solution methods), but rather to a combination of methods and mechanistic investigations in order to obtain high-performance

MOFs for a wide range of applications. In order to realize this target, the synthetic route needs to focus more on the combination of synthetic strategies and mechanistic investigations. In the case of nanostructures, they can be divided into 1D, 2D and 3D according to their specific geometric dimensions.

1D MOFs can be broadly classified as nanowires, nanorods and nanotubes. It is characterized by a high proportion of single dimensions (length, width and diameter) at the nanoscale. This anisotropic growth shortens the transport distance for charge migration. Nanowires tend to exhibit great flexibility due to their extremely high aspect ratio. When the aspect ratio is controlled at about 5, nanorods are easy to form. Hollow structure nanotubes with different winding modes can be divided into single- or multi-wall, which are often used in catalysis because of their high specific surface area. In spite of the limited yields, two strategies, the template and the template-free methods, have proven to be very effective for the production of 1D MOFs nanostructures. However, starting in isotropy without a template and gradually relying on anisotropic growth drives often makes it difficult to form stable one-dimensional structures. From a kinetic point of view, regulating the diffusion and growth of metal sources is a research direction. Under synthetic conditions, many parameters (such as temperature, time and precursor concentration) often influence the sizes and morphologies of MOFs, thus tailoring the MOFs crystals with desired morphology by thermodynamic and kinetic methods is often employed, and also presents challenges and opportunities for controlled synthesis of MOF crystals in future. 1D MOFs have superior properties in terms of catalysts and sensors due to the anisotropy of the crystals, abundant metal nodes and exposed reaction sites. Additionally, due to their porous nature, 1D MOFs can also exist as carriers for loading active nanoparticles.

2D MOFs are generally classified in the literature as single- or multi-layered nanostructures with ordered atomic networks and strong in-plane bonds. The benefits associated with ligand structural diversity (e.g., functionalization, -conjugation, induction effects) allow the customization of 2D MOFs at the molecular level. Mechanically superior multilayer structures are connected by weak van der Waals forces between the layers and can easily be disrupted by breaking the force equilibrium and exfoliating ultrathin nanosheets. These nanosheets are characterized by high sensitivity, neatly aligned planar pores and more unsaturated coordination centers exposed on the surface. This facilitates the use of 2D MOFs for applications such as adsorption and sensing. Furthermore, due to the advantages of the large lateral size of the nanosheets, 2D MOFs can also be found in recent years in the form of carriers for single atoms or molecular catalyst anchoring. Research on 2D MOFs has also evolved from the initial identification of reticular architectures to the study of the relationship between their structures, properties and applications. However, the preparation of 2D MOFs with excellent stability, good homogeneity and controlled thickness is still a challenge.

Compared to 1D MOFs and 2D MOFs, 3D MOFs have more complex structures, great flexibility in morphology and tend to be more robust. More flexible modulation of the pore structure is possible with 3D MOFs that possess a stronger framework structure. Various auxiliary synthesis methods should be developed to synthesize more diverse 3D MOFs. They have larger dimensions, customizable pore sizes and the ability to facilitate hydrophilic/hydrophobic surface functionalization. Because of pores with relatively larger sizes (meso- and macro-porosity), 3D MOFs can greatly improve mass transfer efficiency and offer great advantages for applications in separation and catalysis. The key to creating 3D structures lies in the regulation of the nucleation and growth process of MOF crystals. In other words, it is the process of regulating the self-assembly between metal ions and organic ligands. 3D MOFs can accommodate a wide range of guest species, which in turn form numbers of MOF-hybrids. With the synergistic effect of different components, 3D MOF-hybrids are also popular in adsorption and separation.

Essentially, exploring the synthesis strategies of different MOFs is to investigate MOFs from a morphological perspective without changing their chemical composition. In different dimensions and sizes of MOFs, we expect to draw certain synthetic experiences to enhance the physical designability of these porous materials. The template method, as cited in this review, offers additional possibilities for morphological control of MOFs. Templates can be used as reservoirs for metal sources, reaction sites for MOF nucleation or functional components for MOF hybridization, allowing the synthesis of precisely layered and variable porous structures. The kinetic and thermodynamic investigation of the nucleation and growth of MOFs is also essential to appreciate the morphological changes in MOFs. The rate of coordination between metal sites and organic ligands deeply affects the nucleation of MOFs. In short, the nucleation of MOFs is influenced by coordination bonds, and the stability of coordination bonds in MOFs, enabling them to react or transform to other substances in response to external stimuli. Therefore, it is important to study how to control and improve the stability of coordination bonds in the framework at the molecular level.

In addition, it is essential to establish a link between the variable morphology of MOFs and their properties in order to further investigate the value of MOFs for future applications. The crystallinity of MOFs, pore size, surface area, surface roughness and other factors of their own morphology have a huge impact on the properties of the material. For example, in the energy sector, the surface area of the material has a great influence on the charging and discharging efficiency of the electrodes. Porosity and pore size also deeply influence the rate of transport between the surface of the electrode material and the mediating ions. In catalysis, the catalytic performance of a material is largely dependent on the “recognition” of a specific chemical molecule by the material’s pore structure. It may be possible to combine experimental data, theoretical calculations and machine learning algorithms to create a database of simulations of the morphology and potential applications of MOFs and to select the most suitable MOFs.

While great progress has been achieved in the synthesis of MOFs over the years, great challenges remain as we continue to expand the number of MOFs in the family. Firstly, the mechanism of the genesis and construction of these compounds is not yet fully understood. With the development of technology and the fact that a variety of analytical instruments are nowadays indispensable for systematic studies, it is necessary to combine *in-situ* and *ex-situ* characterization techniques with theoretical methods to study the different stages of the nucleation and growth of MOF crystals. New characterization tools and theories promise to accurately describe the relationship between the coordination environment, framework parameters and stability of MOFs. Current simulation algorithms and computational methods are also useful for understanding the mechanisms, showing great potential for screening the types of MOFs separated by mixed gases. The nucleation and growth of MOFs are highly complicated processes and take place through a variety of different mechanistic processes (solvation-recrystallization, monomer addition, solid-phase conversion, *etc.*), as probed with the help of new techniques^[356]. Combining the development of new techniques will not only help explain the crystal anisotropic growth process, but will also be useful for the further synthesis of MOFs with sub-stable polymorphs and improved properties^[357]. Secondly, the stability of MOFs is still unsatisfactory, such as water, thermal and chemical stability. Finally, most of the materials constructed based on MOFs are currently limited to the laboratory level and have not been produced on a large scale. How to reduce cost, simplify complex synthesis procedures, increase yields and achieve green production are important factors to consider for the commercial application of MOF-based materials.

Perhaps in the longer term, the synthesis of crystals of MOFs by various methods could serve as a cornerstone for a new field of scientific research and the study of the relationship between molecular and macroscopic scale changes promises to be an emerging scientific theme. We wish that the strategies

discussed here for the synthesis of MOFs in different dimensions will provide inspiration for the future fabrication of MOFs with desirable phases, morphologies and properties. We believe that a bright future for MOF-based porous materials will certainly be achieved by the continued exploration of the above challenges.

DECLARATIONS

Acknowledgements

We acknowledge the support from the National Natural Science Foundation of China, the Top-notch Academic Programs Project of Jiangsu Higher Education Institutions (TAPP), Program for New Century Excellent Talents of the University in China, the Six Talent Plan, and Qinglan Project. We also acknowledge the Priority Academic Program Development of Jiangsu Higher Education Institutions and the technical support we received at the Testing Center of Yangzhou University. Liu Y acknowledges Guangdong Basic and Applied Basic Research Foundation, Shenzhen Government's Plan of Science and Technology.

Authors' contributions

Investigation, methodology, data curation, writing original draft: Su Y

Conceptualization, formal analysis: Yuan G

Methodology, conceptualization, formal analysis: Hu J

Investigation: Feng W

Validation: Zeng Q

Methodology, supervision, funding acquisition: Liu Y

Supervision, funding acquisition, writing-review & editing: Pang H

Availability of data and materials

Not applicable.

Financial support and sponsorship

This work was supported by the National Natural Science Foundation of China (NSFC-21671170, 21673203, 21201010 and U1904215), the Top-notch Academic Programs Project of Jiangsu Higher Education Institutions (TAPP), Program for New Century Excellent Talents of the University in China (NCET-13-0645), the Six Talent Plan (2015-XCL-030), and Qinglan Project. We also acknowledge the Priority Academic Program Development of Jiangsu Higher Education Institutions and the technical support we received at the Testing Center of Yangzhou University. Liu Y acknowledges Guangdong Basic and Applied Basic Research Foundation (2019A1515110735) and Shenzhen Government's Plan of Science and Technology (JCYJ20170818144659020).

Conflicts of interest

All authors declared that there are no conflicts of interest.

Ethical approval and consent to participate

Not applicable.

Consent for publication

Not applicable.

Copyright

© The Author(s) 2023.

REFERENCES

1. Yaghi OM, Li G, Li H. Selective binding and removal of guests in a microporous metal-organic framework. *Nature* 1995;378:703-6. DOI
2. Schneemann A, Bon V, Schwedler I, Senkovska I, Kaskel S, Fischer RA. Flexible metal-organic frameworks. *Chem Soc Rev* 2014;43:6062-96. DOI PubMed
3. Zhou HC, Kitagawa S. Metal-organic frameworks (MOFs). *Chem Soc Rev* 2014;43:5415-8. DOI PubMed
4. Islamoglu T, Goswami S, Li Z, Howarth AJ, Farha OK, Hupp JT. Postsynthetic tuning of metal-organic frameworks for targeted applications. *Acc Chem Res* 2017;50:805-13. DOI PubMed
5. Zhao W, Peng J, Wang W, Liu S, Zhao Q, Huang W. Ultrathin two-dimensional metal-organic framework nanosheets for functional electronic devices. *Coord Chem Rev* 2018;377:44-63. DOI
6. Chen L, Xu Q. Metal-organic framework composites for catalysis. *Matter* 2019;1:57-89. DOI
7. Jiao L, Seow JYR, Skinner WS, Wang ZU, Jiang H. Metal-organic frameworks: structures and functional applications. *Materials Today* 2019;27:43-68. DOI
8. Liu D, Wan J, Pang G, Tang Z. Hollow metal-organic-framework micro/nanostructures and their derivatives: emerging multifunctional materials. *Adv Mater* 2019;31:e1803291. DOI PubMed
9. Xiao JD, Jiang HL. Metal-organic frameworks for photocatalysis and photothermal catalysis. *Acc Chem Res* 2019;52:356-66. DOI PubMed
10. Li H, Eddaoudi M, O'keeffe M, Yaghi OM. Design and synthesis of an exceptionally stable and highly porous metal-organic framework. *Nature* 1999;402:276-9. DOI
11. Schubert U. Cluster-based inorganic-organic hybrid materials. *Chem Soc Rev* 2011;40:575-82. DOI PubMed
12. Chen Z, Jiang H, Li M, O'Keeffe M, Eddaoudi M. Reticular chemistry 3.2: typical minimal edge-transitive derived and related nets for the design and synthesis of metal-organic frameworks. *Chem Rev* 2020;120:8039-65. DOI PubMed
13. Kitagawa S, Kondo M. Functional micropore chemistry of crystalline metal complex-assembled compounds. *BCSJ* 1998;71:1739-53. DOI
14. Kitagawa S, Kitaura R, Noro S. Functional porous coordination polymers. *Angew Chem Int Ed Engl* 2004;43:2334-75. DOI PubMed
15. An J, Geib SJ, Rosi NL. Cation-triggered drug release from a porous zinc-adeninate metal-organic framework. *J Am Chem Soc* 2009;131:8376-7. DOI PubMed
16. Stock N, Biswas S. Synthesis of metal-organic frameworks (MOFs): routes to various MOF topologies, morphologies, and composites. *Chem Rev* 2012;112:933-69. DOI PubMed
17. Tian D, Xu J, Xie ZJ, et al. The first example of hetero-triple-walled metal-organic frameworks with high chemical stability constructed via flexible integration of mixed molecular building blocks. *Adv Sci* 2016;3:1500283. DOI PubMed PMC
18. Liu W, Huang J, Yang Q, et al. Multi-shelled hollow metal-organic frameworks. *Angew Chem Int Ed Engl* 2017;56:5512-6. DOI PubMed
19. Liu Y, Liu G, Zhang C, et al. Enhanced CO₂/CH₄ separation performance of a mixed matrix membrane based on tailored MOF-polymer formulations. *Adv Sci* 2018;5:1800982. DOI
20. Peng Y, Huang H, Zhang Y, et al. A versatile MOF-based trap for heavy metal ion capture and dispersion. *Nat Commun* 2018;9:187. DOI PubMed PMC
21. Zhang L, Liu W, Shi W, et al. Boosting lithium storage properties of MOF derivatives through a wet-spinning assembled fiber strategy. *Chemistry* 2018;24:13792-9. DOI PubMed
22. Xue D, Wang Q, Bai J. Amide-functionalized metal-organic frameworks: syntheses, structures and improved gas storage and separation properties. *Coord Chem Rev* 2019;378:2-16. DOI
23. Xie J, Yang X, Xie Y. Defect engineering in two-dimensional electrocatalysts for hydrogen evolution. *Nanoscale* 2020;12:4283-94. DOI PubMed
24. Velásquez-hernández MDJ, Linares-moreau M, Astria E, et al. Towards applications of bioentities@MOFs in biomedicine. *Coord Chem Rev* 2021;429:213651. DOI
25. Tang Y, Zheng S, Cao S, et al. Hollow mesoporous carbon nanospheres space-confining ultrathin nanosheets superstructures for efficient capacitive deionization. *J Colloid Interface Sci* 2022;626:1062-9. DOI PubMed
26. Wang F, Hu J, Liu Y, et al. Turning coordination environment of 2D nickel-based metal-organic frameworks by π -conjugated molecule for enhancing glucose electrochemical sensor performance. *Mater Today Chem* 2022;24:100885. DOI
27. Dybtsev DN, Chun H, Kim K. Rigid and flexible: a highly porous metal-organic framework with unusual guest-dependent dynamic behavior. *Angew Chem* 2004;116:5143-6. DOI PubMed
28. Cohen SM. Postsynthetic methods for the functionalization of metal-organic frameworks. *Chem Rev* 2012;112:970-1000. DOI PubMed
29. Larsson EM, Langhammer C, Zorić I, Kasemo B. Nanoplasmonic probes of catalytic reactions. *Science* 2009;326:1091-4. DOI PubMed
30. Liu G, Yang HG, Pan J, Yang YQ, Lu GQ, Cheng HM. Titanium dioxide crystals with tailored facets. *Chem Rev* 2014;114:9559-612. DOI PubMed
31. Chen D, Zhang N, Tian J, Liu C, Du M. Pore modulation of metal-organic frameworks towards enhanced hydrothermal stability and

- acetylene uptake via incorporation of different functional brackets. *J Mater Chem A* 2017;5:4861-7. DOI
32. Li X, Xue H, Pang H. Facile synthesis and shape evolution of well-defined phosphotungstic acid potassium nanocrystals as a highly efficient visible-light-driven photocatalyst. *Nanoscale* 2017;9:216-22. DOI PubMed
 33. Shi D, Zheng R, Sun MJ, et al. Semiconductive copper(I)-organic frameworks for efficient light-driven hydrogen generation without additional photosensitizers and cocatalysts. *Angew Chem Int Ed Engl* 2017;56:14637-41. DOI PubMed
 34. Cai G, Yan P, Zhang L, Zhou HC, Jiang HL. Metal-organic framework-based hierarchically porous materials: synthesis and applications. *Chem Rev* 2021;121:12278-326. DOI PubMed
 35. Furukawa S, Reboul J, Diring S, Sumida K, Kitagawa S. Structuring of metal-organic frameworks at the mesoscopic/macroscale. *Chem Soc Rev* 2014;43:5700-34. DOI PubMed
 36. Farha OK, Hupp JT. Rational design, synthesis, purification, and activation of metal-organic framework materials. *Acc Chem Res* 2010;43:1166-75. DOI PubMed
 37. Li B, Gu P, Feng Y, et al. Ultrathin nickel-cobalt phosphate 2D nanosheets for electrochemical energy storage under aqueous/solid-state electrolyte. *Adv Funct Mater* 2017;27:1605784. DOI
 38. Abednatanzi S, Gohari Derakhshandeh P, Depauw H, et al. Mixed-metal metal-organic frameworks. *Chem Soc Rev* 2019;48:2535-65. DOI PubMed
 39. Guo F, Yang S, Liu Y, Wang P, Huang J, Sun W. Size engineering of metal-organic framework MIL-101(Cr)-Ag hybrids for photocatalytic CO₂ reduction. *ACS Catal* 2019;9:8464-70. DOI
 40. Li Y, Xu Y, Liu Y, Pang H. Exposing {001} crystal plane on hexagonal Ni-MOF with surface-grown cross-linked mesh-structures for electrochemical energy storage. *Small* 2019;15:e1902463. DOI PubMed
 41. Lerma-Berlanga B, R Ganivet C, Almora-Barrios N, et al. Effect of linker distribution in the photocatalytic activity of multivariate mesoporous crystals. *J Am Chem Soc* 2021;143:1798-806. DOI PubMed
 42. Li W, Guo X, Geng P, et al. Rational design and general synthesis of multimetallic metal-organic framework nano-octahedra for enhanced Li-S battery. *Adv Mater* 2021;33:e2105163. DOI PubMed
 43. Wei Y, Zhu B, Wang J, et al. A series of novel Co(ii)-based MOFs: syntheses, structural diversity, and various properties. *CrystEngComm* 2021;23:6376-87. DOI
 44. Parsaei M, Akhbari K, White J. Modulating carbon dioxide storage by facile synthesis of nanoporous pillared-layered metal-organic framework with different synthetic routes. *Inorg Chem* 2022;61:3893-902. DOI PubMed
 45. Zhang X, Han X, Zhu F, et al. Route to the structure-controlled synthesis of Fe nanobelts and their oxygen evolution reaction application. *Inorg Chem* 2022;61:3024-8. DOI PubMed
 46. Zorainy MY, Sheashea M, Kaliaguine S, Gobara M, Boffito DC. Facile solvothermal synthesis of a MIL-47(V) metal-organic framework for a high-performance Epoxy/MOF coating with improved anticorrosion properties. *RSC Adv* 2022;12:9008-22. DOI PubMed PMC
 47. Ai L, Li L, Zhang C, Fu J, Jiang J. MIL-53(Fe): a metal-organic framework with intrinsic peroxidase-like catalytic activity for colorimetric biosensing. *Chemistry* 2013;19:15105-8. DOI PubMed
 48. Dao X, Ni Y. Al-based coordination polymer nanotubes: simple preparation, post-modification and application in Fe³⁺ ions sensing. *Dalton Trans* 2017;46:5373-83. DOI PubMed
 49. He T, Ni B, Zhang S, et al. Ultrathin 2D zirconium metal-organic framework nanosheets: preparation and application in photocatalysis. *Small* 2018;14:e1703929. DOI PubMed
 50. Zhao M, Wang Y, Ma Q, et al. Ultrathin 2D metal-organic framework nanosheets. *Adv Mater* 2015;27:7372-8. DOI PubMed
 51. Pathak A, Shen JW, Usman M, et al. Integration of a (-Cu-S)_n plane in a metal-organic framework affords high electrical conductivity. *Nat Commun* 2019;10:1721. DOI PubMed PMC
 52. Marsh C, Han X, Li J, et al. Exceptional packing density of ammonia in a dual-functionalized metal-organic framework. *J Am Chem Soc* 2021;143:6586-92. DOI PubMed PMC
 53. Li XX, Liu J, Zhang L, et al. Hydrophobic polyoxometalate-based metal-organic framework for efficient CO₂ photoconversion. *ACS Appl Mater Interfaces* 2019;11:25790-5. DOI PubMed
 54. Zhao S, Wang Y, Dong J, et al. Ultrathin metal-organic framework nanosheets for electrocatalytic oxygen evolution. *Nat Energy* 2016;1. DOI PubMed
 55. Pichon A, Lazuen-garay A, James SL. Solvent-free synthesis of a microporous metal-organic framework. *CrystEngComm* 2006;8:211. DOI
 56. Katsenis AD, Puškarić A, Štrukil V, et al. In situ X-ray diffraction monitoring of a mechanochemical reaction reveals a unique topology metal-organic framework. *Nat Commun* 2015;6:6662. DOI PubMed
 57. Pan ZW, Dai ZR, Wang ZL. Nanobelts of semiconducting oxides. *Science* 2001;291:1947-9. DOI PubMed
 58. Li X, Wang X, Zhang L, Lee S, Dai H. Chemically derived, ultrasoft graphene nanoribbon semiconductors. *Science* 2008;319:1229-32. DOI PubMed
 59. Liu Q, Zhou Y, Kou J, et al. High-yield synthesis of ultralong and ultrathin Zn₂GeO₄ nanoribbons toward improved photocatalytic reduction of CO₂ into renewable hydrocarbon fuel. *J Am Chem Soc* 2010;132:14385-7. DOI PubMed
 60. He J, Liu H, Xu B, Wang X. Highly flexible sub-1 nm tungsten oxide nanobelts as efficient desulfurization catalysts. *Small* 2015;11:1144-9. DOI PubMed
 61. Liang HW, Liu JW, Qian HS, Yu SH. Multiplex templating process in one-dimensional nanoscale: controllable synthesis,

- macroscopic assemblies, and applications. *Acc Chem Res* 2013;46:1450-61. [DOI PubMed](#)
62. Liu Y, Goebel J, Yin Y. Templated synthesis of nanostructured materials. *Chem Soc Rev* 2013;42:2610-53. [DOI PubMed](#)
63. Petkovich ND, Stein A. Controlling macro- and mesostructures with hierarchical porosity through combined hard and soft templating. *Chem Soc Rev* 2013;42:3721-39. [DOI PubMed](#)
64. Yu L, Wu HB, Lou XW. Self-templated formation of hollow structures for electrochemical energy applications. *Acc Chem Res* 2017;50:293-301. [DOI PubMed](#)
65. Pachfule P, Balan BK, Kurungot S, Banerjee R. One-dimensional confinement of a nanosized metal organic framework in carbon nanofibers for improved gas adsorption. *Chem Commun* 2012;48:2009-11. [DOI PubMed](#)
66. Zhang W, Wu ZY, Jiang HL, Yu SH. Nanowire-directed templating synthesis of metal-organic framework nanofibers and their derived porous doped carbon nanofibers for enhanced electrocatalysis. *J Am Chem Soc* 2014;136:14385-8. [DOI PubMed](#)
67. Zhang G, Hou S, Zhang H, et al. High-performance and ultra-stable lithium-ion batteries based on MOF-derived ZnO@ZnO quantum dots/C core-shell nanorod arrays on a carbon cloth anode. *Adv Mater* 2015;27:2400-5. [DOI PubMed](#)
68. Yao MS, Tang WX, Wang GE, Nath B, Xu G. MOF thin film-coated metal oxide nanowire array: significantly improved chemiresistor sensor performance. *Adv Mater* 2016;28:5229-34. [DOI PubMed](#)
69. Zhang W, Cai G, Wu R, et al. Templating synthesis of metal-organic framework nanofiber aerogels and their derived hollow porous carbon nanofibers for energy storage and conversion. *Small* 2021;17:e2004140. [DOI PubMed](#)
70. Jahan M, Bao Q, Yang JX, Loh KP. Structure-directing role of graphene in the synthesis of metal-organic framework nanowire. *J Am Chem Soc* 2010;132:14487-95. [DOI PubMed](#)
71. Caddeo F, Vogt R, Weil D, Sigle W, Toimil-Molares ME, Maijenburg AW. Tuning the size and shape of NanoMOFs via templated electrodeposition and subsequent electrochemical oxidation. *ACS Appl Mater Interfaces* 2019;11:25378-87. [DOI PubMed](#)
72. Arbulu RC, Jiang YB, Peterson EJ, Qin Y. Metal-organic framework (MOF) nanorods, nanotubes, and nanowires. *Angew Chem Int Ed Engl* 2018;57:5813-7. [DOI PubMed](#)
73. Li SC, Hu BC, Shang LM, et al. General synthesis and solution processing of metal-organic framework nanofibers. *Adv Mater* 2022;34:e2202504. [DOI PubMed](#)
74. Steunou N, Livage J. Rational design of one-dimensional vanadium(v) oxide nanocrystals: an insight into the physico-chemical parameters controlling the crystal structure, morphology and size of particles. *CrystEngComm* 2015;17:6780-95. [DOI](#)
75. Pan L, Gao P, Tervoort E, Tartakovsky AM, Niederberger M. Surface energy-driven ex situ hierarchical assembly of low-dimensional nanomaterials on graphene aerogels: a versatile strategy. *J Mater Chem A* 2018;6:18551-60. [DOI](#)
76. Muschi M, Lalitha A, Sene S, et al. Formation of a single-crystal aluminum-based MOF nanowire with graphene oxide nanoscrolls as structure-directing agents. *Angew Chem Int Ed Engl* 2020;59:10353-8. [DOI PubMed](#)
77. Sharifi T, Gracia-Espino E, Barzegar HR, et al. Formation of nitrogen-doped graphene nanoscrolls by adsorption of magnetic γ -Fe₂O₃ nanoparticles. *Nat Commun* 2013;4:2319. [DOI PubMed](#)
78. Qiao S, Wang Q, Zhang Q, Huang C, He G, Zhang F. Sacrificial template method to synthesize atomically dispersed Mn atoms on S, N-codoped carbon as a separator modifier for advanced Li-S batteries. *ACS Appl Mater Interfaces* 2022;14:42123-33. [DOI PubMed](#)
79. Sun JK, Zhan WW, Akita T, Xu Q. Toward homogenization of heterogeneous metal nanoparticle catalysts with enhanced catalytic performance: soluble porous organic cage as a stabilizer and homogenizer. *J Am Chem Soc* 2015;137:7063-6. [DOI PubMed](#)
80. Zhao M, Yuan K, Wang Y, et al. Metal-organic frameworks as selectivity regulators for hydrogenation reactions. *Nature* 2016;539:76-80. [DOI PubMed](#)
81. Zhang W, Liu Y, Lu G, et al. Mesoporous metal-organic frameworks with size-, shape-, and space-distribution-controlled pore structure. *Adv Mater* 2015;27:2923-9. [DOI PubMed](#)
82. Yang Q, Liu W, Wang B, et al. Regulating the spatial distribution of metal nanoparticles within metal-organic frameworks to enhance catalytic efficiency. *Nat Commun* 2017;8:14429. [DOI PubMed PMC](#)
83. Reboul J, Furukawa S, Horike N, et al. Mesoscopic architectures of porous coordination polymers fabricated by pseudomorphic replication. *Nat Mater* 2012;11:717-23. [DOI PubMed](#)
84. Zhan WW, Kuang Q, Zhou JZ, Kong XJ, Xie ZX, Zheng LS. Semiconductor@metal-organic framework core-shell heterostructures: a case of ZnO@ZIF-8 nanorods with selective photoelectrochemical response. *J Am Chem Soc* 2013;135:1926-33. [DOI PubMed](#)
85. Majano G, Pérez-Ramírez J. Scalable room-temperature conversion of copper(II) hydroxide into HKUST-1 (Cu₃(btc)₂). *Adv Mater* 2013;25:1052-7. [DOI](#)
86. Li B, Ma JG, Cheng P. Silica-protection-assisted encapsulation of Cu₂O nanocubes into a metal-organic framework (ZIF-8) to provide a composite catalyst. *Angew Chem Int Ed Engl* 2018;57:6834-7. [DOI](#)
87. Roy P, Berger S, Schmuki P. TiO₂ nanotubes: synthesis and applications. *Angew Chem Int Ed Engl* 2011;50:2904-39. [DOI PubMed](#)
88. Jiang Z, Zhao J, Li C, Liao Q, Xiao R, Yang W. Strong synergistic effect of Co₃O₄ encapsulated in nitrogen-doped carbon nanotubes on the nonradical-dominated persulfate activation. *Carbon* 2020;158:172-83. [DOI](#)
89. Jang W, Kim BG, Seo S, et al. Strong dark current suppression in flexible organic photodetectors by carbon nanotube transparent electrodes. *Nano Today* 2021;37:101081. [DOI](#)
90. Wu L, Wu T, Liu Z, et al. Carbon nanotube-based materials for persulfate activation to degrade organic contaminants: properties, mechanisms and modification insights. *J Hazard Mater* 2022;431:128536. [DOI PubMed](#)
91. Reddy MV, Subba Rao GV, Chowdari BV. Metal oxides and oxyalts as anode materials for Li ion batteries. *Chem Rev* 2013;113:5364-457. [DOI PubMed](#)

92. Yu X, Yu L, Lou XWD. Metal sulfide hollow nanostructures for electrochemical energy storage. *Adv Energy Mater* 2016;6:1501333. DOI
93. Schulze HA, Hoppe B, Schäfer M, Warwas DP, Behrens P. Electrically conducting nanocomposites of carbon nanotubes and metal-organic frameworks with strong interactions between the two components. *ChemNanoMat* 2019;5:1159-69. DOI
94. Hu X, Huang T, Wang S, et al. Separator modified by Co-porphyrin based Zr-MOF@CNT composite enabling efficient polysulfides catalytic conversion for advanced lithium-sulfur batteries. *Electrochimica Acta* 2021;398:139317. DOI
95. Chronopoulos DD, Saini H, Tantis I, Zbořil R, Jayaramulu K, Otyepka M. Carbon nanotube based metal-organic framework hybrids from fundamentals toward applications. *Small* 2022;18:e2104628. DOI PubMed
96. Chen YM, Yu L, Lou XW. Hierarchical tubular structures composed of Co_3O_4 hollow nanoparticles and carbon nanotubes for lithium storage. *Angew Chem Int Ed Engl* 2016;55:5990-3. DOI PubMed
97. Yin Y, Rioux RM, Erdonmez CK, Hughes S, Somorjai GA, Alivisatos AP. Formation of hollow nanocrystals through the nanoscale Kirkendall effect. *Science* 2004;304:711-4. DOI PubMed
98. Liu T, Liu Y, Xu J, Yao L, Liu D, Wang C. Conversion of Cu_2O nanowires into $\text{Cu}_2\text{O}/\text{HKUST-1}$ core/sheath nanostructures and hierarchical HKUST-1 nanotubes. *RSC Adv* 2016;6:91440-4. DOI
99. Li X, Yan Y, Zhang B, Bai T, Wang Z, He T. PAN-derived electrospun nanofibers for supercapacitor applications: ongoing approaches and challenges. *J Mater Sci* 2021;56:10745-81. DOI
100. Li X, Zhou R, Wang Z, Zhang M, He T. Electrospun metal-organic framework based nanofibers for energy storage and environmental applications: current approaches and challenges. *J Mater Chem A* 2022;10:1642-81. DOI
101. Kakade MV, Givens S, Gardner K, Lee KH, Chase DB, Rabolt JF. Electric field induced orientation of polymer chains in macroscopically aligned electrospun polymer nanofibers. *J Am Chem Soc* 2007;129:2777-82. DOI PubMed
102. Sankar SS, Karthick K, Sangeetha K, Karmakar A, Kundu S. Transition-metal-based zeolite imidazolate framework nanofibers via an electrospinning approach: a review. *ACS Omega* 2020;5:57-67. DOI PubMed PMC
103. Sankar SS, Karthick K, Sangeetha K, Karmakar A, Madhu R, Kundu S. Current perspectives on 3D ZIFs incorporated with 1D carbon matrices as fibers via electrospinning processes towards electrocatalytic water splitting: a review. *J Mater Chem A* 2021;9:11961-2002. DOI
104. Dou Y, Zhang W, Kaiser A. Electrospinning of metal-organic frameworks for energy and environmental applications. *Adv Sci* 2020;7:1902590. DOI PubMed PMC
105. Lu AX, McEntee M, Browe MA, Hall MG, DeCoste JB, Peterson GW. MOFabric: electrospun nanofiber mats from PVDF/ UiO-66-NH_2 for chemical protection and decontamination. *ACS Appl Mater Interfaces* 2017;9:13632-6. DOI PubMed
106. McCarthy DL, Liu J, Dwyer DB, et al. Electrospun metal-organic framework polymer composites for the catalytic degradation of methyl paraoxon. *New J Chem* 2017;41:8748-53. DOI
107. Bai Z, Liu S, Chen P, Cheng G, Wu G, Liu Y. Enhanced proton conduction of imidazole localized in one-dimensional Ni-metal-organic framework nanofibers. *Nanotechnology* 2020;31:125702. DOI PubMed
108. Liang H, Yao A, Jiao X, Li C, Chen D. Fast and sustained degradation of chemical warfare agent simulants using flexible self-supported metal-organic framework filters. *ACS Appl Mater Interfaces* 2018;10:20396-403. DOI PubMed
109. Ji D, Fan L, Tao L, et al. The Kirkendall effect for engineering oxygen vacancy of hollow Co_3O_4 nanoparticles toward high-performance portable zinc-air batteries. *Angew Chem Int Ed Engl* 2019;58:13840-4. DOI
110. Niu Q, Guo J, Chen B, Nie J, Guo X, Ma G. Bimetal-organic frameworks/polymer core-shell nanofibers derived heteroatom-doped carbon materials as electrocatalysts for oxygen reduction reaction. *Carbon* 2017;114:250-60. DOI
111. Efome JE, Rana D, Matsuura T, Lan CQ. Insight studies on metal-organic framework nanofibrous membrane adsorption and activation for heavy metal ions removal from aqueous solution. *ACS Appl Mater Interfaces* 2018;10:18619-29. DOI PubMed
112. Topuz F, Abdulhamid MA, Hardian R, Holtz T, Szekeley G. Nanofibrous membranes comprising intrinsically microporous polyimides with embedded metal-organic frameworks for capturing volatile organic compounds. *J Hazard Mater* 2022;424:127347. DOI PubMed
113. Chen LF, Lu Y, Yu L, Lou XW. Designed formation of hollow particle-based nitrogen-doped carbon nanofibers for high-performance supercapacitors. *Energy Environ Sci* 2017;10:1777-83. DOI
114. Huang H, Wang J, Yang X, et al. Unveiling the advances of nanostructure design for alloy-type potassium-ion battery anodes via in situ TEM. *Angew Chem Int Ed Engl* 2020;59:14504-10. DOI PubMed
115. Dou Y, Grande C, Kaiser A, Zhang W. Highly structured metal-organic framework nanofibers for methane storage. *Sci China Mater* 2021;64:1742-50. DOI
116. Zheng J, Wu Y, Deng K, et al. Chirality-discriminated conductivity of metal-amino acid biocoordination polymer nanowires. *ACS Nano* 2016;10:8564-70. DOI PubMed
117. Shi J, Zhang J, Tan D, et al. Rapid, room-temperature and template-free synthesis of metal-organic framework nanowires in alcohol. *ChemCatChem* 2019;11:2058-62. DOI
118. Hwang J, Heil T, Antonietti M, Schmidt BVKJ. Morphogenesis of metal-organic mesocrystals mediated by double hydrophilic block copolymers. *J Am Chem Soc* 2018;140:2947-56. DOI PubMed
119. Chi WS, Sundell BJ, Zhang K, Harrigan DJ, Hayden SC, Smith ZP. Mixed-matrix membranes formed from multi-dimensional metal-organic frameworks for enhanced gas transport and plasticization resistance. *ChemSusChem* 2019;12:2355-60. DOI PubMed
120. Rosnes MH, Nesse FS, Opitz M, Dietzel PD. Morphology control in modulated synthesis of metal-organic framework CPO-27.

- Microporous Mesoporous Mater* 2019;275:207-13. DOI
121. Yu B, Ye G, Chen J, Ma S. Membrane-supported 1D MOF hollow superstructure array prepared by polydopamine-regulated contra-diffusion synthesis for uranium entrapment. *Environ Pollut* 2019;253:39-48. DOI PubMed
 122. Bonnett BL, Smith ED, De La Garza M, et al. PCN-222 metal-organic framework nanoparticles with tunable pore size for nanocomposite reverse osmosis membranes. *ACS Appl Mater Interfaces* 2020;12:15765-73. DOI PubMed
 123. Feng L, Wang KY, Lv XL, Yan TH, Zhou HC. Hierarchically porous metal-organic frameworks: synthetic strategies and applications. *Natl Sci Rev* 2020;7:1743-58. DOI PubMed PMC
 124. Liu X, Kirlikovali KO, Chen Z, et al. Small molecules, big effects: tuning adsorption and catalytic properties of metal-organic frameworks. *Chem Mater* 2021;33:1444-54. DOI
 125. Song Z, Zhang L, Doyle-davis K, Fu X, Luo J, Sun X. Recent advances in MOF-derived single atom catalysts for electrochemical applications. *Adv Energy Mater* 2020;10:2001561. DOI
 126. Wen X, Zhang Q, Guan J. Applications of metal-organic framework-derived materials in fuel cells and metal-air batteries. *Coord Chem Rev* 2020;409:213214. DOI
 127. Wang Q, Astruc D. State of the art and prospects in metal-organic framework (MOF)-based and MOF-derived nanocatalysis. *Chem Rev* 2020;120:1438-511. DOI PubMed
 128. Tsuruoka T, Furukawa S, Takashima Y, Yoshida K, Isoda S, Kitagawa S. Nanoporous nanorods fabricated by coordination modulation and oriented attachment growth. *Angew Chem Int Ed Engl* 2009;48:4739-43. DOI PubMed
 129. Pachfule P, Shinde D, Majumder M, Xu Q. Fabrication of carbon nanorods and graphene nanoribbons from a metal-organic framework. *Nat Chem* 2016;8:718-24. DOI PubMed
 130. Liu X, Jia Q, Fu Y, Zheng T. Exfoliation of metal-organic framework nanosheets using surface acoustic waves. *Ultrason Sonochem* 2022;83:105943. DOI PubMed PMC
 131. Zou L, Kitta M, Hong J, et al. Fabrication of a spherical superstructure of carbon nanorods. *Adv Mater* 2019;31:e1900440. DOI PubMed
 132. Mallick A, Garai B, Díaz DD, Banerjee R. Hydrolytic conversion of a metal-organic polyhedron into a metal-organic framework. *Angew Chem Int Ed Engl* 2013;52:13755-9. DOI PubMed
 133. Shao D, Shi L, Yin L, et al. Reversible on-off switching of both spin crossover and single-molecule magnet behaviours via a crystal-to-crystal transformation. *Chem Sci* 2018;9:7986-91. DOI PubMed PMC
 134. Qu X, Yan B. Zn(ii)/Cd(ii)-based metal-organic frameworks: crystal structures, Ln(iii)-functionalized luminescence and chemical sensing of dichloroaniline as a pesticide biomarker. *J Mater Chem C* 2020;8:9427-39. DOI
 135. Ciupa-litwa A, Janczak J, Peksa P, Sieradzki A. Elucidation of the mechanism of phase transition in a zinc formate framework templated by a diammonium cation - structural, phonon and dielectric studies. *Crystals* 2021;11:213. DOI
 136. Kim J, Ha J, Lee JH, Moon HR. Solid-state phase transformations toward a metal-organic framework of 7-connected Zn₄O secondary building units. *Nano Res* 2021;14:411-6. DOI
 137. Ying P, Zhang J, Zhong Z. Effect of phase transition on the thermal transport in isoreticular DUT materials. *J Phys Chem C* 2021;125:12991-3001. DOI
 138. Zhou CC, Liu HT, Ding L, Lu J, Wang SN, Li YW. Single-crystal-to-single-crystal transformations among three Mn-MOFs containing different water molecules induced by reaction time: crystal structures and proton conductivities. *Dalton Trans* 2021;50:11077-90. DOI PubMed
 139. Lv Y, Mao X, Gong W, et al. Hcp-phased Ni nanoparticles with generic catalytic hydrogenation activities toward different functional groups. *Sci China Mater* 2022;65:1252-61. DOI
 140. Choi SB, Furukawa H, Nam HJ, et al. Reversible interpenetration in a metal-organic framework triggered by ligand removal and addition. *Angew Chem Int Ed Engl* 2012;51:8791-5. DOI PubMed
 141. Coudert F. Responsive metal-organic frameworks and framework materials: under pressure, taking the heat, in the spotlight, with friends. *Chem Mater* 2015;27:1905-16. DOI
 142. Li QQ, Ren CY, Huang YY, et al. Thermally triggered solid-state single-crystal-to-single-crystal structural transformation accompanies property changes. *Chemistry* 2015;21:4703-11. DOI PubMed
 143. Ghoufi A, Benhamed K, Boukli-Hacene L, Maurin G. Electrically induced breathing of the MIL-53(Cr) metal-organic framework. *ACS Cent Sci* 2017;3:394-8. DOI PubMed PMC
 144. Evans JD, Bon V, Senkovska I, Lee HC, Kaskel S. Four-dimensional metal-organic frameworks. *Nat Commun* 2020;11:2690. DOI PubMed PMC
 145. Krause S, Hosono N, Kitagawa S. Chemistry of soft porous crystals: structural dynamics and gas adsorption properties. *Angew Chem Int Ed Engl* 2020;59:15325-41. DOI PubMed
 146. Li R, Liu H, Zhou C, et al. Ligand substitution induced single-crystal-to-single-crystal transformations in two Ni(ii) coordination compounds displaying consequential changes in proton conductivity. *Inorg Chem Front* 2020;7:1880-91. DOI
 147. Han Y, Sinnwell MA, Teat SJ, et al. Desulfurization efficiency preserved in a heterometallic MOF: synthesis and thermodynamically controlled phase transition. *Adv Sci* 2019;6:1802056. DOI PubMed PMC
 148. Chen Y, Feng X, Huang X, et al. A tale of copper coordination frameworks: controlled single-crystal-to-single-crystal transformations and their catalytic C-H bond activation properties. *Chemistry* 2015;21:13894-9. DOI PubMed
 149. Yang Y, Zhu W, Dong Z, et al. 1D coordination polymer nanofibers for low-temperature photothermal therapy. *Adv Mater*

- 2017;29:1703588. DOI PubMed
150. Rappe AK, Casewit CJ, Colwell KS, Goddard WA, Skiff WM. UFF, a full periodic table force field for molecular mechanics and molecular dynamics simulations. *J Am Chem Soc* 1992;114:10024-35. DOI
151. Taylor KM, Rieter WJ, Lin W. Manganese-based nanoscale metal-organic frameworks for magnetic resonance imaging. *J Am Chem Soc* 2008;130:14358-9. DOI PubMed
152. Mazaj M, Logar NZ, Žagar E, Kovačič S. A facile strategy towards a highly accessible and hydrostable MOF-phase within hybrid polyHIPEs through in situ metal-oxide recrystallization. *J Mater Chem A* 2017;5:1967-71. DOI
153. Ding Y, Hu L, He D, et al. Design of multishell microsphere of transition metal oxides/carbon composites for lithium ion battery. *Chem Eng J* 2020;380:122489. DOI
154. Niu H, Cao L, Yang X, Liu K, Liu L, Wang J. In situ growth of the ZIF-8 on the polymer monolith via CO₂-in-water HIPEs stabilized using metal oxide nanoparticles and its photocatalytic activity. *Polym Adv Technol* 2021;32:3194-204. DOI
155. Zou L, Hou CC, Liu Z, Pang H, Xu Q. Superlong single-crystal metal-organic framework nanotubes. *J Am Chem Soc* 2018;140:15393-401. DOI PubMed
156. Novoselov KS, Geim AK, Morozov SV, et al. Electric field effect in atomically thin carbon films. *Science* 2004;306:666-9. DOI PubMed
157. Yi M, Shen Z. A review on mechanical exfoliation for the scalable production of graphene. *J Mater Chem A* 2015;3:11700-15. DOI
158. Dong R, Zhang T, Feng X. Interface-assisted synthesis of 2D materials: trend and challenges. *Chem Rev* 2018;118:6189-235. DOI PubMed
159. Wang J, Wang K, Xu Y. Emerging two-dimensional covalent and coordination polymers for stable lithium metal batteries: from liquid to solid. *ACS Nano* 2021;15:19026-53. DOI PubMed
160. Li C, Wang K, Li J, Zhang Q. Recent progress in stimulus-responsive two-dimensional metal-organic frameworks. *ACS Materials Lett* 2020;2:779-97. DOI
161. Zhao M, Huang Y, Peng Y, Huang Z, Ma Q, Zhang H. Two-dimensional metal-organic framework nanosheets: synthesis and applications. *Chem Soc Rev* 2018;47:6267-95. DOI PubMed
162. Schneemann A, Dong R, Schwotzer F, et al. 2D framework materials for energy applications. *Chem Sci* 2020;12:1600-19. DOI PubMed PMC
163. Zhu H, Liu D. The synthetic strategies of metal-organic framework membranes, films and 2D MOFs and their applications in devices. *J Mater Chem A* 2019;7:21004-35. DOI
164. Faghani A, Donskyi IS, Fardin Gholami M, et al. Controlled covalent functionalization of thermally reduced graphene oxide to generate defined bifunctional 2D nanomaterials. *Angew Chem Int Ed Engl* 2017;56:2675-9. DOI PubMed PMC
165. López-Cabrelles J, Mañas-Valero S, Vitorica-Yrezabal IJ, et al. Isorecticular two-dimensional magnetic coordination polymers prepared through pre-synthetic ligand functionalization. *Nat Chem* 2018;10:1001-7. DOI PubMed
166. Tan C, Yu P, Hu Y, et al. High-yield exfoliation of ultrathin two-dimensional ternary chalcogenide nanosheets for highly sensitive and selective fluorescence DNA sensors. *J Am Chem Soc* 2015;137:10430-6. DOI PubMed
167. Zhang H. Ultrathin two-dimensional nanomaterials. *ACS Nano* 2015;9:9451-69. DOI PubMed
168. Al Obeidli A, Ben Salah H, Al Murisi M, Sabouni R. Recent advancements in MOFs synthesis and their green applications. *Int J Hydrog Energy* 2022;47:2561-93. DOI
169. Liu Y, Cheng H, Lyu M, et al. Low overpotential in vacancy-rich ultrathin CoSe₂ nanosheets for water oxidation. *J Am Chem Soc* 2014;136:15670-5. DOI PubMed
170. Fang Z, Bueken B, De Vos DE, Fischer RA. Defect-engineered metal-organic frameworks. *Angew Chem Int Ed Engl* 2015;54:7234-54. DOI PubMed PMC
171. Lin S, Diercks CS, Zhang YB, et al. Covalent organic frameworks comprising cobalt porphyrins for catalytic CO₂ reduction in water. *Science* 2015;349:1208-13. DOI PubMed
172. Ashworth DJ, Roseveare TM, Schneemann A, et al. Increasing alkyl chain length in a series of layered metal-organic frameworks aids ultrasonic exfoliation to form nanosheets. *Inorg Chem* 2019;58:10837-45. DOI PubMed PMC
173. Hernandez Y, Nicolosi V, Lotya M, et al. High-yield production of graphene by liquid-phase exfoliation of graphite. *Nat Nanotechnol* 2008;3:563-8. DOI PubMed
174. Shen J, He Y, Wu J, et al. Liquid phase exfoliation of two-dimensional materials by directly probing and matching surface tension components. *Nano Lett* 2015;15:5449-54. DOI PubMed
175. Tan C, Yang K, Dong J, et al. Boosting enantioselectivity of chiral organocatalysts with ultrathin two-dimensional metal-organic framework nanosheets. *J Am Chem Soc* 2019;141:17685-95. DOI PubMed
176. Jian M, Qiu R, Xia Y, et al. Ultrathin water-stable metal-organic framework membranes for ion separation. *Sci Adv* 2020;6:eaay3998. DOI PubMed PMC
177. Ding Y, Chen YP, Zhang X, et al. Controlled intercalation and chemical exfoliation of layered metal-organic frameworks using a chemically labile intercalating agent. *J Am Chem Soc* 2017;139:9136-9. DOI PubMed
178. Schoedel A, Li M, Li D, O'Keeffe M, Yaghi OM. Structures of metal-organic frameworks with rod secondary building units. *Chem Rev* 2016;116:12466-535. DOI PubMed
179. Huang J, Li Y, Huang RK, et al. Electrochemical exfoliation of pillared-layer metal-organic framework to boost the oxygen evolution reaction. *Angew Chem Int Ed Engl* 2018;57:4632-6. DOI PubMed

180. Liu L, Chen J, Zhang Y, et al. Fabrication of ultrathin single-layer 2D metal-organic framework nanosheets with excellent adsorption performance. *via* ;9:546-55. DOI
181. Gallego A, Hermosa C, Castillo O, et al. Solvent-induced delamination of a multifunctional two dimensional coordination polymer. *Adv Mater* 2013;25:2141-6. DOI PubMed
182. Wang X, Chi C, Zhang K, et al. Reversed thermo-switchable molecular sieving membranes composed of two-dimensional metal-organic nanosheets for gas separation. *Nat Commun* 2017;8:14460. DOI PubMed PMC
183. Au VK, Nakayashiki K, Huang H, Suginome S, Sato H, Aida T. Stepwise expansion of layered metal-organic frameworks for nonstochastic exfoliation into porous nanosheets. *J Am Chem Soc* 2019;141:53-7. DOI PubMed
184. Lê Anh M, Potapov P, Lubk A, Doert T, Ruck M. Freestanding few-layer sheets of a dual topological insulator. *npj 2D Mater Appl* 2021;5. DOI
185. Lê Anh M, Potapov P, Wolf D, et al. Freestanding nanolayers of a wide-gap topological insulator through liquid-phase exfoliation. *Chemistry* 2021;27:794-801. DOI PubMed PMC
186. Chen JE, Yang Z, Koh HU, et al. Current progress and scalable approach toward the synthesis of 2D metal-organic frameworks. *Adv Materials Inter* 2022;9:2102560. DOI
187. Li X, Zhang G, Bai X, et al. Highly conducting graphene sheets and Langmuir-Blodgett films. *Nat Nanotechnol* 2008;3:538-42. DOI PubMed
188. Dong A, Chen J, Vora PM, Kikkawa JM, Murray CB. Binary nanocrystal superlattice membranes self-assembled at the liquid-air interface. *Nature* 2010;466:474-7. DOI PubMed
189. Yaghi OM. Evolution of MOF single crystals. *Chem* 2022;8:1541-3. DOI
190. Han J, He X, Liu J, et al. Determining factors in the growth of MOF single crystals unveiled by in situ interface imaging. *Chemistry* 2022;8:1637-57. DOI
191. Liu YL, Liu XY, Feng L, et al. Two-dimensional metal-organic framework nanosheets: synthesis and applications in electrocatalysis and photocatalysis. *ChemSusChem* 2022;15:e202102603. DOI PubMed
192. Sakamoto R, Hoshiko K, Liu Q, et al. A photofunctional bottom-up bis(dipyrrinato)zinc(II) complex nanosheet. *Nat Commun* 2015;6:6713. DOI PubMed PMC
193. Ying Y, Zhang Z, Peh SB, et al. Pressure-responsive two-dimensional metal-organic framework composite membranes for CO₂ separation. *Angew Chem Int Ed Engl* 2021;60:11318-25. DOI PubMed
194. Zhang T, Zheng B, Li L, Song J, Song L, Zhang M. Fewer-layer conductive metal-organic Langmuir-Blodgett films as electrocatalysts enable an ultralow detection limit of H₂O₂. *Appl Surf Sci* 2021;539:148255. DOI
195. Lin Y, Li Y, Cao Y, Wang X. Two-dimensional MOFs: design & synthesis and applications. *Chem Asian J* 2021;16:3281-98. DOI PubMed
196. Shi Y, Wang Y, Yu Y, Niu Z, Zhang B. N-doped graphene wrapped hexagonal metallic cobalt hierarchical nanosheet as a highly efficient water oxidation electrocatalyst. *J Mater Chem A* 2017;5:8897-902. DOI
197. Xiao X, Yu H, Jin H, et al. Salt-templated synthesis of 2D metallic MoN and other nitrides. *ACS Nano* 2017;11:2180-6. DOI PubMed
198. Huang L, Zhang X, Han Y, Wang Q, Fang Y, Dong S. In situ synthesis of ultrathin metal-organic framework nanosheets: a new method for 2D metal-based nanoporous carbon electrocatalysts. *J Mater Chem A* 2017;5:18610-7. DOI
199. Huang L, Gao G, Zhang H, Chen J, Fang Y, Dong S. Self-dissociation-assembly of ultrathin metal-organic framework nanosheet arrays for efficient oxygen evolution. *Nano Energy* 2020;68:104296. DOI
200. Talin AA, Centrone A, Ford AC, et al. Tunable electrical conductivity in metal-organic framework thin-film devices. *Science* 2014;343:66-9. DOI PubMed
201. Sun L, Campbell MG, Dincă M. Electrically conductive porous metal-organic frameworks. *Angew Chem Int Ed Engl* 2016;55:3566-79. DOI PubMed
202. Stassen I, Burtch N, Talin A, Falcaro P, Allendorf M, Ameloot R. An updated roadmap for the integration of metal-organic frameworks with electronic devices and chemical sensors. *Chem Soc Rev* 2017;46:3185-241. DOI PubMed
203. Wu G, Huang J, Zang Y, He J, Xu G. Porous field-effect transistors based on a semiconductive metal-organic framework. *J Am Chem Soc* 2017;139:1360-3. DOI PubMed
204. Cui Y, Yan J, Chen Z, et al. [Cu₃(C₆Se₆)_n]: the first highly conductive 2D π -d conjugated coordination polymer based on benzenhexaselenolate. *Adv Sci* 2019;6:1802235. DOI
205. Yang C, Dong R, Wang M, et al. A semiconducting layered metal-organic framework magnet. *Nat Commun* 2019;10:3260. DOI PubMed PMC
206. Arora H, Dong R, Venanzi T, et al. Demonstration of a broadband photodetector based on a two-dimensional metal-organic framework. *Adv Mater* 2020;32:e1907063. DOI PubMed
207. Schwotzer F, Horak J, Senkowska I, et al. Cooperative assembly of 2D-MOF nanoplatelets into hierarchical carpets and tubular superstructures for advanced air filtration. *Angew Chem Int Ed Engl* 2022;61:e202117730. DOI PubMed PMC
208. Dong R, Han P, Arora H, et al. High-mobility band-like charge transport in a semiconducting two-dimensional metal-organic framework. *Nat Mater* 2018;17:1027-32. DOI PubMed
209. Li FL, Wang P, Huang X, et al. Large-scale, bottom-up synthesis of binary metal-organic framework nanosheets for efficient water oxidation. *Angew Chem Int Ed Engl* 2019;58:7051-6. DOI PubMed

210. Liu B, Shekhah O, Arslan HK, Liu J, Wöll C, Fischer RA. Enantiopure metal-organic framework thin films: oriented SURMOF growth and enantioselective adsorption. *Angew Chem Int Ed Engl* 2012;51:807-10. DOI PubMed
211. Haraguchi T, Otsubo K, Sakata O, Fujiwara A, Kitagawa H. Remarkable lattice shrinkage in highly oriented crystalline three-dimensional metal-organic framework thin films. *Inorg Chem* 2015;54:11593-5. DOI PubMed
212. Haraguchi T, Otsubo K, Sakata O, Kawaguchi S, Fujiwara A, Kitagawa H. A three-dimensional accordion-like metal-organic framework: synthesis and unconventional oriented growth on a surface. *Chem Commun* 2016;52:6017-20. DOI PubMed
213. Begum S, Hassan Z, Bräse S, Wöll C, Tsotsalas M. Metal-organic framework-templated biomaterials: recent progress in synthesis, functionalization, and applications. *Acc Chem Res* 2019;52:1598-610. DOI PubMed
214. Lugier O, Pokharel U, Castellanos S. Impact of synthetic conditions on the morphology and crystallinity of FDMOF-1(Cu) thin films. *Cryst Growth Des* 2020;20:5302-9. DOI
215. Sakaida S, Haraguchi T, Otsubo K, Sakata O, Fujiwara A, Kitagawa H. Fabrication and structural characterization of an ultrathin film of a two-dimensional-layered metal-organic framework, {Fe(py)₂[Ni(CN)₄]} (py = pyridine). *Inorg Chem* 2017;56:7606-9. DOI
216. Xiao Y, Zhang W, Jiao Y, Xu Y, Lin H. Metal-phenolic network as precursor for fabrication of metal-organic framework (MOF) nanofiltration membrane for efficient desalination. *J Membr Sci* 2021;624:119101. DOI
217. Liu X, Mazel A, Marschner S, et al. Photoinduced delamination of metal-organic framework thin films by spatioselective generation of reactive oxygen species. *ACS Appl Mater Interfaces* 2021;13:57768-73. DOI PubMed
218. Zhao W, Chen T, Wang W, et al. Layer-by-layer 2D ultrathin conductive Cu₅(HHTP)₂ film for high-performance flexible transparent supercapacitors. *Adv Mater Interfaces* 2021;8:2100308. DOI
219. Cao F, Zhao M, Yu Y, et al. Synthesis of two-dimensional CoS_{1.097}/nitrogen-doped carbon nanocomposites using metal-organic framework nanosheets as precursors for supercapacitor application. *J Am Chem Soc* 2016;138:6924-7. DOI PubMed
220. Liu X, Yan Z, Zhang Y, et al. Two-dimensional metal-organic framework/enzyme hybrid nanocatalyst as a benign and self-activated cascade reagent for in vivo wound healing. *ACS Nano* 2019;13:5222-30. DOI PubMed
221. Hang L, Zhang T, Wen H, et al. Controllable photodynamic performance via an acidic microenvironment based on two-dimensional metal-organic frameworks for photodynamic therapy. *Nano Res* 2021;14:660-6. DOI
222. Wang Z, Wang G, Qi H, et al. Ultrathin two-dimensional conjugated metal-organic framework single-crystalline nanosheets enabled by surfactant-assisted synthesis. *Chem Sci* 2020;11:7665-71. DOI PubMed PMC
223. Liu X, Demir NK, Wu Z, Li K. Highly water-stable zirconium metal-organic framework UiO-66 membranes supported on alumina hollow fibers for desalination. *J Am Chem Soc* 2015;137:6999-7002. DOI PubMed
224. Bai Y, Dou Y, Xie LH, Rutledge W, Li JR, Zhou HC. Zr-based metal-organic frameworks: design, synthesis, structure, and applications. *Chem Soc Rev* 2016;45:2327-67. DOI PubMed
225. Zhang X, Zhang P, Chen C, et al. Fabrication of 2D metal-organic framework nanosheets with tailorable thickness using bio-based surfactants and their application in catalysis. *Green Chem* 2019;21:54-8. DOI
226. Cho W, Lee HJ, Oh M. Growth-controlled formation of porous coordination polymer particles. *J Am Chem Soc* 2008;130:16943-6. DOI PubMed
227. Umemura A, Diring S, Furukawa S, Uehara H, Tsuruoka T, Kitagawa S. Morphology design of porous coordination polymer crystals by coordination modulation. *J Am Chem Soc* 2011;133:15506-13. DOI PubMed
228. Hu M, Ju Y, Liang K, Suma T, Cui J, Caruso F. Void engineering in metal-organic frameworks via synergistic etching and surface functionalization. *Adv Funct Mater* 2016;26:5827-34. DOI
229. Guo X, Zheng S, Zhang G, et al. Nanostructured graphene-based materials for flexible energy storage. *Energy Stor Mater* 2017;9:150-69. DOI
230. Bai XJ, Chen D, Li LL, et al. Fabrication of MOF thin films at miscible liquid-liquid interface by spray method. *ACS Appl Mater Interfaces* 2018;10:25960-6. DOI PubMed
231. Cui J, Gao N, Yin X, et al. Microfluidic synthesis of uniform single-crystalline MOF microcubes with a hierarchical porous structure. *Nanoscale* 2018;10:9192-8. DOI PubMed
232. Geng P, Wang L, Du M, et al. MIL-96-Al for Li-S batteries: shape or size? *Adv Mater* 2022;34:e2107836. DOI PubMed
233. Xiao X, Zou L, Pang H, Xu Q. Synthesis of micro/nanoscaled metal-organic frameworks and their direct electrochemical applications. *Chem Soc Rev* 2020;49:301-31. DOI PubMed
234. Carné-Sánchez A, Imaz I, Cano-Sarabia M, MasPOCH D. A spray-drying strategy for synthesis of nanoscale metal-organic frameworks and their assembly into hollow superstructures. *Nat Chem* 2013;5:203-11. DOI PubMed
235. Xu X, Zhang Z, Wang X. Well-defined metal-organic-framework hollow nanostructures for catalytic reactions involving gases. *Adv Mater* 2015;27:5365-71. DOI PubMed
236. He T, Xu X, Ni B, et al. Fast and scalable synthesis of uniform zirconium-, hafnium-based metal-organic framework nanocrystals. *Nanoscale* 2017;9:19209-15. DOI PubMed
237. He T, Xu X, Ni B, et al. Metal-organic framework based microcapsules. *Angew Chem Int Ed Engl* 2018;57:10148-52. DOI PubMed
238. Qiu T, Gao S, Liang Z, et al. Pristine hollow metal-organic frameworks: design, synthesis and application. *Angew Chem Int Ed Engl* 2021;60:17314-36. DOI PubMed
239. Han L, Yu XY, Lou XW. Formation of prussian-blue-analog nanocages via a direct etching method and their conversion into Ni-Co-mixed oxide for enhanced oxygen evolution. *Adv Mater* 2016;28:4601-5. DOI PubMed
240. Kajiwara T, Fujii M, Tsujimoto M, et al. Photochemical reduction of low concentrations of CO₂ in a porous coordination polymer

- with a ruthenium(II)-CO complex. *Angew Chem Int Ed Engl* 2016;55:2697-700. DOI PubMed
241. Lian X, Fang Y, Joseph E, et al. Enzyme-MOF (metal-organic framework) composites. *Chem Soc Rev* 2017;46:3386-401. DOI PubMed
242. Diercks CS, Liu Y, Cordova KE, Yaghi OM. The role of reticular chemistry in the design of CO₂ reduction catalysts. *Nat Mater* 2018;17:301-7. DOI PubMed
243. Drake T, Ji P, Lin W. Site isolation in metal-organic frameworks enables novel transition metal catalysis. *Acc Chem Res* 2018;51:2129-38. DOI PubMed
244. Li Z, Rayder TM, Luo L, Byers JA, Tsung CK. Aperture-opening encapsulation of a transition metal catalyst in a metal-organic framework for CO₂ hydrogenation. *J Am Chem Soc* 2018;140:8082-5. DOI PubMed
245. Luo L, Lo WS, Si X, et al. Directional engraving within single crystalline metal-organic framework particles via oxidative linker cleaving. *J Am Chem Soc* 2019;141:20365-70. DOI PubMed
246. Khan NA, Jhung SH. Synthesis of metal-organic frameworks (MOFs) with microwave or ultrasound: rapid reaction, phase-selectivity, and size reduction. *Coord Chem Rev* 2015;285:11-23. DOI PubMed
247. Cai X, Xie Z, Li D, Kassymova M, Zang S, Jiang H. Nano-sized metal-organic frameworks: synthesis and applications. *Coord Chem Rev* 2020;417:213366. DOI
248. Thi Dang Y, Hoang HT, Dong HC, et al. Microwave-assisted synthesis of nano Hf- and Zr-based metal-organic frameworks for enhancement of curcumin adsorption. *Microporous Mesoporous Mater* 2020;298:110064. DOI
249. Gabriel C, Gabriel S, Grant EH, Grant EH, Halstead BJS, Mingos DMP. Dielectric parameters relevant to microwave dielectric heating. *Chem Soc Rev* 1998;27:213. DOI
250. Lee Y, Kim J, Ahn W. Synthesis of metal-organic frameworks: a mini review. *Korean J Chem Eng* 2013;30:1667-80. DOI
251. Yang W, Zheng J, Hu S, et al. Self-assembled three-dimensional macroporous Co₂(OH)₃ Cl-MnO₂ spheres synthesized by microwave-assisted method: a new hybrid for high-performance asymmetric supercapacitors. *ACS Sustain Chem Eng* 2017;5:4563-72. DOI
252. Thomas-hillman I, Laybourn A, Dodds C, Kingman SW. Realising the environmental benefits of metal-organic frameworks: recent advances in microwave synthesis. *J Mater Chem A* 2018;6:11564-81. DOI
253. Kumar A, Kuang Y, Liang Z, Sun X. Microwave chemistry, recent advancements, and eco-friendly microwave-assisted synthesis of nanoarchitectures and their applications: a review. *Mater Today Nano* 2020;11:100076. DOI
254. Ma M, Bétard A, Weber I, Al-hokbany NS, Fischer RA, Metzler-nolte N. Iron-based metal-organic frameworks MIL-88B and NH₂-MIL-88B: high quality microwave synthesis and solvent-induced lattice “breathing”. *Cryst Growth Des* 2013;13:2286-91. DOI
255. Li Y, Liu Y, Gao W, et al. Microwave-assisted synthesis of UIO-66 and its adsorption performance towards dyes. *CrystEngComm* 2014;16:7037-42. DOI
256. Babu R, Roshan R, Kathalikkattil AC, Kim DW, Park DW. Rapid, microwave-assisted synthesis of cubic, three-dimensional, highly porous MOF-205 for room temperature CO₂ fixation via cyclic carbonate synthesis. *ACS Appl Mater Interfaces* 2016;8:33723-31. DOI PubMed
257. Chen C, Feng X, Zhu Q, et al. Microwave-assisted rapid synthesis of well-shaped MOF-74 (Ni) for CO₂ efficient capture. *Inorg Chem* 2019;58:2717-28. DOI PubMed
258. Wang W, Sun Z, Chen S, Qian J, He M, Chen Q. Microwave-assisted fabrication of a mixed-ligand [Cu₄(μ₃-OH)₂]-cluster-based metal-organic framework with coordinatively unsaturated metal sites for carboxylation of terminal alkynes with carbon dioxide. *Appl Organomet Chem* 2021:35. DOI
259. Kong Y, Zhang R, Zhang J, et al. Microwave-assisted rapid synthesis of nanoscale MOF-303 for hydrogel composites with superior proton conduction at ambient-humidity conditions. *ACS Appl Energy Mater* 2021;4:14681-8. DOI
260. Firmino AD, Mendes RF, Antunes MM, et al. Robust multifunctional yttrium-based metal-organic frameworks with breathing effect. *Inorg Chem* 2017;56:1193-208. DOI PubMed
261. Kukkar P, Kim K, Kukkar D, Singh P. Recent advances in the synthesis techniques for zeolitic imidazolate frameworks and their sensing applications. *Coord Chem Rev* 2021;446:214109. DOI
262. Cherbański R, Rudniak L. Modelling of microwave heating of water in a monomode applicator - influence of operating conditions. *Int J Therm Sci* 2013;74:214-29. DOI
263. Zhao Z, Li H, Zhao K, Wang L, Gao X. Microwave-assisted synthesis of MOFs: rational design via numerical simulation. *Chem Eng J* 2022;428:131006. DOI
264. Chang HY, Wu KY, Chen WC, et al. Water-induced self-assembly of amphiphilic discotic molecules for adaptive artificial water channels. *ACS Nano* 2021;15:14885-90. DOI PubMed
265. Mohammadi P, Gandier JA, Nonappa, Wagermaier W, Miserez A, Penttilä M. Bioinspired functionally graded composite assembled using cellulose nanocrystals and genetically engineered proteins with controlled biomineralization. *Adv Mater* 2021;33:e2102658. DOI PubMed
266. Morris RE, Čejka J. Exploiting chemically selective weakness in solids as a route to new porous materials. *Nat Chem* 2015;7:381-8. DOI PubMed
267. Huang H, Li JR, Wang K, et al. An in situ self-assembly template strategy for the preparation of hierarchical-pore metal-organic frameworks. *Nat Commun* 2015;6:8847. DOI PubMed PMC
268. Feng L, Wang K, Powell J, Zhou H. Controllable synthesis of metal-organic frameworks and their hierarchical assemblies. *Matter*

- 2019;1:801-24. DOI
269. Wang Z, Ge L, Zhang G, et al. The controllable synthesis of urchin-shaped hierarchical superstructure MOFs with high catalytic activity and stability. *Chem Commun* 2021;57:8758-61. DOI PubMed
270. Zhao X, Feng J, Liu J, et al. Metal-organic framework-derived ZnO/ZnS heteronanostructures for efficient visible-light-driven photocatalytic hydrogen production. *Adv Sci* 2018;5:1700590. DOI PubMed PMC
271. Hu SJ, Guo XQ, Zhou LP, et al. Guest-driven self-assembly and chiral induction of photofunctional lanthanide tetrahedral cages. *J Am Chem Soc* 2022;144:4244-53. DOI PubMed
272. Alivand MS, Mazaheri O, Wu Y, et al. Engineered assembly of water-dispersible nanocatalysts enables low-cost and green CO₂ capture. *Nat Commun* 2022;13:1249. DOI PubMed PMC
273. Avci C, Imaz I, Carné-Sánchez A, et al. Self-assembly of polyhedral metal-organic framework particles into three-dimensional ordered superstructures. *Nat Chem* 2017;10:78-84. DOI PubMed
274. Rosi NL, Eckert J, Eddaoudi M, et al. Hydrogen storage in microporous metal-organic frameworks. *Science* 2003;300:1127-9. DOI PubMed
275. Rowsell JL, Yaghi OM. Strategies for hydrogen storage in metal-organic frameworks. *Angew Chem Int Ed Engl* 2005;44:4670-9. DOI PubMed
276. Ren J, Langmi HW, North BC, Mathe M. Review on processing of metal-organic framework (MOF) materials towards system integration for hydrogen storage: review on processing of MOF materials towards system integration. *Int J Energy Res* 2015;39:607-20. DOI
277. Vilela SMF, Salcedo-Abraira P, Micheron L, Solla EL, Yot PG, Horcajada P. A robust monolithic metal-organic framework with hierarchical porosity. *Chem Commun* 2018;54:13088-91. DOI PubMed
278. Lim GJH, Wu Y, Shah BB, et al. 3D-printing of pure metal-organic framework monoliths. *ACS Mater Lett* 2019;1:147-53. DOI
279. Sumida K, Liang K, Reboul J, Ibarra IA, Furukawa S, Falcaro P. Sol-gel processing of metal-organic frameworks. *Chem Mater* 2017;29:2626-45. DOI
280. Lee J, Lee K, Kim J. Fiber-based gas filter assembled via in situ synthesis of ZIF-8 metal organic frameworks for an optimal adsorption of SO₂: experimental and theoretical approaches. *ACS Appl Mater Interfaces* 2021;13:1620-31. DOI PubMed
281. Asaro F, Benedetti A, Freris I, Riello P, Savko N. Evolution of the nonionic inverse microemulsion-acid-TEOS system during the synthesis of nanosized silica via the sol-gel process. *Langmuir* 2010;26:12917-25. DOI PubMed
282. Lorignon F, Gossard A, Carboni M. Hierarchically porous monolithic MOFs: an ongoing challenge for industrial-scale effluent treatment. *Chem Eng J* 2020;393:124765. DOI
283. Tian T, Zeng Z, Vulpe D, et al. A sol-gel monolithic metal-organic framework with enhanced methane uptake. *Nat Mater* 2018;17:174-9. DOI PubMed
284. Connolly BM, Aragones-Anglada M, Gandara-Loe J, et al. Tuning porosity in macroscopic monolithic metal-organic frameworks for exceptional natural gas storage. *Nat Commun* 2019;10:2345. DOI PubMed PMC
285. Bueken B, Van Velthoven N, Willhammar T, et al. Gel-based morphological design of zirconium metal-organic frameworks. *Chem Sci* 2017;8:3939-48. DOI PubMed PMC
286. Hou J, Sapnik AF, Bennett TD. Metal-organic framework gels and monoliths. *Chem Sci* 2020;11:310-23. DOI PubMed PMC
287. Avrami M. Kinetics of phase change. I general theory. *J Chem Phys* 1939;7:1103-12. DOI
288. Gualtieri AF. Synthesis of sodium zeolites from a natural halloysite. *Phys Chem Miner* 2001;28:719-28. DOI
289. Chen X, Xu Y, Zhou C, et al. Unraveling the physicochemical nature of colloidal motion waves among silver colloids. *Sci Adv* 2022;8:eabn9130. DOI PubMed PMC
290. Pang M, Cairns AJ, Liu Y, Belmabkhout Y, Zeng HC, Eddaoudi M. Synthesis and integration of Fe-soc-MOF cubes into colloidosomes via a single-step emulsion-based approach. *J Am Chem Soc* 2013;135:10234-7. DOI PubMed
291. Pang M, Cairns AJ, Liu Y, Belmabkhout Y, Zeng HC, Eddaoudi M. Highly monodisperse M(III)-based soc-MOFs (M = In and Ga) with cubic and truncated cubic morphologies. *J Am Chem Soc* 2012;134:13176-9. DOI PubMed
292. Zheng S, Sun Y, Xue H, Braunstein P, Huang W, Pang H. Dual-ligand and hard-soft-acid-base strategies to optimize metal-organic framework nanocrystals for stable electrochemical cycling performance. *Natl Sci Rev* 2022;9:nwab197. DOI PubMed PMC
293. di Gregorio MC, Elsoussou M, Wen Q, et al. Molecular cannibalism: sacrificial materials as precursors for hollow and multidomain single crystals. *Nat Commun* 2021;12:957. DOI PubMed PMC
294. Li H, Qin Z, Yang X, Chen X, Li Y, Shen K. Growth pattern control and nanoarchitecture engineering of metal-organic framework single crystals by confined space synthesis. *ACS Cent Sci* 2022;8:718-28. DOI PubMed PMC
295. Wang Y, Wang Y, Zhang L, Liu C, Pang H. Core-shell-type ZIF-8@ZIF-67@POM hybrids as efficient electrocatalysts for the oxygen evolution reaction. *Inorg Chem Front* 2019;6:2514-20. DOI
296. Chen L, Wang HF, Li C, Xu Q. Bimetallic metal-organic frameworks and their derivatives. *Chem Sci* 2020;11:5369-403. DOI PubMed PMC
297. Chuang C, Kung C. Metal-organic frameworks toward electrochemical sensors: challenges and opportunities. *Electroanalysis* 2020;32:1885-95. DOI
298. Guo C, Ma X, Wang B. Metal-organic frameworks-based composites and their photothermal applications. *Acta Chimica Sinica* 2021;79:967. DOI
299. Xu Y, Wang Y, Wan J, Ma Y. Reduced graphene oxide-supported metal organic framework as a synergistic catalyst for enhanced

- performance on persulfate induced degradation of trichlorophenol. *Chemosphere* 2020;240:124849. DOI PubMed
300. Wu Y, Yuan D, He D, et al. Decorated traditional zeolites with subunits of metal-organic frameworks for CH₄/N₂ separation. *Angew Chem Int Ed Engl* 2019;58:10241-4. DOI
301. Xiong Y, Chang X, Qiao X, et al. Co-MOF-74 derived Co₃O₄/graphene heterojunction nanoscrolls for ppb-level acetone detection. *Sens Actuators B Chem* 2019;300:127011. DOI
302. Zhou T, Chen S, Wang X, Xie C, Zeng D. Catalytic activation of cobalt doping sites in ZIF-71-coated ZnO nanorod arrays for enhancing gas-sensing performance to acetone. *ACS Appl Mater Interfaces* 2020;12:48948-56. DOI PubMed
303. Zhao Q, Ge Y, Fu K, Ji N, Song C, Liu Q. Oxidation of acetone over Co-based catalysts derived from hierarchical layer hydroxalcite: influence of Co/Al molar ratios and calcination temperatures. *Chemosphere* 2018;204:257-66. DOI PubMed
304. Lan L, Shi Z, Zhang Q, et al. Defects lead to a massive enhancement in the UV-Vis-IR driven thermocatalytic activity of Co₃O₄ mesoporous nanorods. *J Mater Chem A* 2018;6:7194-205. DOI
305. Zhang Y, Park S. Facile construction of MoO₃@ZIF-8 core-shell nanorods for efficient photoreduction of aqueous Cr (VI). *Appl Catal B: Environ* 2019;240:92-101. DOI
306. Abdollahi N, Akbar Razavi SA, Morsali A, Hu ML. High capacity Hg(II) and Pb(II) removal using MOF-based nanocomposite: cooperative effects of pore functionalization and surface-charge modulation. *J Hazard Mater* 2020;387:121667. DOI PubMed
307. Zheng S, Li Q, Xue H, Pang H, Xu Q. A highly alkaline-stable metal oxide@metal-organic framework composite for high-performance electrochemical energy storage. *Natl Sci Rev* 2020;7:305-14. DOI
308. Li QY, Zhang L, Xu YX, Li Q, Xue H, Pang H. Smart yolk/shell ZIF-67@POM hybrids as efficient electrocatalysts for the oxygen evolution reaction. *ACS Sustain Chem Eng* 2019;7:5027-33. DOI
309. Xiao X, Zhang G, Xu Y, et al. A new strategy for the controllable growth of MOF@PBA architectures. *J Mater Chem A* 2019;7:17266-71. DOI
310. Shan Y, Zhang M, Bai Y, Du M, Guo X, Pang H. Design and synthesis of transition metal oxide/zeolitic imidazolate framework-67 composites. *Chem Eng J* 2022;429:132146. DOI
311. Radhakrishnan S, Mathiyarasu J. Chapter 8 - graphene-carbon nanotubes modified electrochemical sensors. In: editor^editors, editor. Graphene-based electrochemical sensors for biomolecules. Elsevier; 2019. p.187-205.
312. Venkadesh A, Mathiyarasu J, Radhakrishnan S. Voltammetric sensing of caffeine in food sample using Cu-MOF and graphene. *Electroanalysis* 2021;33:1007-13. DOI
313. Khirak BN, Hasanazadeh M, Mojaddami M, Shahriyar Far H, Simchi A. In situ synthesis of quasi-needle-like bimetallic organic frameworks on highly porous graphene scaffolds for efficient electrocatalytic water oxidation. *Chem Commun* 2020;56:3135-8. DOI PubMed
314. Wang W, Xu X, Zhou W, Shao Z. Recent progress in metal-organic frameworks for applications in electrocatalytic and photocatalytic water splitting. *Adv Sci* 2017;4:1600371. DOI PubMed PMC
315. Huang H, Chen Y, Chen Z, Chen J, Hu Y, Zhu JJ. Electrochemical sensor based on Ce-MOF/carbon nanotube composite for the simultaneous discrimination of hydroquinone and catechol. *J Hazard Mater* 2021;416:125895. DOI PubMed
316. Quan X, Sun Z, Xu J, et al. Construction of an aminated MIL-53(Al)-functionalized carbon nanotube for the efficient removal of bisphenol AF and metribuzin. *Inorg Chem* 2020;59:2667-79. DOI PubMed
317. Lin KY, Chang HA. Ultra-high adsorption capacity of zeolitic imidazole framework-67 (ZIF-67) for removal of malachite green from water. *Chemosphere* 2015;139:624-31. DOI PubMed
318. Del Rio M, Turnes Palomino G, Palomino Cabello C. Metal-organic framework@carbon hybrid magnetic material as an efficient adsorbent for pollutant extraction. *ACS Appl Mater Interfaces* 2020;12:6419-25. DOI PubMed
319. Qiu J, Yang L, Li M, Yao J. Metal nanoparticles decorated MIL-125-NH₂ and MIL-125 for efficient photocatalysis. *Mater Res Bull* 2019;112:297-306.
320. Sun D, Li Z. Double-solvent method to Pd nanoclusters encapsulated inside the cavity of NH₂-Uio-66(Zr) for efficient visible-light-promoted suzuki coupling reaction. *J Phys Chem C* 2016;120:19744-50. DOI
321. Wang Y, Chen L, Hou CC, Wei YS, Xu Q. Multiple catalytic sites in MOF-based hybrid catalysts for organic reactions. *Org Biomol Chem* 2020;18:8508-25. DOI PubMed
322. Guan J, Duan Z, Zhang F, et al. Water oxidation on a mononuclear manganese heterogeneous catalyst. *Nat Catal* 2018;1:870-7. DOI
323. Li X, Tung C, Wu L. Semiconducting quantum dots for artificial photosynthesis. *Nat Rev Chem* 2018;2:160-73. DOI
324. Chung HT, Cullen DA, Higgins D, et al. Direct atomic-level insight into the active sites of a high-performance PGM-free ORR catalyst. *Science* 2017;357:479-84. DOI PubMed
325. Fang X, Shang Q, Wang Y, et al. Single Pt atoms confined into a metal-organic framework for efficient photocatalysis. *Adv Mater* 2018;30:1705112. DOI PubMed
326. He T, Chen S, Ni B, et al. Zirconium-porphyrin-based metal-organic framework hollow nanotubes for immobilization of noble-metal single atoms. *Angew Chem Int Ed Engl* 2018;57:3493-8. DOI PubMed
327. Abdel-Mageed AM, Rungtaweeworanit B, Parlinska-Wojtan M, Pei X, Yaghi OM, Behm RJ. Highly active and stable single-atom Cu catalysts supported by a metal-organic framework. *J Am Chem Soc* 2019;141:5201-10. DOI PubMed
328. Zuo Q, Liu T, Chen C, et al. Ultrathin metal-organic framework nanosheets with ultrahigh loading of single Pt atoms for efficient visible-light-driven photocatalytic H₂ evolution. *Angew Chem Int Ed Engl* 2019;58:10198-203. DOI PubMed
329. Qiu J, Zhang X, Xie K, et al. Noble metal nanoparticle-functionalized Zr-metal organic frameworks with excellent photocatalytic

- performance. *J Colloid Interface Sci* 2019;538:569-77. DOI PubMed
330. Chen S, Liu X, Jin J, et al. Individually encapsulated frame-in-frame structure. *ACS Materials Lett* 2020;2:685-90. DOI
331. Kalaj M, Bentz KC, Ayala S Jr, et al. MOF-polymer hybrid materials: from simple composites to tailored architectures. *Chem Rev* 2020;120:8267-302. DOI PubMed
332. Iizuka T, Honjo K, Uemura T. Enhanced mechanical properties of a metal-organic framework by polymer insertion. *Chem Commun* 2019;55:691-4. DOI PubMed
333. DeCoste JB, Denny MS Jr, Peterson GW, Mahle JJ, Cohen SM. Enhanced aging properties of HKUST-1 in hydrophobic mixed-matrix membranes for ammonia adsorption. *Chem Sci* 2016;7:2711-6. DOI PubMed PMC
334. Kalaj M, Denny MS Jr, Bentz KC, Palomba JM, Cohen SM. Nylon-MOF composites through postsynthetic polymerization. *Angew Chem Int Ed Engl* 2019;58:2336-40. DOI PubMed
335. Fu D, Liu X, Zheng X, et al. Polymer-metal-organic framework hybrids for bioimaging and cancer therapy. *Coord Chem Rev* 2022;456:214393. DOI
336. Tan C, Chen J, Wu X, Zhang H. Epitaxial growth of hybrid nanostructures. *Nat Rev Mater* 2018;3. DOI PubMed
337. Liu C, Wang J, Wan J, Yu C. MOF-on-MOF hybrids: synthesis and applications. *Coord Chem Rev* 2021;432:213743. DOI
338. Chai L, Pan J, Hu Y, Qian J, Hong M. Rational design and growth of MOF-on-MOF heterostructures. *Small* 2021;17:e2100607. DOI PubMed
339. Deng X, Yang L, Huang H, et al. Shape-defined hollow structural Co-MOF-74 and metal nanoparticles@Co-MOF-74 composite through a transformation strategy for enhanced photocatalysis performance. *Small* 2019;15:e1902287. DOI PubMed
340. Feng L, Lv XL, Yan TH, Zhou HC. Modular programming of hierarchy and diversity in multivariate polymer/metal-organic framework hybrid composites. *J Am Chem Soc* 2019;141:10342-9. DOI PubMed
341. Zhu K, Fan R, Wu J, et al. MOF-on-MOF membrane with cascading functionality for capturing dichromate ions and p-arsanilic acid turn-on sensing. *ACS Appl Mater Interfaces* 2020;12:58239-51. DOI PubMed
342. Choi S, Kim T, Ji H, Lee HJ, Oh M. Isotropic and anisotropic growth of metal-organic framework (MOF) on MOF: logical inference on MOF structure based on growth behavior and morphological feature. *J Am Chem Soc* 2016;138:14434-40. DOI PubMed
343. Pan Y, Sun K, Liu S, et al. Core-shell ZIF-8@ZIF-67-derived CoP nanoparticle-embedded N-doped carbon nanotube hollow polyhedron for efficient overall water splitting. *J Am Chem Soc* 2018;140:2610-8. DOI
344. Zhan G, Zeng HC. Hydrogen spillover through Matryoshka-type (ZIFs@)(n-1)ZIFs nanocubes. *Nat Commun* 2018;9:3778. DOI PubMed PMC
345. Lee HJ, Cho YJ, Cho W, Oh M. Controlled isotropic or anisotropic nanoscale growth of coordination polymers: formation of hybrid coordination polymer particles. *ACS Nano* 2013;7:491-9. DOI PubMed
346. Chernikova V, Shekhah O, Spanopoulos I, Trikalitis PN, Eddaoudi M. Liquid phase epitaxial growth of heterostructured hierarchical MOF thin films. *Chem Commun* 2017;53:6191-4. DOI PubMed
347. Yang X, Yuan S, Zou L, et al. One-step synthesis of hybrid core-shell metal-organic frameworks. *Angew Chem Int Ed Engl* 2018;57:3927-32. DOI PubMed
348. Kim D, Lee G, Oh S, Oh M. Unbalanced MOF-on-MOF growth for the production of a lopsided core-shell of MIL-88B@MIL-88A with mismatched cell parameters. *Chem Commun* 2018;55:43-6. DOI PubMed
349. Lee S, Oh S, Oh M. Atypical hybrid metal-organic frameworks (MOFs): a combinative process for MOF-on-MOF growth, etching, and structure transformation. *Angew Chem Int Ed Engl* 2020;59:1327-33. DOI PubMed
350. Zha Q, Yuan F, Qin G, Ni Y. Cobalt-based MOF-on-MOF two-dimensional heterojunction nanostructures for enhanced oxygen evolution reaction electrocatalytic activity. *Inorg Chem* 2020;59:1295-305. DOI PubMed
351. Zhao M, Chen J, Chen B, et al. Selective epitaxial growth of oriented hierarchical metal-organic framework heterostructures. *J Am Chem Soc* 2020;142:8953-61. DOI PubMed
352. Haldar R, Wöll C. Hierarchical assemblies of molecular frameworks - MOF-on-MOF epitaxial heterostructures. *Nano Res* 2021;14:355-68. DOI
353. Abdollahzadeh M, Chai M, Hosseini E, et al. Designing angstrom-scale asymmetric MOF-on-MOF cavities for high monovalent ion selectivity. *Adv Mater* 2022;34:e2107878. DOI PubMed
354. Lee G, Lee S, Oh S, Kim D, Oh M. Tip-to-middle anisotropic MOF-On-MOF growth with a structural adjustment. *J Am Chem Soc* 2020;142:3042-9. DOI PubMed
355. Gu Z, Zhang W, Pan T, et al. Anisotropic MOF-on-MOF growth of isostructural multilayer metal-organic framework heterostructures. *Research* 2021;2021:9854946. DOI PubMed PMC
356. Van Vleet MJ, Weng T, Li X, Schmidt JR. In situ, time-resolved, and mechanistic studies of metal-organic framework nucleation and growth. *Chem Rev* 2018;118:3681-721. DOI PubMed
357. Pienack N, Bensch W. In-situ monitoring of the formation of crystalline solids. *Angew Chem Int Ed Engl* 2011;50:2014-34. DOI PubMed